The role of posterior parietal cortex in multisensory decision-making

David Nunes Raposo

Dissertation presented to obtain
the Ph.D degree in Biology - Neuroscience

Instituto de Tecnologia Química e Biológica António Xavier | Universidade Nova de Lisboa

Oeiras,
November 2015

INSTITUTO
DE TECNOLOGIA
QUÍMICA E BIOLÓGICA
ANTÓNIO XAVIER /UNL

Knowledge Creation

The role of posterior parietal cortex in multisensory decision-making

David Nunes Raposo

Dissertation presented to obtain
the Ph.D degree in Biology - Neuroscience

Instituto de Tecnologia Química e Biológica António Xavier | Universidade Nova de Lisboa

Research work coordinated by:

Oeiras, November 2015

INSTITUTO
DE TECNOLOGIA
QUÍMICA E BIOLÓGICA
ANTÓNIO XAVIER /UNL

Knowledge Creation

Acknowledgements

The work presented in this thesis would not have been possible without the help of my colleagues and friends. First, I would like to thank Haley Zamer for helping me set up the lab's first behavioral rigs and conduct the first behavioral experiments with humans and rodents. Petr Znamenskiy and Santiago Jaramillo provided crucial advice on the design of the behavioral experiments, surgical procedures and electrophysiology. A big thanks to Barry Burbach for all the technical knowledge that he shared with me and his devoted assistance. I want to thank John Sheppard, Michael Ryan, Angela Licata and Amanda Brown, for their dedication and close collaboration on many of the experiments that I worked on. Matt Kaufman's analytical thinking and ingenuity are an inspiration to me. I wish to thank him for his invaluable input and collaboration on this project. There are also my classmates and friends, Pedro Garcia da Silva and Diogo Peixoto, who were always available when I needed to discuss any scientific or personal issue. I thank them and wish them the best success for their future endeavors.

I also want to thank the members of my thesis committee, Zach Mainen and Megan Carey, for all the comments and suggestions on my work throughout the PhD. A special thanks to Rui Costa, my co-advisor, for being incomparably enthusiastic and supportive. He, more than I, always believed in my success. Most importantly, I would like to thank my supervisor, Anne Churchland, for daring to accept me as her first student despite my limited experience at the time, for her patience and guidance. I am very fortunate to have her as a mentor and friend.

Finally, I would like to thank my wonderful sisters, my mother and my father. Their support and encouragement were determinant to place me where I am today.

Contributions

Haley Zamer, John Sheppard and Amanda Brown collaborated on the behavioral experiments with humans and rats. John Sheppard was the lead researcher on the cue weighting experiments. Matt Kaufman collaborated on the analysis of electrophysiological data. He developed the PAIRS and Variance Alignment analyses. Michael Ryan, John Sheppard and Angela Licata collaborated on the optogenetic experiments. Anne Churchland contributed to all stages of the research, including the experimental design and the writing of the manuscripts reporting the results presented here.

Funding for this work was provided by FCT – Fundação para a Ciência e a Tecnologia, doctoral fellowship SFRH/BD/51267/2010, NIH – US National Institutes of Health, grants EY019072 and EY022979, the John Merck Fund, the McKnight Foundation, the Marie Robertson Memorial Fund of Cold Spring Harbor Laboratory, and a Swartz Foundation fellowship.

Contents

List of figures

1

Introduction

Making a decision consists of committing to a plan of action, usually selected between two or more competing alternatives. Numerous fields have studied the processes involved in decision-making including psychology, economics, philosophy and statistics, to name only a few. In neuroscience the study of decision-making has been extremely fruitful in recent years and has focused on two main aspects: (1) perceptual decision-making, interested in understanding how external information is perceived by the sensory systems and used to make decisions; (2) value based decision-making, interested in the mechanisms that cause and result from the association of subjective values to the possible outcomes of a decision.

An important feature of decisions is that they can be made on very different and flexible time scales. For example, we can make an immediate decision to stop the car as we drive and see a red light in front of us. But we can also take a longer time to make more complex decisions, such as deciding which career we want to pursue. This characteristic of decision-making depends on the ability that animals have to combine information over time and may be, in general, a hallmark of cognition (Shadlen and Kiani, 2013).

In this thesis we aim at revealing some of the neural computations involved in perceptual decisions that occur over time and are informed by the auditory and visual sensory systems. The following sections will review our current understanding of the mechanisms of perceptual decision-making and integration of sensory evidence over

time and across modalities.

1.1 Perceptual decision-making

In a simplified context of decision-making, a subject is given two alternative choices and has to commit to one of them based on information provided by the external world. Faced with this problem the brain must implement at least three transformation steps (Graham, 1989) from the moment when the sensory inputs arrive until the moment the choice is made. First, it must transform the sensory input into a higher-order representation that is informative for the decision (sensory evidence). For example, when deciding which of two rectangles is wider, our brain needs to have access to a representation of the width of the two rectangles to be able to compare them. Second, it must use this representation of the input to select the most appropriate response. This step can also be viewed as computing a "decision variable" or, in other words, the probability of choosing one of the two alternative responses. Third, it must implement the action associated with the appropriate choice, by instantiating the probabilistic representation into a discrete behavioral output (for review, see Sugrue et al., 2005).

These transformations have been explored extensively in the primate visual and oculomotor systems. In these studies monkeys were typically asked to discriminate noisy visual stimuli and report their perceptual judgments using eye movements. Primary and secondary visual areas of the cortex (V1 and V2) and higher visual areas, such as V4 and middle temporal area (MT, also known as V5), were found to play a critical role in the representation of sensory evidence. For example, neurons in area MT respond to the direction of visual motion. On the other hand, areas in the frontal and parietal cortices — e.g. lateral intraparietal area (LIP), frontal eye fields (FEF) and supplementary eye field (SEF) — intermediate between sensory areas and the oculomotor nuclei in the brainstem, are thought to be responsible for translating visual evidence into a "decision variable" that will inform the ultimate choice.

1.1.1 Motion discrimination task

The random-dot motion direction discrimination task is, perhaps, the most successful paradigm used in the study of perceptual decisions. It relies on the presentation of dots that appear randomly on a circumscribed area of a screen ($\sim$ 5–10°) which is positioned in front of the subject. Some of these dots move towards one of two possible predefined directions. The goal of the subjects is to report which direction the dots are moving towards, usually by making an eye movement (saccade) into one of two targets on the screen. This task is designed in such a way that allows the experimenter to change the difficulty of each trial by varying the percentage of coherently moving dots.

Variants of this paradigm have been used in multiple studies to show that neurons in the cortical visual area MT carry signals that can be used by the subjects to discriminate the direction of visual motion. Here we list some of the findings:

1. The majority of neurons in area MT are tuned to the direction of visual motion (Albright et al., 1984);

2. The response of individual MT neurons correlates with behavioral accuracy / psychophysical performance (Britten et al., 1992; Shadlen et al., 1996);

3. The firing rate of single neurons in MT significantly predicts the subjects' choices, even on error trials, on a trial by trial basis (choice probability, Britten et al., 1996);

4. Lesioning MT causes an impairment in subjects' ability to discriminate the direction of visual motion (Newsome and Paré, 1988), suggesting the area is necessary for the task;

5. Microstimulation of MT, taking advantage of the anatomical organization of the area in terms of motion direction tuning, indicated that this area has a causal role in the subjects' ability to perform the task (Salzman et al., 1990).

These experiements not only showed the importance of MT in motion discrimination, they also led to new hypotheses. Britten, Newsome and colleagues suggested that, in this task, the brain makes a decision based on the comparison between the firing rate of two pools of neurons, each of them most sensitive to one of the two possible directions of motion (Newsome et al., 1989; Britten et al., 1992). As an example, if on a particular trial the random dots move leftwards, a pool of neurons with a "preference" for motion towards the left (more tuned to that direction of motion) would on average fire more than a pool of neurons with a preference for motion in the opposite direction (rightward motion). The difference between the firing rates of these two pools of neurons can be used as a decision variable — if the difference is positive (on average), choose 'left'; if the difference is negative, choose 'right'.

In the case of a weak stimulus (low proportion of coherently moving dots) the difference between the firing rate of the two pools of neurons becomes close to zero. This compels the subjects to take some time before committing to a particular choice. In other words, the subjects need to accumulate evidence for a certain period of time in order to make accurate decisions. This corresponds to allowing the decision variable to be integrated over time, as more evidence arrives, until it is possible to determine with confidence if its value is positive or negative.

Together, these studies established a new paradigm for investigating the neural mechanisms of decision formation by making it possible to characterize neural responses as the decision process unfolds.

One other key aspect of this task is that it sets up a clear association between a decision about a stimulus and a behavioral response to report that decision: a saccade towards one of two targets. This allowed scientist to look for a signature of the decision variable in particular brain areas involved in the guiding or planning of eye movements, like the lateral intraparietal area (LIP), the superior colliculus (SC) and the frontal eye fields (FEF).

1.1.2 Drift diffusion model

Decisions that are based on noisy, unreliable information may benefit from the process of integrating that same information over time. The reason is that integration provides a way to average out the noise and therefore achieve more accurate decisions. This is the idea behind integration models such as the *drift diffusion model* (DDM). The DDM assumes that infinitesimally small samples of a noisy signal are added together continuously and that this summation represents evidence accumulated over time. When this accumulated evidence reaches an upper or a lower bound, an appropriate response is triggered (Ratcliff, 1978).

To be more specific, let's assume that a "decision system" implementing the DDM receives an input signal corrupted by gaussian noise (stimulus), with mean μ and standard deviation σ (Figure 1.1, top). This device will sum this stochastic stimulus over time (integrated evidence), producing a drift that fluctuates over time (Figure 1.1, bottom). At some point this drifting integrated evidence will cross one of two thresholds — A or B (upper or lower bound). This event triggers the response of the system: if threshold A was crossed, the systems returns the response R_A (e.g. select target 'A'); if threshold B was crossed, the system returns the response R_B (e.g. select target 'B').

In the context of the motion discrimination task, the parameter μ is defined by the stimulus strength (motion coherence) and the noise parameter σ is considered constant. The distance between the decision boundaries A and B and the initial value of integrated evidence (evidence = 0) depends on the response bias of the subject, as measured by the point of subjective equality (PSE) of the psychometric curve (see Methods for explanation on psychometric curves).

This is a very simple model that, nonetheless, fits the behavioral data remarkably well (Palmer et al., 2005). Furthermore, neurophysiological data collected from subjects performing the task come in support of this view of integration of evidence at the level of individual neurons.

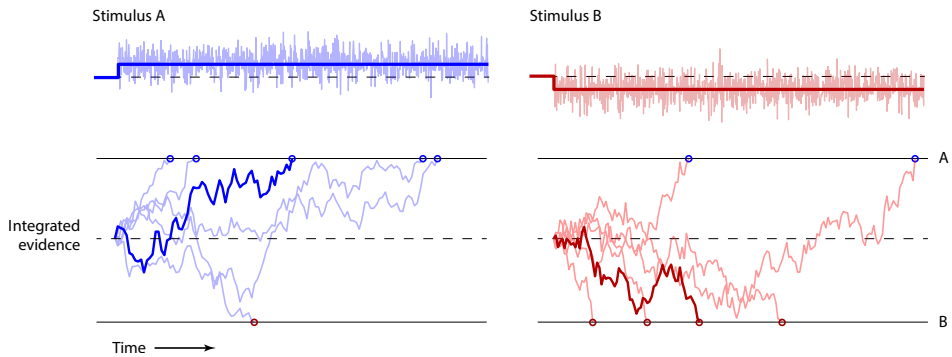

Figure 1.1: **Drift diffusion model.** Adapted from Uchida et al. (2006). Top, schematic of two example input signals (saturated blue/red line) and signal with added gaussian noise (stimulus; faded ragged blue/red trace). Bottom, cumulative sum of six instantiations of the two example stimuli (representing the integrated evidence), in which the signal was kept constant and the added noise varied. The noise makes the integrated evidence drift over time. At some point in time this integrated evidence crosses one of two thresholds (A or B), which is indicated by the blue/red circles.

1.1.3 A signature of the decision variable

The lateral intraparietal area (LIP) is a subregion of the posterior parietal cortex (PPC). It receives inputs from visual areas such as V3, V4 and MT (Felleman and Van Essen, 1991) and the pulvinar (Hardy and Lynch, 1992). Neurons in this area encode the direction and amplitude of an intended saccade (Gnadt and Andersen, 1988) and send these signals to structures involved in the control of eye movements (Andersen et al., 1990). Researchers soon hypothesized that the activity of LIP neurons could be correlated with a decision variable.

Indeed, experiments using the motion discrimination task described above revealed that some neurons in LIP reflect the accumulation of evidence in favor of one choice versus the other, i.e., the integration of the difference in firing between the two pools of MT neurons (Shadlen and Newsome, 1996). Moreover, the firing rate of these LIP neurons increased proportionally to the motion coherence and reached the same singular value, across trials, just before the decision was reported (Roitman and Shadlen, 2002). These suggest a mechanism of integration of evidence over time until

a specific threshold — or level of confidence in the decision — is crossed, very much consistent with the drift diffusion model.

Although microstimulation of LIP neurons during motion discrimination produces a contralateral response bias (Hanks et al., 2006), this effect is much smaller compared to the one observed from microstimulation of MT neurons. It was not yet established if LIP is, indeed, necessary for motion discrimination or if, instead, evidence integration occurs elsewhere and this computation is simply reflected in LIP. One the reasons why it has been difficult to state the importance of LIP in the motion discrimination task relates to the absence of techniques that would allow stimulation or inactivation of the specific outputs of MT that connect to LIP. Optogenetics opens up this possibility but methods for using this technique in primates are still in an early stage of development.

1.2 Integrating multiple sensory modalities

In the previous section we discussed how integration over time can ameliorate the problem of making decisions based on noisy and unreliable evidence. In the current section we will examine how the use of more than one sensory modality benefits decision-making under the same conditions.

Our observation of the world may sometimes lead to ambiguous or uncertain judgments. For example, imagine a situation where we are sitting inside an immobile train at the station and there is a second train, also immobile, next to ours. If that second train slowly starts moving, we sometimes perceive as if the train we are on is the one moving instead. This illusion happens because this is an ambiguous visual scene — based on our visual system, either scenario ('my train is moving' versus 'the other train is moving') would be conceivable. In situations like this one our judgment typically improves when we use another sensory modality to disambiguate our perception of the scene. In this case, using our vestibular system, for example, would help us to recognize that we are not moving.

Many studies have approached this question of how the brain combines multiple pieces of sensory information in order to achieve a more accurate perception and,

therefore, be able to make more accurate decisions. Here we will introduce some of the current views about multisensory integration.

1.2.1 Cue combination framework

The word 'cue' refers to a piece of sensory information that gives rise to a sensory estimate of a particular scene. The process of combining different cues is referred to as "cue combination" (or "cue integration").

If we try to estimate the precise location of a bird that hides behind the leaves of a tree, we may use both our vision and our audition, if the bird is singing, to do so. Our perception of the location of the bird must then be given by a mixture between our visual and auditory perceptions. But how exactly does the brain combine the two? One possibility is that the brain computes a separate estimate for each cue (visual cue and auditory cue) and then combines these estimates by computing a weighted average of the two, creating a final estimate (Clark and Yuille, 1990).

The maximum likelihood estimation framework provides an 'optimal', i.e. most advantageous, solution to the problem of determining how heavily each of the individual estimates should be weighted to compute the final estimate. Assuming that the noise corrupting each individual estimate is independent and gaussian, the best final estimate is the one that weighs each estimate by the inverse of their variances — *maximum likelihood estimate*, or MLE (see Methods for detailed deduction; for review, see Ernst and Bülthoff, 2004). This 'optimal' way of integrating evidence achieves a final estimate that is unbiased and that has the lowest possible variance.

From a Bayesian perspective, suppose that we want to estimate an external variable, S, using two sensory cues. It is fair to assume that the neural representation of these two cues, r_1 and r_2, is noisy and can, therefore, be seen as probabilistic. The possible values of S are then given by a probability density function, $P(S \mid r_1, r_2)$. If the noise affecting each cue is independent, $P(S \mid r_1, r_2)$ can be calculated using the Bayes' theorem:

$$P(S \mid r_1, r_2) = \frac{P(r_1 \mid S)\ P(r_2 \mid S)\ P(S)}{P(r_1)\ P(r_2)} \tag{1.1}$$

The left hand side of this equation, called the *posterior distribution*, can be used to estimate S (by taking the mean of this distribution, for example) and includes the uncertainty associated with that estimate (its variance). $P(r_1 \mid S)$ and $P(r_2 \mid S)$ are called the *likelihood* functions and quantify the probability of observing a particular neural response for each of the two cues. $P(S)$, the *prior distribution*, represents the probability of a particular event S occurring in the first place. Here, our goal is to find the value of S that maximizes the *posterior*. This optimization process is independent of the terms $P(r_1)$ and $P(r_2)$. Assuming gaussian likelihoods and a uniform prior, it follows that the solution S with the smallest variance is the MLE (Knill and Pouget, 2004; Angelaki et al., 2009).

Many studies have shown that this model describes well the behavior of human subjects in cue combination tasks. In a target localization task, humans combine auditory and visual cues, in an optimal way, according to each cue's reliability (Battaglia et al., 2003; Alais and Burr, 2004; Ghahramani and Wolpert, 1997). Humans combine visual and haptic cues to optimally estimate object size (Ernst and Banks, 2002). Surface slant estimates by humans using depth and texture cues result from optimal cue combination (Knill and Saunders, 2003).

Most multisensory integration studies, like the ones mentioned above, have relied on careful behavior and psychophysics with human subjects. Only a few recent studies have gone further and approached this problem with a combination of phychophysics and neural recordings in non-human primates, in search for a signature of multisensory integration in the brain.

1.2.2 Heading discrimination task

Gu, Angelaki and colleagues designed a two-alternative forced choice task that asked subjects to judge their heading direction using visual and vestibular cues. In this task, subjects (macaque monkeys) were seated on a platform that moved on the horizontal plane. A projector attached to the platform displayed a three-dimensional field of moving dots that provided optic flow on a given direction. For a subject seating on the platform, this optic flow simulates the translation of the platform in

the opposite direction of flow. In each trial, the subjects experienced forward motion with a small leftward or rightward component and were asked to report the perceived heading direction. They found that subjects performed significantly better when they used both cues (multisensory condition), compared to when they used only one (single sensory condition). Subjects' choices and how much they improved were well predicted by the maximum likelihood model described above. Moreover, when the reliability of the visual and vestibular cues changed, subjects quickly adjusted the relative weighting of two cues as the model predicted (Gu et al., 2008).

Many neurons in the dorsal medial superior temporal area (MSTd) had been found to respond strongly to both optic flow and translational movement (Duffy, 1998), making this area a good candidate in the search for a signature of heading perception. In a subset of neurons that had the same heading preference with both visual and vestibular cues ("congruent neurons"), heading tuning became steeper — more sensitive — in the multisensory condition. This finding suggested that these neurons could be involved in heading discrimination. Furthermore, choice probability analysis showed that trial-to-trial fluctuations in the firing rate of "congruent neurons" was strongly correlated with the fluctuations in the subjects' perceptual decisions, consistent with the hypothesis that monkeys monitored these neurons to perform the task.

Together these studies established the foundation for future research on the neural basis of multisensory decisions and opened doors to new models of sensory integration.

1.2.3 Models of multisensory integration

One of the main findings in the studies mentioned above was that cue weighting was adjusted on-the-fly as the reliability of each cue was changed by the experimenter from trial to trial. This revelation suggests that optimal integration, which requires knowledge of the variance of the estimates, can be accomplished on-line, as the evidence arrives and allows us to exclude particular neural models of sensory integration. Models that rely on plasticity to compute the uncertainty associated with a perceptual estimate, for example, may be too slow to follow the rapid changes observed in

cue weighting. Instead, the neural implementation of cue combination may, perhaps, be depended on network dynamics.

A plausible mechanism for determining the variance of a sensory estimate on-line is one that monitors the different responses of a population of neurons to a single sensory cue — referred to, in the literature, as a *population code*. As an example, consider a population of neurons in primary auditory cortex that are sensitive to tone frequency. This means that each neuron will fire the most in response to its preferred tone and will fire less as the frequency of the tone diverges away from its preferred one (tunning) In response to a particular tone, the firing of a population of auditory neurons will follow a distribution that peaks at the presented tone frequency and with a variance proportional to the uncertainty of the neural representation of the stimulus. Moreover, combining the activity of two such populations of neurons, by multiplying the two population firing distributions, results in an overall response distribution that corresponds to the solution provided by maximum likelihood estimation (Ernst and Bülthoff, 2004). In a Bayesian context, this corresponds to multiplying the likelihood functions to obtain the posterior distribution (assuming a flat prior). This is true not only for two populations of neurons that respond to only one sensory modality (e.g. two populations of auditory neurons), but also for two populations of neurons that respond to different sensory modalities — e.g. a population of auditory neurons and a population of visual neurons.

Many studies have proposed neural models of sensory integration using populations codes (Pouget et al., 2000; Zemel and Dayan, 1997). Ma, Pouget and colleagues demonstrated that, by taking advantage of the probabilistic nature of neural firing — assuming Poisson-like variability — cue combination could be implemented as a simple linear combinations of populations of neural activity (Ma et al., 2006). However, their model assumes fixed cue weighting and, thus, fails to explain the impact of cue reliability in the combination rule (Morgan et al., 2008).

Ohshiro and colleagues proposed that "divisive normalization" could explain many of the features of multisensory integration, including the change in neural weights with cue reliability (Ohshiro et al., 2011). In this model, two sensory neurons (e.g.,

one auditory neuron and one visual neuron) with overlapping receptive fields provide input to the same multisensory neuron. In summary, the activity of each multisensory neuron depends on a linear combination of the inputs, followed by an expansive power-law nonlinearity, and is divided by the net activity of all multisensory neurons.

"Divisive normalization" (Heeger, 1992) has been used to explain how neurons in primary visual cortex respond to a combination of stimuli with different contrasts and orientations (Carandini et al., 1997) and proposed to be involved in attention modulation (Reynolds and Heeger, 2009). It may, therefore, be a prevalent cortical computation that relies on relatively simple operations, making it a plausible model of multisensory integration.

1.3 The posterior parietal cortex

The posterior parietal cortex (PPC) is an association area of the brain traditionally seen as critical for visuo-spatial perception and spatial attention. However, in recent years, multiple studies have proposed its involvement in a wide range of cognitive functions, such as working memory and decision-making.

In primates, the PPC receives inputs from the pulvinar and lateral posterior nuclei of the thalamus. It is extensively connected with multiple sensory areas — visual, auditory, somatosensory and vestibular sensory systems (Avillac et al., 2005) and with subcortical structures, such as the superior colliculus (SC) and striatum. PPC is also strongly interconnected with the prefrontal cortex (PFC), traditionally associated with higher cognitive operations and executive functions (Miller and Cohen, 2001), premotor cortex and frontal eye fields (FEF). Its anatomical characteristics have led researchers to propose that PPC is involved in directed spatial attention. Indeed, unilateral and bilateral lesioning of PPC in humans cause strong deficits in attentional processing, such as the notorious hemispatial neglect (for review, see Reep and Corwin, 2009). Situated between multiple sensory inputs and a motor output, PPC is also in a privileged position for the computation of the variables necessary for decision-making. In fact, in decision-making tasks, neural responses in PPC re-

flect, for example, evidence accumulation (see Section 1.1.3), categorization of visual stimuli (Freedman and Assad, 2006), estimation of numerical quantities (Nieder and Miller, 2004) and reward expectation (Platt and Glimcher, 1999). These studies show a remarkable correlation between the neural activity in PPC and the decisions the subjects were asked to make. However, it is not yet known whether PPC neurons simply reflect a neural correlate of these decision-related signals or whether they are indeed responsible for the computations of these signals. If the latter is true, it would require downstream areas to be able to de-multiplex — i.e., independently decode — the different signals carried by PPC neurons (Huk and Meister, 2012).

In rodents, the existence of a PPC has only recently been established, with several studies identifying PPC as an autonomous region of the rodent brain (Kolb and Tees, 1990). In studies using retrograde tracers, Chandler, Reep and colleagues have found that PPC in rodents could be defined based on its afferents from the lateral dorsal and lateral posterior nuclei of the thalamus (Chandler et al., 1992; Reep et al., 1994). Unilateral lesioning of this brain area in rodents produces severe multimodal neglect — visual, tactile and auditory — similar to that observed in humans (Corwin et al., 1994; King and Corwin, 1993). However, it is not yet clear the degree to which the rodent PPC is homologous to the primate PPC. Other studies have shown the importance of PPC in spatial attention as well as in learning (Robinson and Bucci, 2012) and memory (Myskiw and Izquierdo, 2012) in rodents, but its importance in perceptual decisions has not been established in this model system.

1.4 Mixed selectivity and the argument against neural categories

Neurons in early sensory areas typically (although not exclusively; see Saleem et al., 2013) respond to a particular feature of the sensory environment. For example, some neurons in primary visual cortex are active when a moving bar with a specific orientation crosses the neuron's receptive field. In contrast, neurons in higher order brain structures often have more complex response properties and reflect more than one

feature of the task the organism is dealing with. This ability that neurons in some brain areas have to respond to multiple features is called "mixed selectivity". The PFC is predominantly composed of neurons with mixed selectivity. This makes its responses very heterogeneous and, therefore, difficult to interpret. However, mixed selectivity might be crucial in giving areas like PFC the ability to be involved in multiple tasks. Rigotti, Fusi and colleagues have shown that, whilst neurons in PFC encode distributed information about many task-relevant features, each of those features could be easily decoded from this population of *mixed-selective* neurons. They argue that mixed selectivity is a signature of high-dimensional neural representations. This high-dimensionality is what allows a linear classifier — such as a simple neuron model that combines information from a population of neurons — to decode information about any task-relavant feature (Rigotti et al., 2013).

Recent studies have extended mixed selectivity to neurons in PPC. Monkey LIP neurons were found to frequently respond to a mixture of decision signals, such as the accumulated evidence, and decision-irrelevant signals — other parameters of the task that do not inform the decision process, such as the presence of a choice target in the neurons receptive field (Meister et al., 2013). Other studies have emphasized this property of LIP neurons by showing that, while these neurons are strongly influenced by visual-spatial factors, such as the direction of a future saccade, they also carry signals about more abstract, nonspatial factors, such as the learned category of the direction of moving dots (Freedman and Assad, 2009).

Here we argue that the view that individual neurons belong to specialized classes, apt for particular computations, while important for understanding early sensory areas, may be inappropriate for the study of higher order brain areas. Instead, we speculate that single neurons in areas such as PPC and PFC may reflect a random combination of task-related parameters, therefore challenging the idea of neural categories. Mixed selectivity does not imply random combination of parameters per se. However, there is a major advantage to this kind of configuration: a task parameter that is randomly distributed across a population of neurons can be decoded by linearly combining an arbitrary group of neurons from that population (for review,

see Ganguli and Sompolinsky, 2012). An important consequence of this is that if a population with these characteristics is randomly connected to multiple downstream neurons, each of these neurons would receive enough information to be able to read out (decode) any particular task parameter that is encoded by the neural population.

1.5 Thesis outline

The following chapters report the main findings that came out of this research work (Chapters 2–4), the methodologies and details of the analyses used (Chapter 5) and, lastly, a summary of the conclusions we take and their relevance in the larger picture of understanding the computations that allow multisensory decision-making to take place in the brain (Chapter 6).

Chapter 2 describes our efforts to bring the rodent model to the field of multisensory decision-making. We lay out a new task that allowed us to observe that rodents, as humans, are able to combine auditory and visual information to make more accurate decisions.

In Chapter 3 we reveal the response properties of neurons in the posterior parietal cortex of rats performing a multisensory decision-making task. The neural recordings that we have conducted reveal mixed selectivity of PPC neurons and suggest that the population is category-free — characteristics that allow them to encode multiple task parameters, while granting easy decoding of those same parameters by downstream neurons. In this chapter we also analyze the impact of PPC inactivation during multisensory decision-making.

Chapter 4 describes the consequences of disrupting the normal activity of PPC in a spatially and temporally precise manner, using optogenetics. Our findings suggest that disruption impairs the use of sensory evidence in decisions and is followed by a slow network recovery.

2

Multisensory decision-making in rats and humans

A large body of work has shown that animals and humans are able to combine information across time to make decisions in some circumstances (Roitman and Shadlen, 2002; Mazurek et al., 2003; Palmer et al., 2005; Kiani et al., 2008). Specifically, combining information across time can be a good strategy for generating accurate decisions when incoming signals are noisy and unreliable (Link and Heath, 1975; Gold and Shadlen, 2007). For noisy and unreliable signals, combining evidence across sensory modalities might likewise improve decision accuracy, but little is known about whether the framework for understanding combining information over time might extend to combining information across sensory modalities.

The ability of humans to combine multisensory information to improve perceptual judgments for static information has been well established (for review, see Alais et al., 2010). Psychophysical studies have shown that multisensory enhancement requires that information from the two modalities be presented within a temporal "window" (Slutsky and Recanzone, 2001; Miller and D'Esposito, 2005). Physiological studies suggest the same: SC neurons show enhanced responses for multisensory stimuli only when those stimuli occur close together in time (Meredith et al., 1987). Such a temporally precise mechanism would serve a useful purpose for localizing or detecting objects. Therefore, temporal synchrony (or near-synchrony) provides an important cue that two sensory signals are related to the same object (Lovelace et al., 2003;

Burr et al., 2009).

In other circumstances, multisensory decisions might have more lax requirements for the relative timing of events in each modality. For example, when multiple auditory and visual events arrive in a continuous stream, temporal synchrony of individual events might be difficult to assess. Auditory and visual stimuli drive neurons with different latencies (Pfingst and O'Connor, 1981; Maunsell and Gibson, 1992; Recanzone et al., 2000), making it difficult to determine which events belong together. It is not known whether information in streams of auditory and visual events can be combined to improve perceptual judgments; if they can, this could be evidence for a different mechanism of multisensory integration that has less strict temporal requirements compared with the classic, synchrony-dependent mechanisms.

To invite subjects to combine information across both time and sensory modalities for decisions, we designed an audiovisual rate discrimination decision task. In the task, subjects are presented with a series of auditory and/or visual events and report whether they perceive the event rates to be high or low. Because of differing latencies for the auditory and visual systems, our stimulus would pose a challenge to synchrony-dependent mechanisms of multisensory processing. Nevertheless, we saw a pronounced multisensory enhancement in both humans and rats. Importantly, this enhancement was present whether the event streams were identical and played synchronously or were independently generated, suggesting that the enhancement did not rely on mechanisms that require precise timing. Together, these results suggest that some mechanisms of multisensory enhancement might exploit abstract information that is accumulated over the trial duration and therefore must rely on neural circuitry that does not require precise timing of auditory and visual events.

2.1 Rate discrimination task

We developed a novel behavioral task designed to invite subjects to combine information across time and sensory modalities. Each trial consisted of a series of auditory or visual "events" (duration: 10 ms for humans, 15 ms for rats) with background

noise between events (Figure 2.1a, top). Visual events were flashes of light, and auditory events were brief sounds (see below for methodological details particular to each species). The amplitude of the events was adjusted for each subject so that on the single-sensory trials performance was $\sim$70–80% correct and matched for audition and vision. We chose these values because previous studies have indicated that multisensory enhancement is the largest when individual stimuli are weak (Stanford et al., 2005). This appears to be particularly true for synchrony-dependent mechanisms of multisensory integration (Meredith et al., 1987).

Trials were generated so that the instantaneous event rate fluctuated over the course of the trial. Each trial was created by sequentially selecting one of two interevent intervals: either a long duration or a short duration (Figure 2.1a, bottom) until the total trial duration exceeded 1000 ms (or occasionally slightly longer/shorter durations for "catch trials"; see below). Trial difficulty was determined by the proportion of interevent intervals from each duration. As the proportion of short intervals varied from zero to one, the average rate smoothly changed from clearly low to clearly high. For example, when all of the interevent intervals were long, the average rate was clearly low (Figure 2.1a, left), and similarly when all of the interevent intervals were taken from the short interval, the average rate was clearly high (Figure 2.1a, right). When interevent intervals were taken more evenly from the two values, the average of the fluctuating rate was intermediate between the two (Figure 2.1a, center). When the number of long intervals exceeded the number of short intervals, subjects were rewarded for making a "low rate" choice and vice versa. When the numbers of short and long intervals in a trial were equal, subjects were rewarded randomly. Note that in terms of average rate this reward scheme places the low rate–high rate category boundary closer to the lower extreme (all long durations) than to the higher extreme (all short durations) because of the differing duration of the intervals. The strategies of both human and rat subjects reflected this: typically, subjects' points of subjective equality (PSEs) were closer to the lowest rate and less than the median of the set of unique stimulus rates presented. Nevertheless, for simplicity, we plotted subjects' choices as a function of stimulus rate. Nearly equivalent results were achieved when

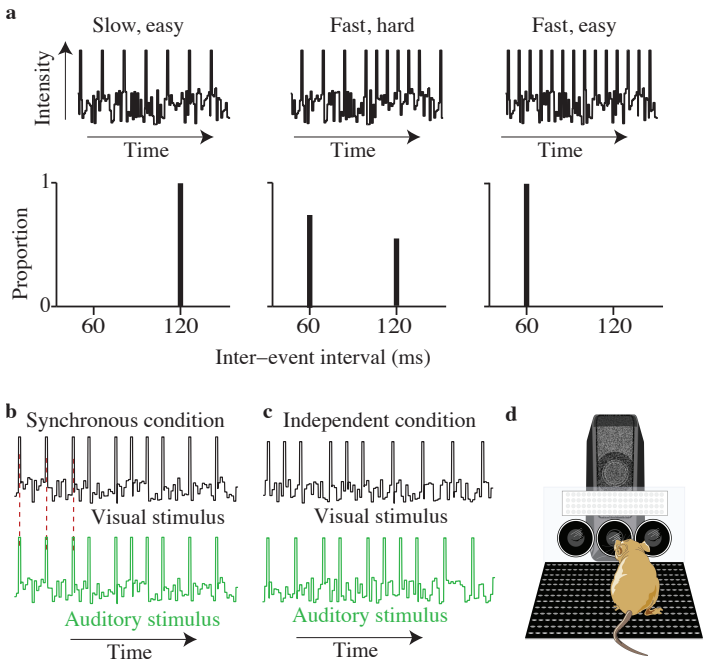

Figure 2.1: **Schematic of rate discrimination decision task and experimental setup.** **a,** Each trial consists of a stream of events (auditory or visual) separated by long or short intervals (top). Events are presented in the presence of ongoing white noise. For easy trials, all interevent intervals are either long (left) or short (right). More difficult trials are generated by selecting interevent intervals of both values (middle). Values of interevent intervals (bottom) reflect those used for all human subjects. **b,** Example auditory and visual event streams for the synchronous condition. Peaks represent auditory or visual events. Red dashed lines indicate that auditory and visual events are simultaneous. **c,** Example auditory and visual event streams for the independent condition. **d,** Schematic drawing of rodent in operant conditioning apparatus. Circles are the "ports" where the animal pokes his nose to initiate stimuli or receive liquid rewards. The white rectangle is the panel of LEDs. The speaker is positioned behind the LEDs.

we analyzed subjects' responses as a function of the number of short intervals in a trial rather than stimulus rate.

For single-sensory trials, event streams were presented to just the auditory or just the visual system. Visual trials were always 1000 ms long. Auditory trials were usually 1000 ms long, but we sometimes included catch trials that were 800 or 1200 ms. Catch trials were collected for four human subjects. The purpose of the catch trials

was to determine whether subjects' decisions were based on just event counts or event counts relative to the total duration over which those counts occurred. Catch trials constituted a total of 2.31% of the total trials. We reasoned that using such a small percentage of the trials for variable durations would make it possible to probe subjects' strategy without encouraging them to alter it. For these trials, we rewarded subjects based on event counts rather than the rate. This should have increased the likelihood that subjects would have made their decisions based on count, if they were able to detect that stimuli were sometimes of variable duration.

For multisensory trials, both auditory and visual stimuli were present and played for 1000 ms. To distinguish possible strategies for improvement on multisensory trials, we used two conditions. First, in the synchronous condition, identically timed event streams were presented to the visual and auditory systems simultaneously (Figure 2.1b). Second, in the independent condition, auditory and visual event streams were on average in support of the same decision (i.e., the proportion of interevent intervals taken from each duration was the same), but each event stream was generated independently (Figure 2.1c). As a result, auditory and visual events frequently did not occur at the same time. Auditory and visual events did not occur simultaneously even for the highest stimulus strengths because we imposed a 20 ms delay between events. Although a 20 ms delay does prevent auditory and visual events from being synchronous at the highest and lowest rates, the delay may be too brief to prevent auditory and visual stimuli from being perceived as synchronous (Fujisaki and Nishida, 2005). To be sure that our conclusions about the independent condition were not affected by these "perceptually synchronous" trials at the highest and lowest rates, we analyzed the independent condition both with and without the easiest trials (see Section 2.3). The multisensory effects we observed were very similar regardless of whether or not we included the easy trials.

Because auditory and visual event streams were generated independently, trials for this condition fell into one of four categories:

- Matched trials, where auditory and visual event streams had the same number of events (example match trials are shown in Figure 2.1c);

- Bonus trials, where both modalities provided evidence for the same choice, but one modality provided evidence that was one events/s stronger than the other (i.e., auditory and visual streams had proportions of short or long durations both above or below 0.5, but were not equal);
- Neutral trials, where only one modality provided evidence for a particular choice, whereas the other modality provided evidence that was so close to the PSE that it did not support one choice or the other;
- Conflict trials, where each modality provided evidence for a different choice.

Conflict trials were used to reveal differential weighting of sensory cues by explicitly varying the reliability of the single-sensory stimuli (see Section 2.5), as previously described in other multisensory paradigms (Fine and Jacobs, 1999; Hillis et al., 2004; Fetsch et al., 2009).

2.2 Rats, as humans, combine auditory and visual stimuli to improve decision accuracy

We examined whether subjects could combine information about the event rate of a stimulus when the information was presented in two modalities. Combining evidence should produce lower multisensory thresholds relative to single sensory thresholds. We first describe results from the synchronous condition where the same stream of events was presented to the auditory and visual systems, and the events occurred simultaneously (Figure 2.1b).

We quantified subjects' performance by computing their probabilities of high-rate decisions across the range of trial event rates and fitting psychometric functions to the choice data using standard psychophysical techniques (see Methods). Figure 2.2a shows results for the synchronous condition for a representative human subject: the subject's psychophysical threshold (σ) was lower for multisensory trials compared with single-sensory trials (Figure 2.2a, blue line is steeper than green and black lines), demonstrating that subjects made more correct choices on multisensory trials. The

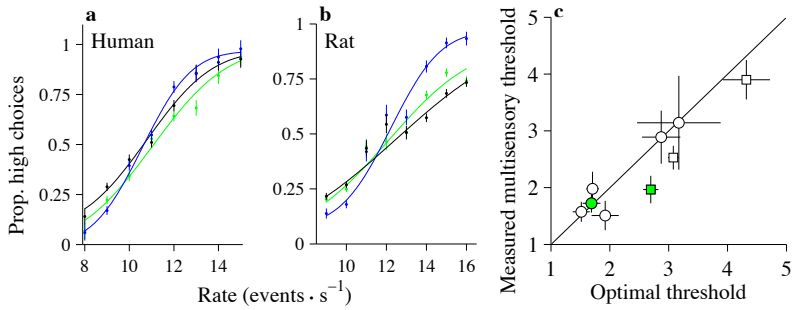

Figure 2.2: **Subjects' performance is better on multisensory trials. a,** Performance of a single subject plotted as the fraction of responses judged as high against the event rate. Green trace, auditory only; black trace, visual only; blue trace, multisensory. Error bars indicate SEM (binomial distribution). Smooth lines are cumulative Gaussian functions fit via maximum-likelihood estimation. $n = 7680$ trials. **b,** Same as a but for one rat (rat 3). $n = 12459$ trials. **c,** Scatter plot comparing the observed thresholds on the multisensory condition with those predicted by the single-cue conditions for all subjects. Circles, human subjects; squares, rats. Green symbols are for the example rat and human shown in a and b. Black solid line shows $x = y$; points above the line show a suboptimal improvement. Error bars indicate 95% CIs. Prop, Proportion.

difference between the single-sensory and multisensory thresholds was highly significant (auditory: $p = 0.0001$; visual: $p < 0.0003$); the change in threshold was not significantly different from the optimal prediction (see 'Optimal cue weighting', Equation 5.4 in Methods for details; measured: 1.75 [1.562, 1.885]; predicted: 1.69 [1.54, 1.84]; $p = 0.38$). In contrast, the PSE for multisensory trials was similar to those seen on single-sensory trials (auditory: $p = 0.06$; visual: $p = 0.52$).

The example was typical: all subjects we tested showed an improvement on the multisensory condition, and this improvement was frequently close to optimal (Figure 2.2c, circles are close to the $x = y$ line, indicating optimal performance). On average, this improvement was not accompanied by a change in PSE (mean PSE difference between visual and multisensory: 0.54 [0.48, 1.56], $p = 0.23$; mean PSE difference between auditory and multisensory: 0.05 [−0.66, 0.75], $p = 0.87$).

Significant multisensory enhancement was also observed in all three rats. Figure 2.2b shows results for a single rat. The difference in thresholds between the single-sensory and the multisensory trials was highly significant (auditory: $p < 10^{-5}$; visual:

$p < 10^{-5}$). The improvement exceeded that predicted by optimal cue combination (measured: 1.97 [1.72, 2.21]; predicted: 2.70 [2.57, 2.83]; $p < 10^{-5}$). This improvement was also seen in the remainder of our rat cohort (Figure 2.2c, squares); the improvement was significantly greater than the optimal prediction in one of the two additional animals (rat 1, $p < 10^{-5}$); the improvement nearly reached significance in a third (rat 2, $p = 0.06$).

Multisensory enhancement on our task could be driven by decisions based on estimates of event rate of the stimulus or estimates of the number of events. Human subjects have previously been shown to be adept at estimating counts of sequentially presented events, even when they occur rapidly (Cordes et al., 2007). In principle, either strategy could give rise to uncertain estimates in the single-sensory modalities that could be improved with multisensory stimuli. To distinguish these possibilities, we included a small number of random catch trials that were either longer or shorter than the standard trial duration. Consider an example trial that has 11 events (Figure 2.3a, arrow). If subjects use a counting strategy, they would make the same proportion of high choices whether the 11 events are played over 800, 1000, or 1200 ms. We did not observe these results in our data. Rather, subjects made many fewer high choices when the same number of events were played over a longer duration (Figure 2.3a, blue trace) compared with a shorter duration (Figure 2.3a, red trace).

These findings argue that subjects normalize the total number of events by the duration of the trial. In fact, the example subject in Figure 2.3, a and b, normalized quite accurately: he made the same proportion of high choices for a given rate (Figure 2.3c, arrow) whether that rate consisted of a small number of events played over a short duration (red traces) or a larger number of events played over a longer durations (green and blue traces). The tendency to make choices based on stimulus rate rather than stimulus count was evident when examined in a single subject (Figure 2.3a,b) and in the population of four subjects (Figure 2.3c,d). Note that our subjects exhibited such a rate strategy despite the fact that we rewarded them based on the absolute event count, not the event rate (see Methods).

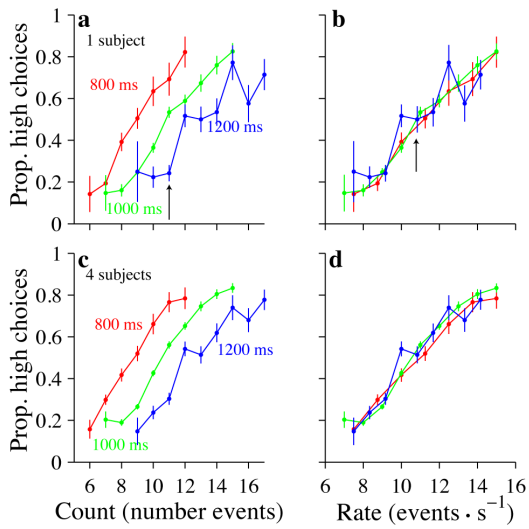

Figure 2.3: **Subjects make decisions according to event rates, not event counts. a,** Example subject. Abscissa indicates the number of event counts. Each colored line shows the subject's performance for trials where the event count on the abscissa was presented over the duration specified by the labels. For a given event count (11 events, black arrow) the subject's choices differed depending on trial duration. $n = 3656$ trials. **b,** Same data and color conventions as in a except that the abscissa indicates event rate instead of count. For a given event rate (11 events/s, black arrow), the subject's choices were very similar for all trial durations. **c, d,** Data for four subjects; conventions are the same as in a and b. $n = 9727$ trials. Prop, Proportion.

2.3 Multisensory enhancement occurs even when audio-visual events are asynchronous

The multisensory enhancement observed for our task (Figure 2.2) might simply have resulted because the auditory and visual stimuli were presented amid background noise and therefore were difficult to detect. Thus, in the synchronous condition, multisensory information may have enhanced subjects' performance by increasing the effective signal-to-noise ratio for each event by providing both auditory and visual events at the same time. To evaluate this possibility, we tested subjects on a condition designed to prevent multisensory information from facilitating event detection: we

achieved this by generating auditory and visual event streams independently. We term this the "independent condition". On each trial, we used the same ratio of short to long events for the auditory and visual stimuli. First, we restricted our analysis to the case where the resulting rates were identical or nearly identical (matched trials). Importantly, the auditory and visual events did not occur at the same time and could have had different sequences of long and short intervals (Figure 2.1c). Because the events frequently did not occur simultaneously, subjects had little opportunity to use the multisensory stimulus to help them detect individual events. Despite this, subjects' performance still improved on the multisensory condition compared with the single-sensory condition. This is evident in the performance of a single human and rat subject (Figure 2.4a,c). For both the human and the rat, thresholds were significantly lower on multisensory trials compared with visual or auditory trials (human: auditory, $p = 0.0002$, visual, $p < 10^{-5}$; rat: auditory, $p < 10^{-5}$, visual, $p < 10^{-5}$). The change in threshold was close to the optimal prediction for the human (measured: 2.08 [1.70, 2.46]; optimal: 2.39 [2.60, 2.17]; $p = 0.09$) and was lower than the optimal prediction for the rat (measured: 2.64 [2.47, 2.81]; optimal: 3.26 [3.10, 3.38]; $p < 10^{-5}$). This example was typical: all subjects we tested showed an improvement on the multisensory condition, and multisensory thresholds were frequently slightly lower than the optimal prediction (Figure 2.4e, many circles are below the $x = y$ line); the improvement was significantly greater than the optimal prediction for one additional rat (rat 1, $p < 10^{-5}$). On average, this improvement was not accompanied by a change in PSE, for neither the humans (mean PSE difference between visual and multisensory condition: 0.45 [−1.93, 1.04], $p = 0.47$; mean PSE difference between auditory and multisensory conditions: 0.62 [−0.4, 1.65], $p = 0.18$) nor the rats (mean PSE difference between visual and multisensory condition: 0.48 [−0.33, 1.29], $p = 0.13$; mean PSE difference between auditory and multisensory conditions: 0.55 [−2.04, 3.14], $p = 0.46$). To ensure that subjects' improvement on the independent condition was not driven by changes at the highest and lowest rates (where stimuli might be perceived as synchronous), we repeated this analysis excluding trials at those rates. The multisensory improvement was still evident for the example human and was

again very close to the optimal prediction (measured: 2.45 [1.85, 3.05]; optimal: 2.79 [2.40, 3.18]; $p = 0.82$). The multisensory improvement for the example rat was also present and was still better than the optimal prediction (measured: 2.75 [2.41, 3.09]; optimal: 3.53 [3.19, 3.88]; $p = 0.0008$). For the collection of human subjects, we found that thresholds were lower for multisensory trials compared with visual ($p = 0.039$) or auditory ($p = 0.003$) trials. For the rats, thresholds were lower for multisensory trials compared with visual ($p = 0.02$) or auditory ($p = 0.04$) trials. Excluding trials with the highest/lowest rates did not cause significant changes in the average ratio of multisensory to single-sensory thresholds for either modality or either species ($p < 0.05$).

Subjects might have shown a multisensory improvement on the independent condition for two trivial reasons. First, the presence of two modalities together might have been more engaging and therefore recruited additional attentional resources compared with single-sensory trials. Second, events in the independent condition might sometimes occur close enough in time to aid in event detection. We performed two additional analyses that ruled out both of these possibilities.

First, we examined subsets of trials from the independent condition where the rates were different for the auditory and visual trials (bonus trials). For these trials, evidence from one modality (say, vision) provided stronger evidence about the correct decisions than the other modality (say, audition). For example, the auditory stimulus might be 10 Hz, a rate that is quite close to threshold, but still in favor of a low rate choice, while the visual stimulus is 9 Hz (Figure 2.4b, arrow, cyan line). We compared such trials possessing different auditory and visual rates with "matched-evidence" trials where both stimuli had the same rate (Figure 2.4b, arrow, blue line). If subjects exhibit improved event detection on the multisensory condition because of near-simultaneous events, they should perform worse on the bonus evidence trials (at least for low rates), because the likelihood of events occurring at the same time is lower when there are fewer events (10 and 10 events for matched trials; 10 and 9 events for bonus trials). To the contrary, we found that performance improved on bonus evidence trials: in the example, the subject made fewer high choices on the bonus

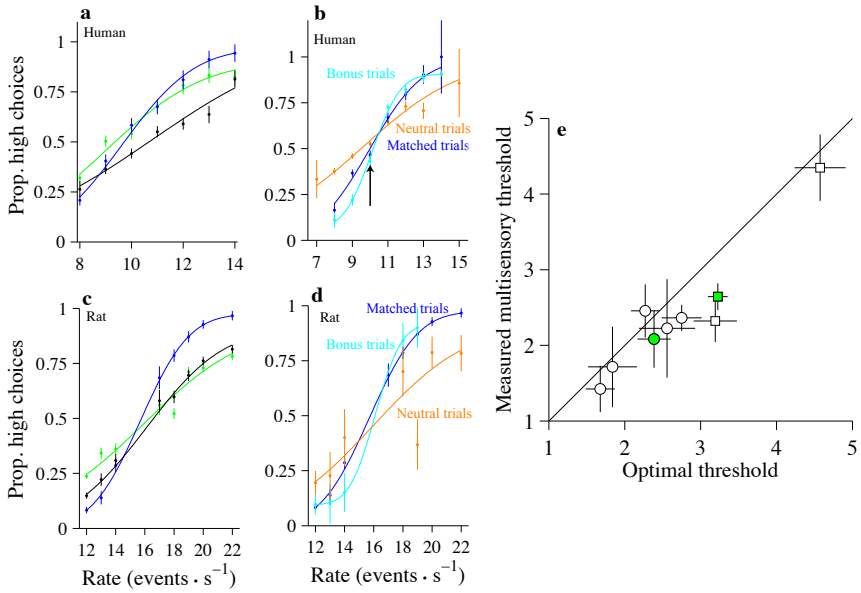

Figure 2.4: **The multisensory enhancement is still present for the independent condition. a,** Performance of a single subject. Conventions are the same as in Figure 2a. $n = 4255$ trials. **b,** A comparison of accuracy for matched trials (blue trace), bonus trials (cyan trace), and neutral trials (orange trace). Abscissa plots the rate of the auditory stimulus. Data are pooled across six humans. $n = 1957$ (matched condition), 2933 (bonus condition), and 3825 (neutral condition). **c,** Same as a, but for a single rat (rat 1). $n = 13116$ trials. **d,** Same as b, but for a single rat. $n = 3725$ (matched condition), 244 (bonus condition), and 247 (neutral condition) **e,** Scatter plot for all subjects comparing the observed thresholds on the multisensory condition with the predicted thresholds. Conventions are the same as in Figure 2c. Error bars indicate 95% CIs. Prop, Proportion.

trials at low rates (Figure 2.4b, arrow, cyan trace below blue trace), demonstrating improved performance. Accuracy was improved at the higher rates as well, leading to a significantly lower threshold for bonus trials (matched: $\sigma = 2.3$ [2.00, 2.57]; bonus: $\sigma = 1.3$ [1.12, 1.38]; $p < 10^{-5}$). The enhanced performance seen in this subject was typical: five of six subjects showed lower thresholds for bonus evidence trials, and this reached statistical significance ($p = 0.05$) in three individual subjects. Data from an example rat subject supported the same conclusion (Figure 2.4d): performance on bonus trials was better than performance on matched trials (matched: $\sigma = 2.6$ [2.42, 2.78]; bonus: $\sigma = 1.4$ [0.71, 2.09]; $p = 0.02$). Bonus trials were collected from one of

the remaining two rats; for this rat also, performance on bonus trials was better than performance on matched trials (rat 2; matched: $\sigma = 4.4 \pm 0.22$; bonus: $\sigma = 2.6 \pm 0.70$; $p = 0.008$).

Next, we examined subsets of neutral trials for which the rate of one modality (say, vision) was so close to the PSE that it did not provide compelling evidence for one choice or the other. If multisensory trials are simply more engaging and help subjects pay attention, performance should be the same on matched trials and neutral trials. To the contrary, we found that performance was worse for neutral trials compared with matched trials: the example subject made many more errors on neutral trials and had elevated thresholds (matched: $\sigma = 2.3$ [2.00, 2.57]; neutral: $\sigma = 4.2$ [3.56, 4.57]; $p < 10^{-5}$). The decreased performance seen on neutral trials was typical: all subjects showed higher thresholds for neutral trials, and this was statistically significant ($p = 0.05$) in five subjects. Data from an example rat subject support the same conclusion (Figure 2.4d): performance on the neutral trials was worse than performance on matched trials ($\sigma = 2.6$ [2.42, 2.78]; neutral: $\sigma = 5.0$ [3.80, 6.20]; $p < 10^{-5}$). Neutral trials were collected from one of the remaining two rats; for this rat also, performance on neutral trials was worse than performance on matched trials (matched: $\sigma = 4.4$ [4.03, 4.76]; neutral: $\sigma = 6.6$ [5.09, 8.11]; $p = 0.01$).

Because we typically collected data from only the independent condition or the synchronous condition on a given day, we could not rule out the possibility that subjects developed different strategies for the two conditions. If true, then their performances should decline when the trials from the two conditions were mixed within a session. To test this, we collected data from four additional subjects on a version of the task where the synchronous and independent conditions were presented in alternating blocks of 160 trials over the course of each day. Because the condition switched so frequently within a given experimental session, subjects would have a difficult time adjusting their strategy. Therefore, a comparable improvement on the two tasks can be taken as evidence that subjects can use a similar strategy for both conditions. Indeed, we found that subjects showed a clear multisensory enhancement on both conditions, even when they were presented in alternating blocks (Figure

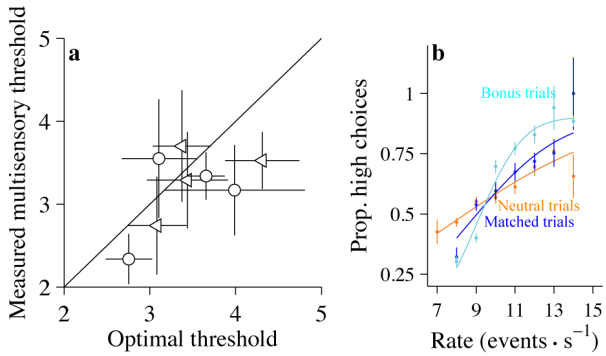

Figure 2.5: **Human subjects' performance is better on multisensory trials even when the synchronous and independent conditions are presented in alternating blocks. a,** Scatter plot for all subjects comparing the observed thresholds on the multisensory condition with the predicted thresholds. Data from the synchronous (circles) and independent (triangles) conditions are shown together. Error bars indicate 95% CIs. **b,** Subjects perform better on bonus trials compared with the matched trials and slightly worse on neutral trials. Conventions are the same as in Figure 4c. $n = 1390$ (matched condition), 2591 (bonus condition), and 2464 (neutral condition). Prop, Proportion.

2.5a, triangles and circles close to the $x = y$ line). Further, this group of subjects showed the same enhancement on bonus trials as did subjects who were tested in the more traditional configuration (Figure 2.5b; matched: $\sigma = 3.7$ [2.93, 4.45]; bonus: $\sigma = 1.9$ [1.67, 2.04]; $p < 10^{-5}$). Individual subjects all showed reduced thresholds for the bonus condition; this difference reached significance for one individual subject. This group of subjects also showed significantly increased thresholds on neutral trials relative to matched trials (Figure 2.5b) (matched: $\sigma = 3.7$ [2.93, 4.45]; neutral: $\sigma = 6.4$ [4.91, 7.89]; $p = 0.0008$). This effect was also observed in all four individual subjects.

2.4 Subjects' decisions reflect evidence accumulated over the course of the trial

Our stimulus was deliberately constructed so that the stimulus rate fluctuated over the course of the trial. We exploited these moment-to-moment fluctuations in rate

to determine which time points in each trial influenced the subjects' final decisions. To explain this analysis, consider a group of trials that was selected because they had the same average rate during the first 700 ms of the trial (Figure 2.6a, top). By examining the average stimulus rate in the last 300 ms of the trial and comparing it for trials that end in high versus low choices, we can determine whether rates during that late interval influenced the subjects' final choice. In the schematic example, trials preceding low choices (Figure 2.6a, red traces, top) had a lower rate during the final 300 ms compared with trials preceding high choices (Figure 2.6a, blue traces, top). We denote differences in rate within such windows as the "excess rate" supporting one choice over the other. The same process can be repeated for other windows within the trial (Figure 2.6a, bottom). Systematically varying the temporal window makes it possible to generate a time-varying weighting function, termed the choice-triggered average (Kiani et al., 2008; Nienborg and Cumming, 2006; Sugrue et al., 2004), that describes the degree to which each moment in the trial influenced the final outcome of the decision. When excess rate > 0 at a particular time point, we conclude that stimuli at that time influence the decision. By comparing the timecourse of the excess rate curves between different trial types, we gain insight into the animals underlying strategies. For example, if the excess rate was elevated only very late in the trial, this suggests that the subjects either did not pay attention early in the trial or did not retain the information (a leaky integrator) and simply based their decision on what happened at the end of the trial. By contrast, if the excess rate was elevated for the entire duration of the trial, this suggests that subjects exploited information presented at every moment.

The excess rate that we computed was elevated over the course of the entire trial for human subjects (Figure 2.6b) and over ~ 600 ms for rodents (Figure 2.6c). This suggests that subjects integrate evidence over time for the majority of the trial. The integration time appears to be longer for humans compared with rats: the choice-triggered average for rats was not elevated during the first 200 or last 100 ms of the trials. On average, humans' excess rates were significantly larger for multisensory trials compared with auditory-only or visual-only trials (multisensory: 1.63 ± 0.05;

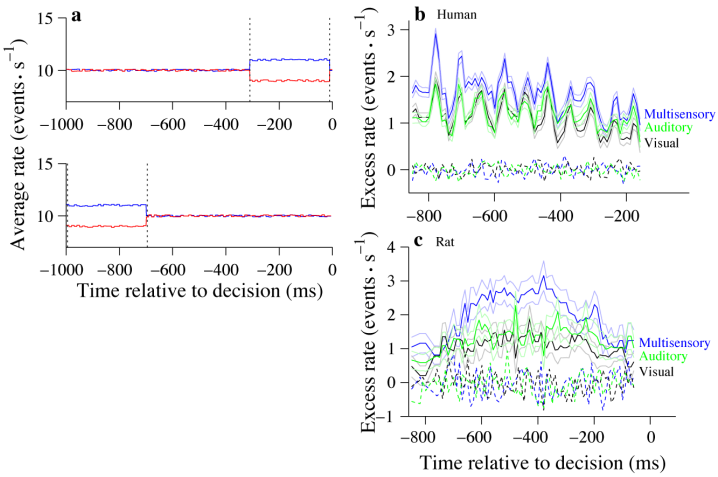

Figure 2.6: **Subjects' decisions reflect evidence accumulated over the course of the trial.** **a,** Schematic of average stimulus frequencies for trials supporting opposing decisions. Top, Trials were selected if their average stimulus rate from 0 to 700 ms was 10 Hz (seven events over 700 ms). Trials were then grouped according to whether the subject chose low (red) or high (blue) on each trial. Average stimulus rate within the bin of interest (700–1000 ms; dashed lines) was then compared for stimuli preceding left and right choices. Bottom, Same as in top panel except that the window of interest occurred early in the trial (0–300 ms). **b,** Solid traces indicate difference in average event rate for trials that preceded left versus right choices for all time points in a trial. Color conventions are the same as in Figure 2, a and b. Thin lines indicate SEM computed via bootstrapping. Dashed traces indicate difference in average rate for trials assigned randomly to two groups. Data were pooled from six human subjects. Trial numbers differed slightly for each time point; $\sim$ 1800 trials were included at each point. **c,** Same as b but for an individual rat. Trial numbers differed slightly for each time point; $\sim$3200 trials were included at each point.

visual: 1.16 ± 0.04; auditory: 1.19 ± 0.03; multisensory $>$ auditory, $p < 10^{-5}$; multisensory $>$ visual, $p < 10^{-5}$). The multisensory excess rate was also elevated in the example rat (multisensory: 1.99 ± 0.08; visual: 1.05 ± 0.04; auditory: 1.29 ± 0.04; multisensory $>$ auditory, $p < 10^{-5}$; multisensory $>$ visual, $p < 10^{-5}$). Similar results were observed in the other two rats: the choice-triggered averages exhibited similar shapes and the magnitude of the multisensory trials was larger than that of the single-sensory trials (rat 2: multisensory $>$ auditory, $p < 10^{-5}$; multisensory $>$ visual, $p < 10^{-5}$; rat 3: multisensory $>$ auditory, $p > 10^{-5}$; multisensory $>$ visual, $p > 10^{-5}$).

2.5 Perceptual weights change with stimulus reliability

We examined the decisions of rat and human subjects on a version of the rate discrimination task in which we systematically varied both the stimulus strength (i.e., the trial-averaged event rate) and the reliability (i.e., SNR) of auditory and visual stimuli.

On single-sensory trials, estimated psychophysical thresholds (σ) were comparable across modalities for matched reliability trials but significantly smaller for high- relative to low-reliability trials of either modality, as highlighted in a representative human subject (Figure 2.7a, green and black lines steeper than blue and gray lines; $\sigma \pm$ SE: high-reliability auditory: $1.01 \pm 0.12 <$ low-reliability auditory: 3.20 ± 0.21, $p < 10^{-5}$; high-reliability visual: $1.24 \pm 0.11 <$ low-reliability visual: 3.40 ± 0.30, $p < 10^{-5}$). Rats were similarly presented low-reliability and high-reliability auditory stimuli, but only a single reliability level was used for the visual stimuli. Rats' thresholds also differed significantly between the two auditory reliability levels, as demonstrated in an example rat (Figure 2.7c, green line steeper than blue line; high-reliability auditory: $1.93 \pm 0.35 <$ low-reliability auditory: 5.32 ± 0.95, $p = 0.0004$), with an intermediate threshold for visual trials (black line; visual: 2.72 ± 0.31). In both species, we attempted to minimize bias; however, achieving zero bias for all three (rat) or four (human) single sensory trial types proved challenging. Analyses that could in principle be affected by subject bias were always repeated in subsampled data where biases were minimal.

As in the experiments described in Section 2.2, both rats' and humans' performances improved on multisensory trials, and the performances were frequently close to the optimal prediction. The magnitude of the multisensory improvement ($\sigma_{predicted}/\sigma_{observed}$; see Methods) was unrelated to the magnitude of the cue conflict (mean correlations averaged across trial types, 95% CIs; humans: $r = 0.07$ [-0.13, 0.26], rats: $r = 0.03$ [-0.25, 0.31]). We took advantage of cue conflict trials and asked whether subjects' multisensory decisions reflected the relative reliabilities of the au-

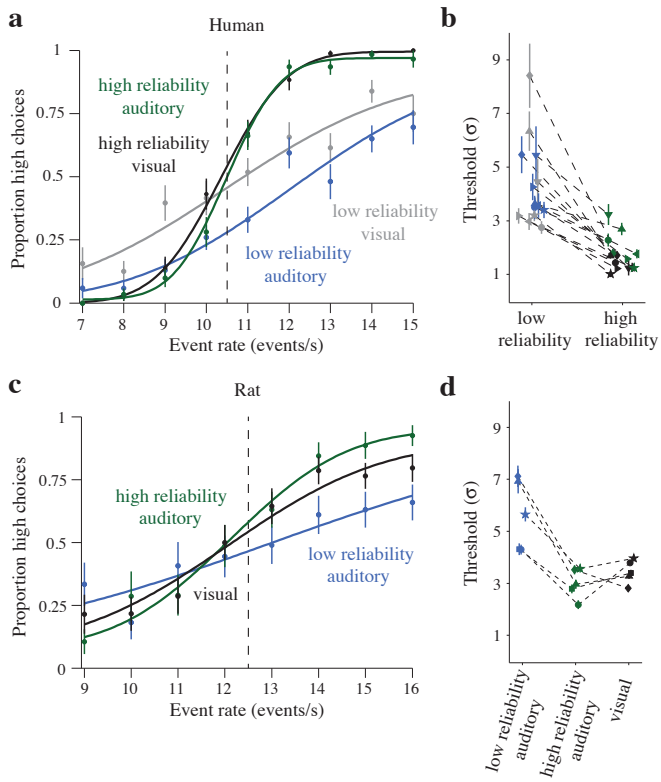

Figure 2.7: **Single sensory performance on rate discrimination task depends on sensory reliability. a,** Performance of an individual human subject, displayed as the proportion of high-rate decisions plotted against the trial-averaged event rate. Data are presented separately for each single sensory trial type. Lines indicate psychometric functions fit via maximum likelihood estimation. Data were combined across multiple behavioral sessions (2161 trials). **b,** Psychophysical thresholds obtained from seven human subjects for each single sensory trial type (low/high reliability auditory: blue/green; low/high reliability visual: gray/black). Symbols depict individual subjects. **c,** Single sensory performance in an individual rat, pooled from two consecutive sessions (975 trials). **d,** Single sensory thresholds obtained across cohort of 5 rat subjects (symbols). Thresholds in b and d were estimated from data combined across multiple behavioral sessions (humans/rats: 19143/62363 total single sensory trials). Star symbols indicate the example human and rat subjects used in a and c. Error bars indicate standard errors in all panels.

ditory and visual stimuli as estimated from subjects' single sensory psychophysical thresholds. To assess the relative weights subjects assigned to the auditory and visual stimuli, we compared subjects' decisions on multisensory trials across a range of

conflict levels for each of the possible reliability pairings.

Both humans' and rats' decisions on multisensory trials were influenced by the relative reliabilities of the auditory and visual stimuli. The effects of stimulus reliability on subjects' decisions can be visualized by comparing subjects' choice data on trials with different levels of conflict between the auditory and visual event rates. When auditory and visual reliabilities are matched, subjects should weigh both modalities equally. Indeed, on matched reliability trials, conflict in the event rates did not systematically bias subjects' decisions towards either cue. When sensory reliabilities were unequal, however, subjects preferentially weighted the more reliable modality, and their PSEs were systematically shifted towards this cue on conflict trials (Figure 2.8a,b; red, blue curves). These results are in agreement with previous observations from experiments using static stimuli (Ernst and Banks, 2002; Jacobs, 1999). The shifts in the psychometric functions for the example rat subject were smaller than in the human. The smaller magnitude of the shift in the rat relative to the human reflects the fact that the single sensory thresholds (and thus the sensory reliabilities) were more disparate between the two modalities in the human than in the rat (i.e., compare human and rat psychometric curves in Figure 2.7a,c).

The magnitude and direction of the shift in PSE depended on the magnitude and direction of the stimulus conflict as well as the relative reliabilities of the two modalities. Figure 2.8, c and d, displays the example subjects' estimated PSEs as a function of conflict level for two multisensory trial types. For multisensory trials featuring low-reliability visual and high-reliability auditory stimuli in the example human, linear regression of PSE against conflict level (Δ) produced slopes significantly greater than zero (Figure 2.8c, left; slopes, 95% CIs: 0.36 [0.26, 0.46]). On the other hand, the slope of this regression was significantly less than zero for multisensory trials featuring high-reliability visual and low-reliability auditory stimuli (Figure 2.8c, right; slopes, 95% CIs: -0.46 [-0.59,-0.33]). The positive and negative slopes of the regression lines indicate stronger and weaker weighting of the auditory stimulus (respectively) relative to the visual stimulus; thus, this subject weighed the high-reliability modality more strongly than the low-reliability modality in either case.

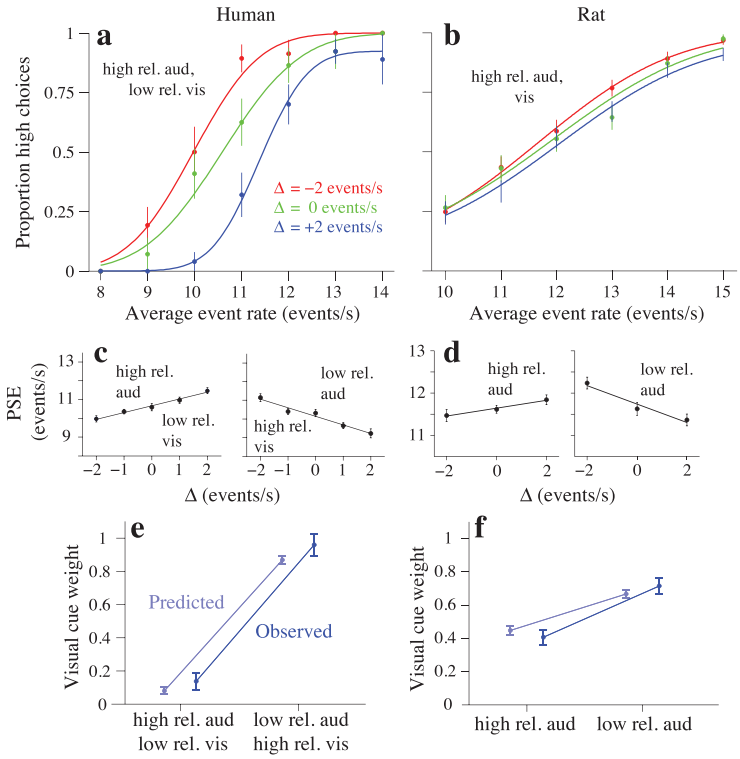

Figure 2.8: **Subjects weigh auditory and visual evidence in proportion to sensory reliability. a,** Performance on multisensory trials in an individual human pooled over multiple sessions (values on abscissae indicate mean trial event rates averaged between auditory and visual stimuli). Colors indicate level of conflict between modalities ($\Delta = \textit{visual rate} - \textit{auditory rate}$). Presented human data were obtained from the low-reliability visual/high-reliability auditory condition. **b,** Same as a but for one rat. Data were obtained from the visual/high-reliability auditory condition. **c,** Points of subjective equality (PSEs) from multisensory trials plotted as a function of conflict level for different pairings of auditory and visual stimulus reliabilities, shown for the same subject as in a. Fitted lines were obtained via linear regression. Plotted data correspond to trials consisting of low- and high-reliability auditory stimuli paired with high- and low-reliability visual stimuli, respectively. Analogous fits were obtained for the other pairings of auditory and visual reliabilities presented to human subjects. **d,** Same as c but for the single rat subject in b. **e,** Comparisons of the observed visual weights to the values predicted from the example human's single sensory thresholds. Data pertain to the same two multisensory trial types reported in c. $N = 3,861$ trials. **f,** same as e but for the rat in b and d. $N = 4,018$ trials. Error bars indicate standard errors in all panels.

Similarly, slopes of the PSE versus Δ regression lines differed significantly between the two multisensory trial types in the example rat, reflecting the relative reliabilities of auditory and visual stimuli (Figure 2.8d: visual/high-reliability auditory: 0.09 [0.005, 0.18]; visual/low-reliability auditory: -0.22 [-0.32, -0.12], $p < 10^{-5}$).

The changes in subjects' PSEs across the range of cue conflicts agreed well with predictions based upon the sensory reliabilities we inferred from subjects' performance on single sensory trials. To test whether subjects' cue weighting approximated statistically optimal behavior, we compared the observed sensory weights estimated from the slopes of the regression lines with the theoretical weights predicted by subjects' thresholds on the corresponding unisensory auditory and visual trials (see Methods; Young et al., 1993). The observed and predicted weights were in close agreement for all multisensory trial types in both example subjects (Figure 2.8e,f).

The weighting of multisensory stimuli seen in the example human and rat was typical: nearly all humans and rats weighed sensory information in a manner that reflected the relative reliabilities of auditory and visual stimuli (Figure 2.9). For each subject, we computed the difference in w_V between multisensory trials consisting of high-reliability auditory/low-reliability visual versus low-reliability auditory/high-reliability visual stimulus pairings. This change was significantly greater than zero for six of seven individual humans (Figure 2.9a, $p < 0.007$, one-tailed Z-tests). This indicates that nearly all human subjects increasingly relied on the visual or auditory evidence when its reliability was increased relative to the other modality. The increase in w_V between multisensory trials containing low- versus high-reliability auditory stimuli was likewise significant in four out of five rats (Figure 2.9d; $p < 0.032$, Z-tests). The remaining human and rat also showed changes in w_V in the expected direction, but the changes did not reach significance ($p > 0.19$).

2.5.1 Optimal cue weighting

Having established that both humans and rats dynamically changed their perceptual weights on multisensory trials in a manner that reflected the relative reliabilities of the auditory and visual evidence, we examined the degree to which these changes

matched the statistically optimal predictions. These predictions are based on the sensory reliabilities inferred by subjects' performance on single sensory trials (see Methods). In humans, observed visual weights were generally closely matched to predictions within the individual subjects (Figure 2.9b); seven of 28 comparisons (7 subjects $\times$ 4 multisensory trial types) exhibited significant deviations between predicted and observed weights ($p < 0.05$, Z-tests). The observed deviations were distributed across four subjects. Interestingly, six of the seven deviations involved overweighting of visual evidence relative to predictions when the auditory reliability was high (Figure 2.9b, green and orange symbols). The remaining 21 comparisons for the other human subjects revealed no significant differences between observed and predicted weights. A limitation of our analysis is that we cannot rule out the possibility that some of the apparent deviations from optimality were, in fact, false positives arising from the large number of comparisons; however, all seven deviations remained robust to multiple comparisons correction after allowing for a false discovery rate of 20% (Benjamini and Hochberg, 1995).

In rats, as in humans, the perceptual weights for many individual subjects were close to the optimal predictions (Figure 2.9e). In general, rats came closest to the optimal prediction on high-reliability auditory trials (observed visual weights did not differ significantly from predictions in any of the rats; $p > 0.18$, two-tailed Z-tests). Deviations from the optimal prediction were observed more frequently on trials where the auditory stimulus reliability was low. On such trials, the perceptual weights for three of five rats differed significantly from optimality ($p < 0.05$, Z-tests). One other rat's perceptual weights also differed from the optimal prediction on such trials, though the effect was only marginally significant ($p = 0.07$). In all four of these cases, observed visual weights were lower than predicted, suggesting that rats may systematically under-weigh visual evidence relative to the optimal prediction when auditory reliability is low (Figure 2.9e: black square, triangle, diamond, and circle). This contrasted with the deviations from optimality observed in humans, in which subjects occasionally overweighted visual evidence when auditory reliability was high. Note that these observations do not mean that the rats ignored the visual

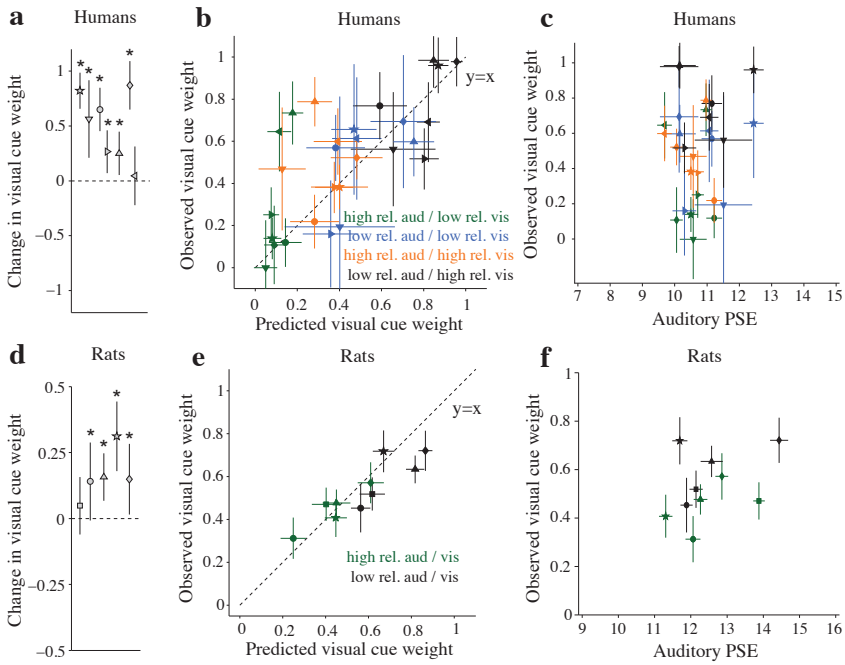

Figure 2.9: **Reliability-based sensory weighting is observed consistently across subjects.** Cue weights were estimated from data pooled over multiple behavioral sessions (humans/rats = 23,873/17,984 total multisensory trials). **a,** Data points indicate the change in observed cue weights observed in seven individual human subjects, computed as the differences in subjects' visual cue weights between high-reliability visual/low-reliability auditory and low-reliability visual/high-reliability auditory trials. Asterisk indicates significant change in visual cue weights ($p < 0.05$, within-subjects one-tailed Z-tests). **b,** Scatterplot compares observed visual cue weights (ordinate) to predicted values (abscissa) for all multisensory trial types in the individual human subjects. Legend indicates colors corresponding to each multisensory trial type. **c,** Comparison of the observed visual cue weights (ordinate) to the PSE for unisensory auditory trials (abscissa). Color conventions are the same as in b. **d,** Same as a but for five individual rats. **e,** Same as b but showing data for five rats. **f,** Same as c but for five rats. Error bars indicate 95% confidence intervals in all panels.

stimulus; when auditory reliability was low, rats generally relied more heavily on the visual stimulus than on the auditory stimulus (i.e., $w_V > 0.5$). The deviations from optimality here imply that the rats would have made better use of the available information had they relied even more heavily on the visual stimulus than observed.

It is unlikely that our changing cue weights were driven by unisensory biases. First,

unisensory biases have previously been shown to have very little effect on weights measured during multisensory trials (Fetsch et al., 2012). This is because although nonnegligible single sensory biases are assumed to systematically shift the PSE on multisensory trials in proportion to the relative reliabilities of either cue, such biases should shift the PSE in an identical manner on conflict trials and nonconflict trials. Therefore, our estimates of w_V and w_A, which are generated by taking the slope of the line relating PSE and cue conflict (Figure 2.8c), should not be affected by unisensory bias under the classic cue integration framework (Young et al., 1993). Nevertheless, we took two additional steps to guard against the possibility that our results were confounded by single sensory bias. The first step was to examine whether w_V (and by extension w_A) was related to unisensory bias. We found that for every multisensory trial type considered individually in both rats and humans, w_V was unrelated to the PSE measured from corresponding unisensory auditory trials (all p-values > 0.05, across-subject Pearson's correlations, Figure 2.9c,f). In other words, subjects who had a slight bias on auditory trials were just as likely as any other subject to demonstrate a particular cue weight. This was also true for the relationship between w_V and visual PSE (all p-values > 0.05). These observations are consistent with theoretical predictions and provide reassurance that discrepant biases on the two unisensory conditions had no systematic effects on cue weights. Our second step to guard against artifacts from unisensory bias was to recompute w_V for humans and rats after restricting the included data to behavioral sessions for which subjects' single-sensory PSEs were all equal within a tolerance of ± 2 events/second (i.e., less than the range of cue conflicts presented), and obtained nearly equivalent results in both species.

2.6 Discussion

In this chapter we report five main findings:

1. Subjects can combine multisensory information for decisions about an abstract quantity, event rate, which arrives sequentially over time;

2. Similar, near-optimal multisensory enhancement was observed in humans and rats. This suggests that the neural mechanisms underlying this multisensory enhancement are very general and are not restricted to a particular species;

3. Multisensory enhancement is present both when the sensory inputs presented to each modality were redundant and when they were generated independently. This finding is consistent with a model where event rates are estimated independently for each modality and then are fused into a single estimate at a later stage;

4. Most subjects based decisions on sensory evidence presented throughout the trial duration;

5. Dynamic weighting of sensory inputs extends to time-varying stimuli and is not restricted to primates.

Our results differ from previous observations about multisensory integration in a number of ways. First, our stimulus is unique in that the relevant information, event rate, is not available all at once but must be accumulated over time. Most prior studies of multisensory integration have not explicitly varied the incoming evidence with respect to time (Ernst et al., 2000; Ernst and Banks, 2002; Alais and Burr, 2004). Some previous studies have presented time-varying rates in a multisensory context (Recanzone, 2003), but have not, to our knowledge, asked whether subjects can exploit the multisensory information to improve performance. Second, we have shown multisensory enhancement in both humans and rodents. Most of the multisensory integration studies in animals have been performed with nonhuman primates (Avillac et al., 2007; Gu et al., 2008). There have been some studies of multisensory integration in rodents (Sakata et al., 2004; Hirokawa et al., 2008), but our study goes further than those in several ways. Previous studies did not establish animals' thresholds or PSEs. Our approach allowed us to determine the animals' psychophysical thresholds and PSEs and therefore compare changes on multisensory trials to a maximum-likelihood prediction. Further, previous studies in rodents also did not

compare human data alongside the animals, making it difficult to know whether the two species use similar strategies when combining multisensory information.

Our results are perhaps consistent with a different mechanism for multisensory integration than has been thus far observed physiologically. Recordings from the SC in anesthetized animals have made it clear that temporal synchrony (or near-synchrony) of individual stimulus events is a requirement for multisensory integration (Meredith et al., 1987). Because we observed multisensory integration in the absence of temporal synchrony, the circuitry in the SC probably does not underlie the improvement we observed. Instead, our observations point to mechanisms that estimate more abstract quantities, such as the average rate over a long time interval.

Critical features of the task we used may have invited modality-independent combination of evidence. First of all, auditory and visual events probably arrived in the brain with different latencies even on the synchronous condition (Pfingst and O'Connor, 1981; Maunsell and Gibson, 1992; Recanzone et al., 2000). More importantly, the stimulus rates were sufficiently high that connecting individual auditory and visual events was likely not feasible for most subjects. Previous research has shown that when auditory and visual events are embedded in periodic pulse trains, the detection of temporal synchrony falls to chance levels at only 4 Hz (Fujisaki and Nishida, 2005). A separate study found that discrimination thresholds for time interval judgments are approximately five times longer for multisensory stimuli than for auditory of visual stimuli alone (Burr et al., 2009).Together, those studies and ours suggest that the brain faces a major challenge when trying to associate specific auditory or visual events that are arriving quickly. A reasonable solution to this problem is to generate separate estimates for each modality and then combine them at a later stage, perhaps in an area outside of the SC that receives both auditory and visual inputs, such as the parietal cortex (Reep et al., 1994; Mazzoni et al., 1996). This type of strategy may not be necessary for stimuli that lack discrete events. It remains to be seen whether other continuously varying stimuli would likewise be integrated over time at an early stage and then combined later on (Fetsch et al., 2009).

We have argued that our subjects use data presented over the entire duration of the trial. Because we presented stimuli for a fixed duration (1000 ms), however, we make this conclusion with caution. The choice-triggered average we report suggests that subjects use information over long periods of time in the trial, but a reaction time paradigm is necessary to make this conclusion with complete confidence.

Although we conclude that rats and humans are both quite capable of multisensory integration, there are small differences in the behavior of the two species. Specifically, humans' decisions were influenced by stimuli at all times during the trial (Figure 2.6b), whereas rats' decisions were influenced mainly by the middle 650 ms (Figure 2.6c). The weak influence of stimuli at the very beginning of the trial is consistent with a "leaky integrator" that accumulates evidence but leaks it away according to a time constant that is shorter than the trial. An alternative explanation is that the rats had little time to prepare for the onset of the stimulus. The stimulus began as soon as the rats initiated a nose poke into the center port. The human subjects, by contrast, began each trial with a brief fixation period before the stimulus began, providing them with some preparation time. Accordingly, humans' decisions were clearly influenced by stimuli very early on in the trial. Several explanations are consistent with the weak influence of stimuli near the end of the trial. One possibility is that the rats accumulated evidence up to a threshold level or bound that was frequently reached before the end of the trial. If this were the case, stimuli arriving after the bound was reached would not influence the animals' decisions, leading to the pattern of results that we observed. A signature of this has been previously reported in monkeys (Kiani et al., 2008). A second possibility is that stimuli late in the trial did not influence the rats' choices because the rats used the last 200 ms of the trial to prepare the full-body movement that was required to report their decisions. Human observers, by contrast, made much smaller movements to report their decisions, so they might not have needed the additional movement preparation time. Further, human subjects almost never responded before the stimulus was over. Rodents' more frequent early responses were consistent with the possibility that they used part of the stimulus presentation time to plan a movement. Note that other aspects of the choice triggered average

were quite similar for the two species. For example, we observed a reliable difference in the magnitude of the choice-triggered average for single-sensory and multisensory trials. This suggests that multisensory stimuli exert more influence over the choice compared with single sensory stimuli, a conclusion that is in agreement with the overall improvements we observed on multisensory trials.

A final caveat is the observation that our subjects, particularly the rats, frequently showed multisensory enhancements that were larger than one would expect based on maximum-likelihood combination. Individual sessions with superoptimal enhancements have been observed previously in animals (Fetsch et al., 2009, 2012), so our observations are not without precedent. Nevertheless, the tendency toward supraoptimality is more prevalent and consistent in our dataset than in previous ones. The most likely explanation is that performance on single-sensory trials provides an imperfect estimate of a modality's reliability. The apparent supraoptimal cue combination likely indicates that, at least for a few subjects, we underestimated the reliability of the single-sensory stimulus. A possible explanation is that the animals had different levels of motivation on single-sensory versus multisensory trials. One reason for this might be as follows: the rats are, in general, very sensitive to overall reward rate. For example, we have observed improved overall performance on a given modality when we decrease the proportion of easy trials for that modality. This suggests that the animals may strive for a particular reward rate and adjust their motivation levels when they exceed or fall short of that rate. Because single-sensory trials yield lower average reward rates compared with multisensory trials, animals might have decreased motivation on those trials, particularly when they are interleaved with higher-reward rate multisensory trials. Although this explanation is a speculative one, we favor it over other possibilities, such as the possibility that there is an additive noise source: high-level decision noise, for example. Additive noise would indeed cause underestimates of the subjects' reliability on the single-sensory condition; however, it has been previously demonstrated to have only a very small effect on the relationship between the measured and predicted behavior on the multisensory condition (Knill and Saunders, 2003). Indeed, if high-level decision noise were present and constant

across single-sensory and multisensory trials (Hillis et al., 2004), it would result in an overestimate of multisensory improvement, whereas we observed multisensory improvements greater in magnitude than predicted by the maximum-likelihood model.

Our behavioral evidence argues for the existence of neural circuits that make it possible to flexibly fuse information across time and sensory modalities. Our observations suggest that this kind of multisensory integration may use different circuitry compared with the synchrony-dependent mechanisms that have been reported previously. The existence of many mechanisms for multisensory integration likely reflects the fact that multisensory stimuli in the world probably activate neural circuits on a variety of timescales. As a result, many different mechanisms, each of them suited to the particular constraints of a class of stimuli, may operate in parallel in the brain.

Extending dynamic weighting to rodents indicates that the ability to estimate stimulus reliability for dynamic stimuli is conserved across diverse species in the mammalian lineage. Although previous behavioral studies on multisensory integration have been conducted in rats (Sakata et al., 2004; Hirokawa et al., 2008, 2011), they have not systematically varied stimulus reliability in a way that made it possible to estimate perceptual weights. The dynamic weighting we observed in rats suggests that the ability to estimate reliability and use such estimates to guide decisions likely relies on neural mechanisms common across many species. Further, by establishing dynamic weighting for rodents, we open the possibility of using this species to examine the underlying neural circuits that drive this behavior.

The ease with which rats dynamically reweighed inputs, even when reliability levels changed unpredictably from trial to trial, suggests that rodents, like primates, possess flexible neural circuits that are designed to exploit all incoming sensory information regardless of its modality. What neural mechanisms might underlie this ability to flexibly adjust perceptual weights? Although a wealth of multisensory experiments have been carried out in anesthetized animals (Jiang et al., 2001; Meredith et al., 1987; Stanford et al., 2005), many fewer have been carried out in behaving animals; as a result, much about the underlying neural mechanisms for optimal integration remain unknown. Here, our subjects reweighed sensory inputs even when the

relative reliabilities varied from trial to trial, suggesting that the dynamic weighting could not have resulted from long-term changes in synaptic strengths (for instance, between primary sensory areas and downstream targets). The required timescales of such mechanisms are far too long to explain dynamic weighting. One possibility is that populations of cortical neurons automatically encode stimulus reliability due to the firing rate statistics of cortical neurons. Assuming Poisson-like firing statistics, neural populations naturally reflect probability distributions (Salinas and Abbott, 1994; Sanger, 1996). Unreliable stimuli may generate population responses with reduced gain and increased variability at the population level (Beck et al., 2008; Deneve et al., 2001; Ma et al., 2006). Such models of probabilistic population coding offer an explanation for how dynamic cue weighting might be automatically implemented as a circuit mechanism without changes in synaptic strengths. A plausible circuit implementation of such a coding scheme has been recently described in the context of multisensory integration (Ohshiro et al., 2011); this model allows for random connectivity among populations of sensory neurons and achieves sensitivity to stimulus reliability using well-established mechanisms of divisive normalization (Sclar and Freeman, 1982; Heeger, 1993; Carandini et al., 1997).

A competing explanation for multisensory enhancement is that it arises from synchronous activity between areas responsive to each individual sensory modality (for review, see Senkowski et al., 2008). Indeed, classic work in the superior colliculus suggests that precise timing of sensory inputs is crucial for multisensory enhancement of neural responses (Meredith et al., 1987), and psychophysical effects can likewise require precise timing of the relevant inputs (Lovelace et al., 2003; Shams et al., 2002). By contrast, multisensory improvements on our task do not require synchronous auditory and visual stimuli. Our subjects' ability to combine independent streams of stochastic auditory and visual information bearing on a single perceptual judgment is testament to the flexibility of multisensory machinery in the mammalian brain.

3

A category-free neural population supports evolving demands during decision-making

Individual neurons are often seen as members of highly specialized categories, with response properties making them suitable for particular classes of computations (Barlow, 1953; Kuffler, 1953). This view has been fruitful for understanding early sensory areas, where single neurons can be strongly tuned for task parameters, such as direction of motion (Britten et al., 1996) or disparity (Nienborg and Cumming, 2006).

The assumption of neural categories is reflected in many experimental designs and analysis methods, even those focusing on neural structures far downstream of early sensory areas. This assumption can be evident in the way neurons are sampled: sometimes, neurons must meet certain response criteria to be included for study, such as responsiveness to certain stimuli or activity during a delay period (Roitman and Shadlen, 2002; Balan et al., 2008; Georgopoulos et al., 1982; Churchland et al., 2008). Implicit in this approach is the idea that the cell's response during one stimulus identifies it as a member of the category being examined. The assumption of categories can also be evident during analysis: pie charts, a common way of summarizing population data (Arimura et al., 2013; Viswanathan and Nieder, 2013; Roth et al., 2012), explicitly assign neurons to categories. Another way of summarizing a population response, averaging over many neurons, likewise reflects the assumption that each

neuron is an exemplar of a category, different from other category members mainly because of noise.

An alternative hypothesis is that neurons reflect random combinations of parameters, leading to neural populations in which neurons' responses defy categorization. Theoretical work suggests a major advantage for category-free populations: when parameters are distributed randomly across neurons, an arbitrary group of them can be linearly combined to estimate the parameter needed at a given moment (Ganguli and Sompolinsky, 2012; Salinas, 2004; Pouget and Sejnowski, 1997). This obviates the need for precisely prepatterned connections between neurons and their downstream targets and also means that all information is transmitted. This latter property could allow the same network to participate in multiple behaviors simply by using different readouts of the neurons. Experimental work has not tested directly whether neural populations are category free, but many observations are broadly consistent with this possibility. Specifically, recent studies have demonstrated that neurons in parietal (Rishel et al., 2013; Meister et al., 2013; Freedman and Assad, 2009; Park et al., 2014) and frontal (Rigotti et al., 2013; Mante et al., 2013) areas have mixed selectivity: individual neurons are modulated by multiple task parameters. Mixed selectivity would be expected if neurons reflect random mixtures of parameters, but it also might exist under other assumptions. Other experimental work has probed for the existence of neural categories defined by the timing of a neuron's response (Harvey et al., 2012). That work argued against categories, but it tested only for categories defined by response sequence. A more general test is thus required. Further, because neurons in that study responded sparsely, it was not possible to test whether the same neurons participated statically or dynamically in the network as the behavioral demands evolved from decision to movement.

Here, we developed a multisensory decision task rich enough to expose the functional organization of a neural population, both at a single moment and over the course of a complex choice with evolving behavioral demands. Our data suggest that in the PPC, the population is category free: response features are randomly distributed across neurons. A possible explanation for this configuration is that it

confers flexibility, allowing the brain to use the same neurons in different ways, depending on the needs of the animal. In keeping with this explanation, we found that the population can be decoded instantaneously to estimate multiple task parameters and that the population activity explored different dimensions as the animal's needs evolved from decision formation to movement.

3.1 PPC inactivation reduces visual performance

We trained a new cohort of rats on the rate discrimination task described in Section 2.1. As before, animals reported a judgment about a 1-second series of auditory clicks and/or full-field visual flashes. In this chapter we refer to this 1-second period as "decision formation" because we have demonstrated that stimuli throughout this period influence the animals' decisions (see Section 2.4; Raposo et al., 2012; Sheppard et al., 2013). Once the stimulus terminated, animals reported whether the event rate of the stimulus was above or below an experimenter-imposed category boundary. They reported decisions via movement to one of two choice ports. Rats were mostly stationary during stimulus presentation and did not typically move toward or away from the direction of the port they ultimately chose (Figure 3.1b,c). Rats mastered the ability to categorize the stimulus and report the decision regardless of whether stimuli were unisensory (visual-only or auditory-only) or multisensory. As in other studies (Angelaki et al., 2009), when auditory and visual stimuli were presented together (multisensory trials), performance was enhanced (Figure 3.1a).

We first evaluated whether PPC inactivation affected decisions in any of the modalities tested. Even if the area is not causally involved in every modality, having multiple task parameters that modulate neurons can greatly aid our understanding: it allows a broad search for categories that could be defined by a number of features. In addition, modulation from a second, noncausal modality could still be of interest to the animal, since these inputs might be required for behaviors beyond those studied here.

We suppressed spiking activity of PPC neurons using two complementary strate-

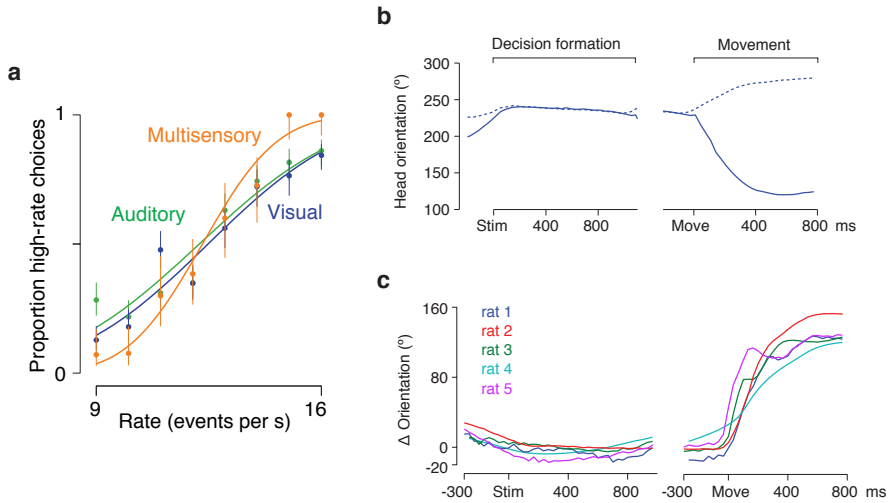

Figure 3.1: **Rats' behavior in the rate discrimination task. a,** Example behavioral data (818 trials; 1 session) from a single animal (rat 4). Smooth lines are cumulative Gaussian fits. Error bars reflect the Wilson binomial confidence interval. **b,** Head angle measured during a single session. Dashed: trials that ended in a high-rate choice; solid: trials that ended in a low-rate choice. Dashed/solid traces are largely overlapping during decision formation (while animals are still) but diverge during the time animals report their choices. **c,** Difference in head or body angle for trials ending in right vs. left choices (i.e., dashed minus solid traces in b). Each trace reflects the average of multiple sessions in which neurons were recorded: Stim, stimulus onset; Move, withdrawal time from center port.

gies. First, we made double bilateral infusions of muscimol, a $GABA_A$ agonist, into PPC (2 rats). We compared performance for inactivation versus control days and observed shallower psychometric functions (more errors) on inactivation days (Figure 3.2a, $\sigma_{saline} = 2.640.39$; $\sigma_{muscimol} = 4.670.67$; standard errors computed by bootstrapping, see Methods). This example was typical: PPC inactivation reliably impaired visual decisions (Figure 3.2b, middle; Mann-Whitney U test; $p < 0.001$, pooled across animals). Animals retained some ability to make visual judgments despite the inactivation, suggesting either that inactivation was incomplete or that structures in addition to PPC support the task, consistent with other studies of parietal inactivation (Balan and Gottlieb, 2009; Li et al., 1999).

Impairment was specific to visual trials and had no consistent effect on auditory

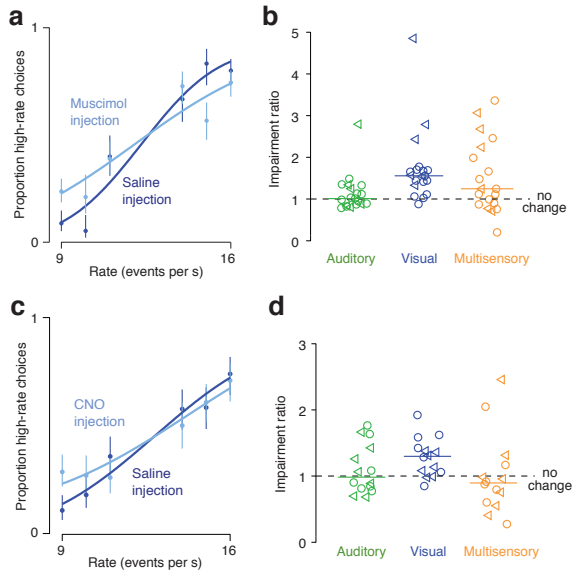

Figure 3.2: **Effect of PPC inactivation during audio-visual decisions. a,b,** Effects of muscimol inactivation. **a,** Example psychometric functions for 1 animal (visual trials only). Dark blue, a single session following saline injection; light blue, a single session the next day following muscimol injection. **b,** Effects of inactivation on performance for auditory (green), visual (blue) and multisensory (orange) trials. Ordinate, impairment ratio: the ratio of values for σ parameter from cumulative Gaussian fit to the data (see Methods). A value of 1 indicates no effect; values > 1 indicate performance was worse on a single inactivation session (muscimol) relative to the previous control session (saline). Symbols, individual animals ($N = 2$); horizontal lines, median across animals and sessions. **c,d,** Same as a,b, but for separate inactivation experiments implemented with DREADD ($N = 2$). CNO, clozapine N-oxide.

decisions (Figure 3.2b, left; $p = 0.41$, pooled across animals). The sparing of auditory decisions reveals that inactivation did not reduce the animal's motivation or introduce confusion about the stimulus-response contingency. Further, we observed sparing of the multisensory enhancement, the improved sensitivity for multisensory relative to unisensory decisions (Figure 3.2b, right). This spared enhancement implies that PPC likely does not drive multisensory enhancement and leaves open the possibility that PPC may process visual inputs before they are integrated with other modalities. Under this scenario, we would predict only a small change in multisensory performance

even when visual inputs are impaired. This is because multisensory mechanisms can still use the remaining, weak visual signal to improve their estimation alongside the spared auditory signal. The framework for multisensory integration therefore predicts a very minor change in enhancement during inactivation of one modality, even if that modality is clearly impaired.

One possible explanation for impaired visual decision-making is that the muscimol might have spread to portions of neighboring visual areas, posterior to PPC. This seems unlikely to have driven the effect because the retinotopic organization of visual areas means that restricted spread of muscimol would only have affected a portion of the visual field. Since our stimulus was full field, the unaffected parts of the visual field could likely have supported the behavior (Glickfeld et al., 2013). Nevertheless, we wished to determine the spread of the inactivation.

To achieve this, we used a second inactivation strategy: DREADD (designer receptor exclusively activated by designer drug), a pharmacogenetic inactivation method that permits visualization of the agent to determine its spread (Rogan and Roth, 2011). These effects were similar to the effects of muscimol inactivation in a second set of 2 rats: impairment of visual decisions (Figure 3.2c, $\sigma_{saline} = 3.890.64$; $\sigma_{CNO} = 5.290.71$) and sparing of auditory decisions and multisensory integration (Figure 3.2d; visual trials impaired: $p = 0.011$; auditory trials spared: $p = 0.91$, pooled across animals). Histological examination (Figure 3.3a–e) revealed that DREADD expression was minimal beyond the posterior border of PPC, defined as 5.0 mm posterior to bregma (Reep et al., 1994). For one rat, expression was less than 0.12% of maximal expression; for the second rat, expression was 20.3% of maximal expression (Figure 3.3a-e; see Methods). The more posterior expression was apparently not the source of the impairment because the rat with more expression posterior to PPC had weaker visual impairment compared to the other rat. We did not detect DREADD expression in other areas. Overall, results were similar for all animals with both muscimol and DREADD inactivation. Effects were individually significant in 3 of 4 cases for visual trials and 0 of 4 cases for auditory trials.

Impairments on visual decision making might be driven by a change in the reliabil-

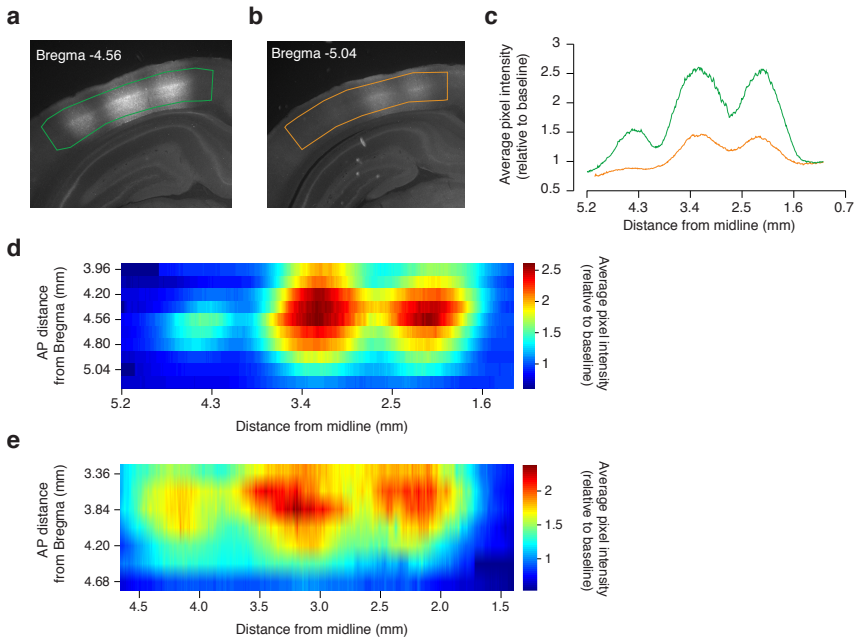

Figure 3.3: **DREADDs expression and hystology. a,** Histological section showing DREADD expression in the PPC of one rat and the region that was manually selected for quantification of expression (ROI, green contour). **b,** Same as a but for brain section closer to the border between PPC and secondary visual cortex. **c,** Quantification of expression levels in PPC (green trace) and near the border of PPC (orange trace; see Methods). DREADD expression near the border of PPC was weak or absent. **d,** Quantification of DREADD expression levels (see Methods). Heat map of average pixel intensity across columns of pixels for 7 brain sections, spanning 3.36 to 4.68 mm posterior to Bregma. Sections' anterior-posterior locations were estimated using the Paxinos brain atlas. **e,** Same as in d, but for second rat injected with DREADD.

ity of incoming visual signals or by a change in the animal's decision-making strategy. Changes in decision-making strategy could include making 'snap judgments' that relied only on evidence presented at the beginning of the trial or 'leaking' evidence causing decisions to be made using only evidence presented late in the trial. To distinguish changes in stimulus reliability from changes in strategy, we performed an analysis of animals' decisions that took advantage of the ongoing fluctuations in visual and auditory rates that occur throughout the 1-second decision formation period (see

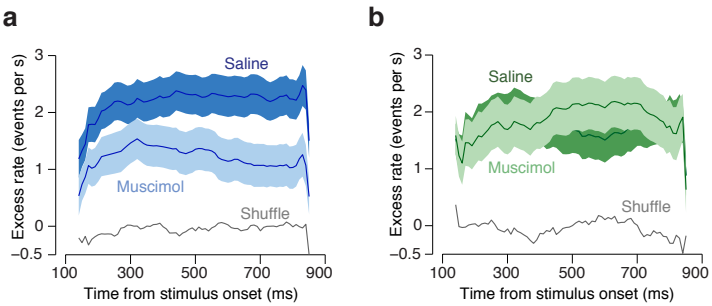

Figure 3.4: **Effect of PPC inactivation on use of evidence. a,** Excess rate is higher for a single rat on visual trials in saline (dark blue) than in muscimol (light blue) sessions. Values on abscissa, centers of sliding windows; shaded regions, confidence bounds (mean ± s.e.m.). **b,** Excess rate for the same rat on auditory trials with saline (dark green) and muscimol (light green).

Methods and Section 2.4; Brunton et al., 2013). This analysis revealed no evidence of snap judgments or evidence leak. Instead, the analysis indicates that inactivation reduced the signal-to-noise of incoming evidence (Figure 3.4a). No effects were observed on auditory trials (Figure 3.4b). The reduced excess rate on visual trials and unchanged excess rate on auditory trials also confirms the outcome of the previous analysis using a model-free approach that does not rely on fitted parameters.

The reduced excess rate over the entire course of visual trials suggests that inactivation reduced the reliability or signal-to-noise of visual signals. Behavioral experiments in which we reduced the brightness of visual flashes affected psychometric functions and excess rate nearly identically to these inactivations (Sheppard et al., 2013). Taken together, our inactivation experiments and analyses suggest that PPC is required for accurate visual decision-making, perhaps by converting incoming visual signals into evidence for a decision. These observations point to PPC as causal for visual decision-making, laying the foundation for subsequent recording experiments that probe the functional organization and dynamics of cortical networks within PPC.

3.2 Choice and modality both modulate neural responses

To evaluate whether PPC neurons demonstrate mixed selectivity, we recorded from single, well-isolated neurons in the left PPC of five trained rats. Trials were grouped by modality and by the animal's choice. Rare neurons had pure choice selectivity (Figure 3.5a) or pure modality selectivity (Figure 3.5b). However, most neurons mixed information about modality and choice (Figure 3.5c,d). For such neurons, the mixing sometimes resulted in identical firing rates for different conditions (Figure 3.5c).

We assessed the effect of the animal's choice on neural responses during decision formation. We used ROC analysis to generate an index of choice divergence that measures how strongly a neuron's firing rate for a correct leftward response diverges from the firing rate for a correct rightward response (Figure 3.5a). The divergence could be driven by a number of factors, including accumulation of evidence for a decision, a developing motor plan, or a sensory preference for a particular stimulus frequency. Choice divergence became positive about 200 ms after stimulus onset and continued to grow over the course of the decision (Figure 3.5e). Choice divergence here was computed using 'easy' unisensory trials (stimulus rates > 2 events/s from the category boundary) and was similar for auditory and visual stimuli (Figure 3.5e; for multisensory, see Figure 3.6a). Stronger choice divergence was evident on multisensory trials at many points during the trial (Figure 3.6b,c); stronger choice divergence was also evident on easy versus more difficult trials (Figure 3.6d–f).

Responses on multisensory trials were usually well predicted by a linear combination of auditory and visual responses. Simple linear regression revealed that 80.1% of neurons (218 of 272 units) had a multisensory response that was better predicted by the auditory and visual responses than by the multisensory mean (assessed on left-out data). Across all neurons, a linear combination of visual and auditory responses accounted for a median 68.2% of the multisensory variance.

An additional index, choice preference, captured not only the magnitude of the

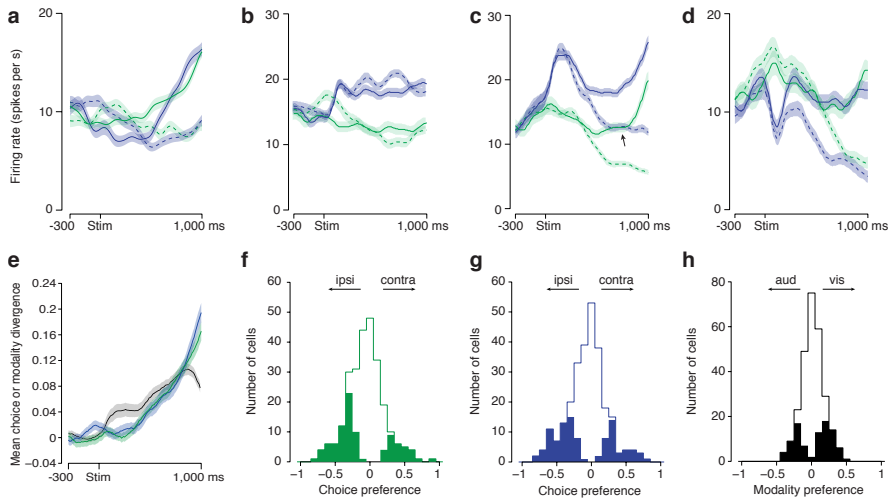

Figure 3.5: **PPC neurons show mixed selectivity for choice and modality.** Plots display visual and auditory trials (blue and green, respectively). **a–d,** Peristimulus time histograms for four single neurons. Mean spike counts were computed in 10-ms time windows smoothed with a Gaussian ($\sigma = 50$ ms). Error trials were excluded. Trials grouped by stimulus rate. Solid line, low-rate stimulus; dashed line, high-rate stimulus. Auditory trials, green; visual trials, blue. Shaded fills, s.e.m. Responses aligned to the time the visual or auditory stimulus began (Stim). **a,** A neuron reflecting mainly categorical choice (392 trials). **b,** A neuron reflecting mainly stimulus modality (414 trials). **c,** A neuron mixing categorical choice and modality (586 trials). Arrow highlights ambiguous moment in which high-rate visual and low-rate auditory stimuli gave rise to the same firing rate. **d,** A neuron mixing categorical choice and modality and displaying complex temporal dynamics (440 trials). **e,** Choice divergence (see Methods) for auditory trials (green; average of 262 neurons) and visual trials (blue; average of 268 neurons), and modality divergence (black; average of 266 neurons). Shaded fills, s.e.m. (bootstrap). **f,** Histogram of choice preference for auditory trials, measured 200 ms before decision end. Filled bars indicate neurons for which index was significantly different from 0 ($p < 0.01$, 1000 bootstraps). **g,** Same as f but for visual trials. **h,** Same as f,g, but for modality.

choice divergence but also whether it was in favor of a high-rate or low-rate choice (see Methods). Choice preference was significant 200 ms before movement in over a third of individual neurons for both auditory and visual trials (Figure 3.5f,g; 35.5% and 37.3% of neurons were significant on auditory and visual trials, respectively; for multisensory, see Figure 3.6g). Strong choice preferences for both ipsi- and contralateral decisions were observed. For both auditory and visual decisions, a slight majority of

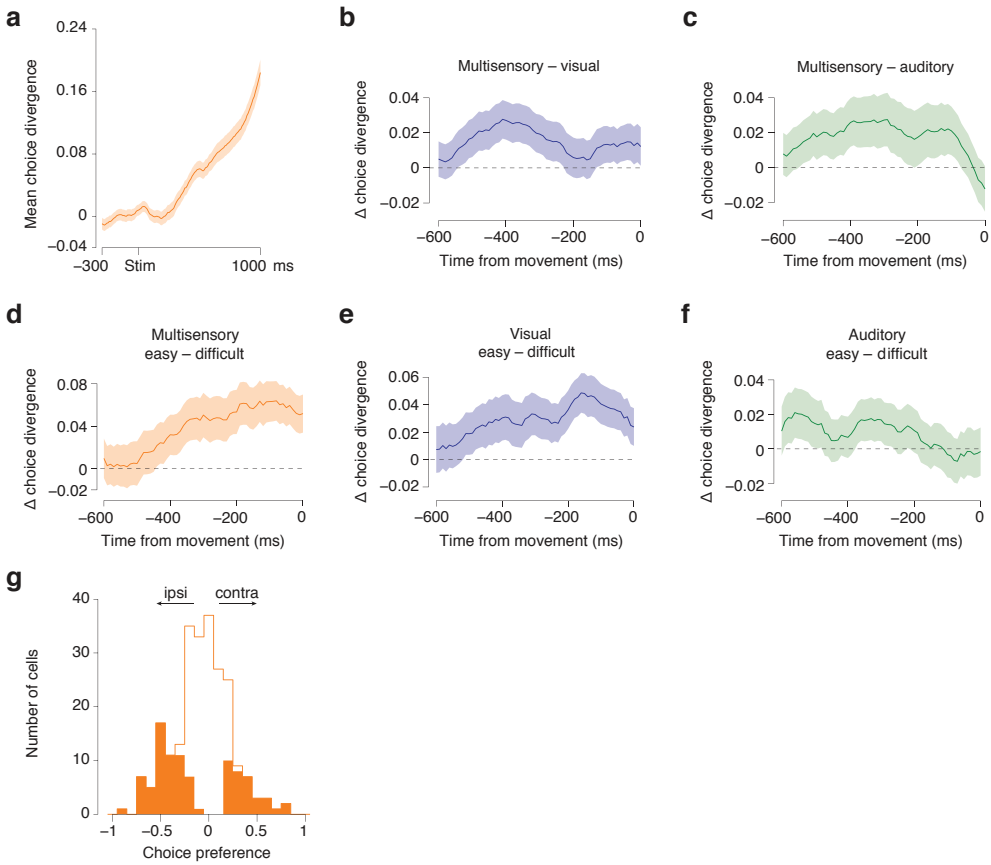

Figure 3.6: **Choice preference/divergence are stronger on multisensory trials and easy unisensory trials. a,** Magnitude and time course of choice divergence for multisensory trials was similar to that seen in auditory/visual trials (Figure 3.5e). **b,** Choice divergence was stronger on multisensory trials than unisensory. Abscissa: time relative to the rat's movement to report the decision. Ordinate: the difference in choice divergence for multisensory versus visual trials. Values > 0 indicate stronger divergence on multisensory trials. **c,** Same as b but comparing multisensory with auditory trials. **d–f**, Choice divergence was significantly stronger on easy trials (rates > 2 events/s from the category boundary) compared to difficult trials (rates that were 1 or 2 events/s from the category boundary). **g,** Histogram of choice preference for multisensory trials, measured 200 ms before decision end. 39.8% of neurons (of 236 total) had significantly nonzero choice preference.

neurons fired more in advance of ipsilateral as compared to contralateral choices (two-sided sign test; auditory, median choice preference $= -0.061$, $p = 0.0011$, $N = 262$

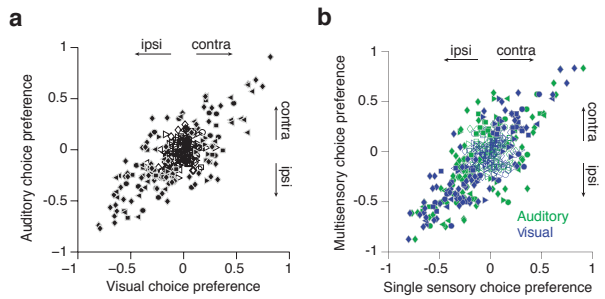

Figure 3.7: **Choice preference is strongly correlated between auditory, visual and multisensory trials. a,** Auditory choice preference was strongly correlated with visual choice preference, $N = 262$ neurons, $r = 0.74$, $p < 10^{-4}$). Shading indicates significance. **b,** Multisensory choice preference was strongly correlated with both auditory choice preference (green symbols; $N = 236$ neurons, $r = 0.668$, $p < 0.001$) and visual choice preference (blue symbols; $N = 236$ neurons, $r = 0.807$, $p < 0.001$). Shading indicates significance.

neurons; visual, median choice preference $= -0.038$, $p = 0.0502$, $N = 268$ neurons). Choice preferences computed during visual and auditory trials were strongly correlated (Figure 3.7a, $N = 262$ neurons, $r = 0.74$, $p < 10^4$); preferences during each unimodal stimulus were also correlated with preference during multisensory stimuli (Figure 3.7b, $N = 236$ neurons; auditory, $r = 0.668$, $p < 0.001$; visual, $r = 0.807$, $p < 0.001$).

We next assessed the effect of stimulus modality on responses during decision formation. "Modality divergence" measured how strongly a neuron's responses diverged for auditory versus visual trials (for example, Figure 3.5b). Compared to choice divergence, modality divergence increased earlier and faster during the stimulus presentation but was weaker overall (Figure 3.5e). "Modality preference" captured not only the magnitude of the modality divergence but also whether it was in favor of visual versus auditory stimuli. A third of the neurons (33.8%) had significant modality preference (Figure 3.5h). Visual-preferring and auditory-preferring neurons were observed in nearly equal numbers (Figure 3.5h; median modality preference was 0.017 and did not differ significantly from 0; $p = 0.088$; $N = 269$ neurons). For both choice and modality, similar results were achieved when we assessed selectivity using

a rate-based rather than ROC-based analysis (data not shown).

3.3 PPC is category-free

The data thus far indicate that many individual neurons are strongly modulated by modality or choice. We next investigated how frequently individual neurons had mixed selectivity for modality and choice. If mixed selectivity is common, many neurons should have a nonzero choice preference and a nonzero modality preference. This is exactly what we observed (Figure 3.8a). Neural responses were not restricted to pure selectivity. Instead, most neurons had mixed selectivity for modality and choice. Moreover, a major component of the mixed selectivity was linear: that is, when predicting the neuron's response to a given choice and modality (for example, a high-rate choice for visual stimuli), linear sensitivity to each task parameter alone was more important than a nonlinear interaction between parameters (data not shown). The nonlinear component we observed in PPC was smaller and more variable than for neurons in the prefrontal cortex (Rigotti et al., 2013), perhaps suggesting that nonlinear mixed selectivity emerges gradually across cortical areas or depends on the nature of the task.

The existence of individual cells with mixed selectivity would be expected under two scenarios: response features might be randomly distributed across PPC neurons, or particular response features might cluster together, defining categories of neurons that are specialized for particular computations. The data (Figure 3.8a) hint that choice and modality selectivity are randomly distributed across neurons. For example, choice and modality preferences were uncorrelated ($N = 268$ neurons, $r = 0.074$, $p = 0.23$). This is in keeping with studies from monkey PPC in which selectivity for spatial versus category parameters were likewise unrelated (Rishel et al., 2013).

However, lack of correlation does not conclusively rule out the existence of functional categories: selectivity for task features could still define categories. This could be the case if, for instance, the points in Figure 3.8a formed an "X" or formed clusters that were symmetrically arranged around the origin. We therefore wished to

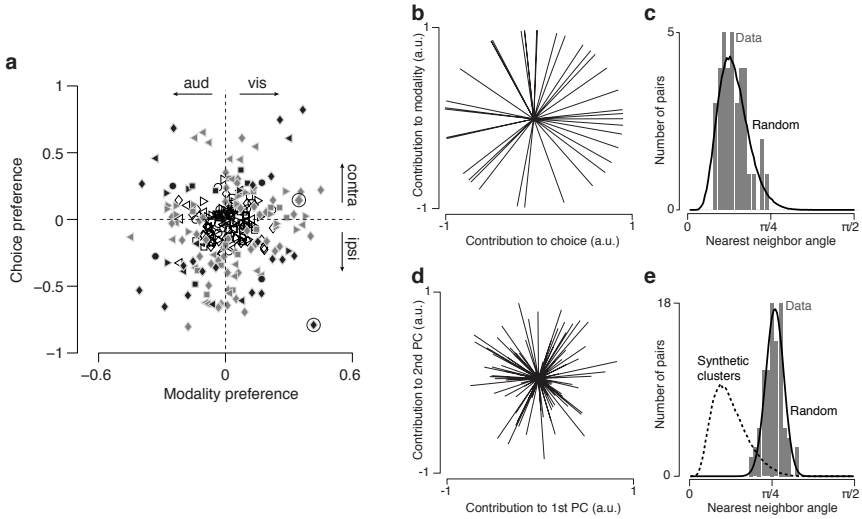

Figure 3.8: **Neural responses defy categorization.** **a,** Choice and modality preferences are unrelated. Each point shows values for a single neuron. Abscissa, average modality preference for high- and low-rate trials; ordinate, choice preference for visual trials. A nearly identical outcome was achieved when choice preference was computed from auditory trials (data not shown). Shading indicates significance: open, neither choice nor modality preference was significant; gray, choice or modality preference was significant; black, choice and modality preference were significant. Top circled point shows modality-selective neuron in Figure 2b; bottom circled point shows mixed-selectivity neuron in Figure 3.5c. Dashed lines define a region along which neurons would tend to cluster if they had pure selectivity for choice or modality. **b,** Low-dimensional summaries of neurons' responses. Each line is a feature vector showing the degree to which each neuron contributes to choice and modality; a.u., arbitrary units. **c,** Neurons are rarely more similar to one another than expected by chance. Histogram shows the distribution of angles between each neuron and its nearest neighbors ($N = 45$ neurons, rat 5). Black line, distribution of nearest-neighbor angles for random two-dimensional vectors. **d,** Low-dimensional summaries of neurons' responses. Responses are shown projected into two dimensions of eight used total. Each vector shows the contribution of one neuron to the two dimensions. The apparently random distribution of vectors suggests that neurons do not tend to cluster. **e,** Neurons are rarely more similar to one another than expected by chance. Histogram shows the distribution of angles between each neuron and its nearest neighbors ($N = 77$ neurons; rat 1). Solid line, distribution of nearest-neighbor angles for random eight-dimensional vectors; dashed, left-shifted distribution of nearest-neighbor angles obtained when 'synthetic clusters' are introduced (see Methods).

test whether neurons formed categories (broadly construed) or whether, instead, tuning for one feature was independent of tuning for others. To do so, we examined each neuron's "feature vector" the pair of values describing how strongly the neuron contributed to decoding choice and modality (see Section 3.4 and Figure 3.8b). Each neuron's feature vector was compared with its nearest neighbors in this feature space. If some neural responses fell into categories, these neurons would tend to have closer neighbors in feature space than if there were not categories (Indyk and Motwani, 1998). The distribution of nearest-neighbor angles for the population can thus distinguish the presence or absence of such neural categories. We used these nearest-neighbor angles to compute a statistic indicating whether the population had an excess of small nearest-neighbor angles. We term this statistic "PAIRS": projection angle index of response similarity (see Methods).

The PAIRS test did not indicate categories (Figure 3.8c). The distributions of nearest-neighbor angles were statistically indistinguishable from a control distribution generated by randomly oriented two-dimensional vectors (for rat 5, PAIRS index $= -0.052$; $p = 0.632$). No evidence for clear categories was present in any animal (PAIRS indices for rats 14: -0.135, 0.117, -0.080, -0.142; p-values from Monte Carlo simulations: 0.236, 0.253, 0.399, 0.004; the one significant p-value indicated less clustering than expected by chance). This observation is critical: it argues that neurons with pure selectivity (for example, Figure 3.5a,b) are exceptions and occur about as often as would be expected by chance.

This analysis argues that choice and modality selectivity do not define categories. However, this leaves open the possibility that there are categories defined by other features of the data. More generally, a category might be defined by a shared pattern of firing rates across conditions and time. To test for this, we used principal component analysis to identify a set of neural response features that were not imposed by us. This version of the test is thus quite general because it captures whatever features of the responses were strongest and is sensitive to numerous such features (Figure 3.9). The PAIRS test again pointed to a category-free population (Figure 3.8d,e). The overall lack of categories was not simply because neural variability caused our analysis to

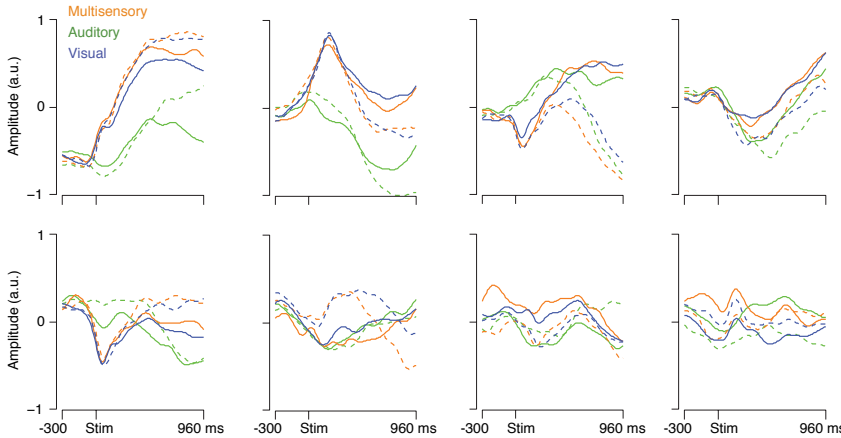

Figure 3.9: **Time-varying firing rate patterns across neurons.** The eight principal components used in the PAIRS analysis. These were generated from the population data ($N = 94$ neurons) from one animal (Rat 4). Colors indicate modality; dashed lines: data from high rate trials; solid lines: data from low rate trials.

miss structure: when we introduced synthetic categories into the population with noise derived from the real neural data, a strikingly different PAIRS distribution was evident (Figure 3.8e; see Methods). Relatively close neuron pairs were occasionally observed, but these differed from chance in only 1 of 5 cases (PAIRS index for rats 15: -0.011, 0.108, -0.038, 0.011, -0.007; p-values from Monte Carlo simulations: 0.621, 0.001, 0.209, 0.491, 0.857). These deviations from the random distribution indicate that a small fraction of neurons do have pairs in feature space. However, such neurons are rare; most neurons reflect a unique combination of response features. Most individual neurons participate in random combinations of response patterns: that is, they randomly mix task parameters and temporal response features.

3.4 Decoding choice and modality from a mixed population

Here we evaluate whether the mixed selectivity of PPC neurons poses any problem for decoding the key task variables. We first tested whether the animal's choice could be

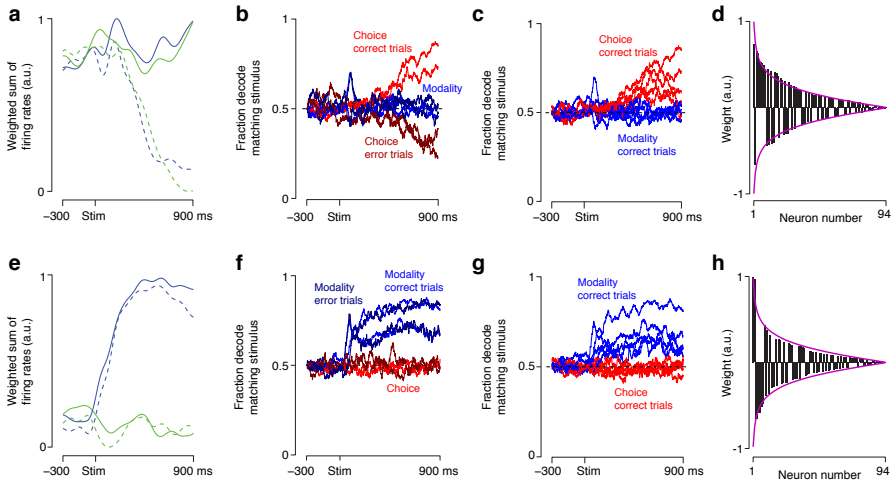

Figure 3.10: **Choice and modality can be decoded from population activity. a,** Weighted sums of neural responses; weights were chosen by the classifier. Blue, visual; green, auditory; dashed lines, high-rate trials; solid lines, low-rate trials. Data from rat 4, $N = 94$ neurons. **b,** The choice decoder could correctly classify responses as left versus right on trials where the rat was successful (bright red traces, one per rat), but is at chance for auditory versus visual (blue traces). On trials where the rat chose the incorrect port, the decoding tracked the rats choice (brown traces). Traces reflect the average of 1000 classifications. **c,** Same as b for all five rats, correct trials only. Each animal has one trace for modality and one for choice. **d,** Bars, values of the weights used to generate the traces in a, ordered by magnitude. Purple lines, values of randomly generated 94-dimensional vectors ordered by magnitude. **e–h,** Same as a–d but for the modality decoder. The modality decoding was nearly identical whether the rats chose the correct or incorrect port (f, light versus dark blue).

decoded from the population response during decision formation. To achieve this, we used a machine learning classifier (support vector machine, SVM; Cortes and Vapnik, 1995; Rust and Dicarlo, 2010) as our decoder, trained with single-trial population responses for correct high-rate versus low-rate choices (see Methods). The decoder successfully identified neural weights so that a weighted sum of the neural population was strongly choice dependent but mostly modality independent (Figure 3.10a).

We trained the decoder using a portion of the stimulus epoch (500–700 ms after stimulus onset), then tested the decode over the entire epoch. Time windows outside the training window test the generality of the decoder and probe the consistency of the population response throughout decision formation. We first examined both

correct and incorrect choices for animals with sufficient error trials (2 rats). For both rats (Figure 3.10b), PPC activity tracked the animal's choice. As expected, decoder performance grew over the course of the trial. For all 5 rats (Figure 3.10c), we examined correct-choice trials at the time point 700–800 ms after stimulus onset (outside the decoder's training epoch). Decoder performance was significantly better than chance for all animals tested (Figure 3.10c; decoding performances were 68.9%, 61.2%, 59.4%, 80.2%, 70.1%; 4 rats $p < 0.001$, rat 3 $p = 0.002$). The same decoder did not perform significantly better than chance when estimating stimulus modality (Figure 3.10c; performance of 48.0%, 51.0%, 54.3%, 48.8%, 48.6%, all rats $p > 0.2$). Our decoding of choice was not perfect, but this is unsurprising: decoding was performed on a sample of tens of neurons out of many thousands, on a task where the animal's performance is likely noise limited. Further, since the decoder indicated the opposite choice for error trials, this implies that correct choices could be distinguished from errors. Moreover, unlike in typical monkey experiments (Britten et al., 1996; Roitman and Shadlen, 2002; Churchland et al., 2008), the stimulus was not optimized for each neuron's preference and neurons were not selected on the basis of tuning properties.

The analysis above was restricted to auditory and visual trials. We next tested the ability of the same decoder, trained only on unisensory trials, to classify performance on multisensory trials. Decoder performance was significantly better than chance for all animals tested (Figure 3.11; all $p < 0.001$). This speaks to the generality of the decoder and also highlights that the network is used similarly during decision formation regardless of the modality.

One concern is that the choice decoder's success might have resulted from heavily weighting rare neurons with pure selectivity for choice (for example, Figure 3.5a). This was not the case. The neural weights were nonzero for all neurons, indicating that every member of the population contributed (Figure 3.10d). Importantly, the distribution of neural weights in the data did not differ from those that would be expected by chance if neurons reflected random weightings (Figure 3.10d; for rats 1–5, p-values for kurtosis were 0.696, 0.470, 0.134, 0.198, 0.430; see Methods). This is an independent indicator that neurons mix information about task parameters with

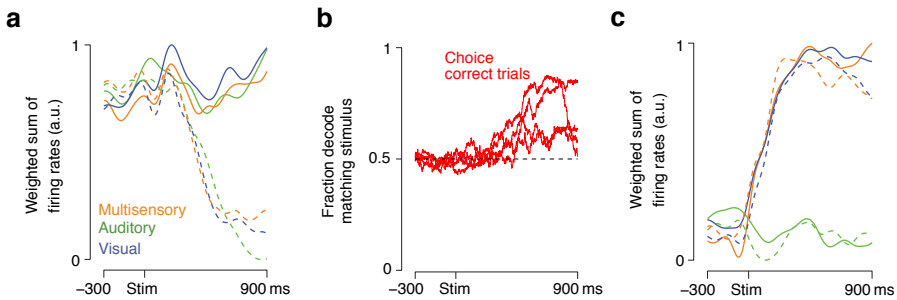

Figure 3.11: **Choice can be estimated on multisensory trials, even when the decoder is trained on data from unisensory trials. a,** Weighted sums of neural responses; weights were chosen by the classifier. Blue, visual; green, auditory; orange, multisensory; dashed lines: high-rate trials; solid lines: low-rate trials. Data from unisensory trials is the same as in Figure 4a. Data from Rat 4, $N = 94$ neurons. **b,** The choice decoder could correctly classify responses as left vs. right on multisensory trials where the rat was successful (bright red traces, one per rat). Decoder performance was significantly better than chance for all animals tested. Rat 5 was excluded from this analysis because of insufficient days on which multisensory trials were presented. **c,** Same as a but for the modality decoder.

random weights.

Having examined choice, we tested whether stimulus modality could also be decoded from the population response during decision formation. Again, we trained an SVM classifier with single-trial population responses, this time to distinguish auditory versus visual trials. The decoder successfully identified a weighted sum of neurons such that the population readout was strongly modality dependent but choice independent (Figure 3.10e). The decoder was able to estimate modality at a rate better than chance when testing generalization for all 5 animals tested (Figure 3.10g; decoding performances were 59.8%, 56.6%, 60.4%, 83.7%, 70.0%; p-values 0.010, 0.045, 0.002, < 0.001, < 0.001).

Modality was decoded nearly identically whether the animal's choice was correct or incorrect (Figure 3.10f); this is expected because errors do not reflect incorrect categorization of modality. As before, the accurate performance seen at the end of the trial was for time points outside the training window. The same decoder did not perform significantly better than chance when estimating choice (Figure 3.10g,

performance of 48.0%, 51.6%, 50.4%, 50.2%, 51.5%, all p-values > 0.5). Again, the decoder achieved this performance using all the neurons; the distribution of weights, as with choice, did not differ significantly from the random distribution (Figure 3.10h; for rats 1–5, all p-values > 0.4).

The ability of the same population of neurons to reliably and independently represent information about both choice and modality is a direct consequence of mixed selectivity: the joint modulation of neurons by choice and modality allows them to be combined in different ways to give rise to whatever estimate is needed. The above results have two implications. First, the fact that choice and modality can be decoded independently implies that these two representations are nearly orthogonal in the population. That is, presenting a high versus low rate stimulus evokes one pattern of activity across neurons, presenting a visual versus auditory stimulus evokes another (different) pattern of activity across neurons, and these two patterns are unrelated. More operationally, a decoder vector summarizes the pattern of activity (across the population) evoked in response to one stimulus versus another. Since choice and modality can be decoded independently, the patterns of activity for different parameters must be uncorrelated, as expected from Figure 3a. This can be verified directly: the average angle between the choice decoder and the modality decoder was 86.5°, only slightly less than a perfectly orthogonal 90°. Second, the consistent decoding performance over time implies that the choice representation remains in the same neural dimension (covariance pattern across neurons) in PPC over the course of decision formation, and the modality representation does the same.

3.5 The network explores different dimensions during decision and movement

Perhaps the neural state explores yet other dimensions (patterns of neural covariance) when the animal's brain needs to perform a substantially different function (Harvey et al., 2012). This could permit PPC to control what signals are routed to different areas at different times. As shown recently, exploiting additional dimensions can be

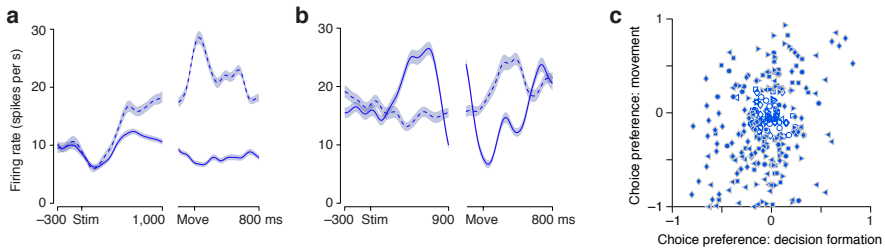

Figure 3.12: **Many PPC neurons switch preference between decision formation and movement. a,** Example neuron with a sustained preference for high-rate stimuli (dashed line) over low-rate ones (solid line). Responses were aligned to stimulus onset (left) and to movement onset (right). Alignment to these two events was necessary because the time between the stimulus end and the animal's movement varied slightly from trial to trial. Traces reflect averaged responses of all correct visual trials (and s.e.m.) computed as in Figure 3.5a–d. **b,** Example neuron that switched its preference over the course of the trial. **c,** Choice preference during decision formation (200 ms before decision end, abscissa) and movement (200 ms after animal leaves choice port, ordinate) frequently differed but were nonetheless correlated across all cells; $N = 268$ neurons, $r = 0.302$, $p < 0.001$; symbols, individual animals.

particularly useful to control when movement should be produced (Kaufman et al., 2014). We searched for a signature of the neural states either aligning (using the same dimensions at different times) or exploring different dimensions during different epochs. To do so, we compared two moments in the trial where the animal's behavior differed: during decision formation, when animals remain still to integrate sensory signals (Figure 3.1b) and during movement, when they rapidly reorient their bodies to harvest a reward. Examination of PSTHs (Figure 3.12a,b) shows that neural activity can differ substantially during decision formation and movement. For example, the neuron in Figure 3.12b has an elevated response during trials preceding a leftwards choice but is then suppressed during the leftwards movement used to report the choice. Such switching of preference from decision formation to movement was observed frequently (Figure 3.12c).

To quantify the alignment of state spaces during decision and movement, we developed an analysis that we term variance alignment (see Methods). The intuition behind this analysis is that if neurons' firing rates co-vary in similar ways during decision and movement, then the dimensions that best capture the variance for one

epoch will also capture much of the variance for the other epoch. The alternative is that the dimensions that account for much variance in one epoch will account for little variance in the other epoch: that is, that neurons will co-vary in completely different patterns from one epoch to the other. In this latter scenario, the neural state spaces for the two epochs can be described as misaligned.

We tested for alignment by computing an index that describes whether the dimensions that capture most of the variance during movement likewise capture the variance during decision formation. Crucially, this measure describes whether the neural state moves through the same dimensions (that is, maintains the same patterns of covariance), not whether the trajectories are similar within those dimensions. Four two-dimensional projections of decision epoch data are shown in Figure 3.13a–d. A projection onto the first two principal components is shown in Figure 3.13a. For comparison, we can view different two-dimensional projections of the exact same data, with the projection chosen based on the movement-epoch activity (Figure 3.13b), a random projection (Figure 3.13c), or the smallest two principal components (Figure 3.13d). The key element of these plots is the size of the ellipse representing the s.d.: if a space captures the decision-epoch variance well, then the s.d. should be nearly as large as in Figure 3.13a. Surprisingly, we found that dimensions that captured considerable variance during the movement captured the variance during decision formation far less well (Figure 3.13b), arguing against aligned state spaces for decision formation and movement. Indeed, the amount of alignment was slightly less than would be expected by chance (Figure 3.13e). This absence of alignment (index near zero) or even significant misalignment (index near -1) was present in all animals tested (rat 1, index $= -0.498$, $p = 0.0012$; rat 2, index $= -0.145$, $p = 0.51$; rat 3, index $= -0.559$, $p = 0.003$; rat 4, index $= -0.230$, $p = 0.27$; rat 5, index $= -0.219$, $p = 0.20$).

For comparison as a positive control, we repeated the variance alignment analysis on neural responses during decision formation, comparing two different stimulus conditions: visual and multisensory. This analysis, by contrast, revealed strong alignment (Figure 3.13f, index near 1 for rat 4; index $= 0.840$, $p < 10^{-4}$), present in all rats tested (indices were 0.644, 0.883 and 0.812 for rats 1, 2 and 3, $p < 10^{-4}$ in all

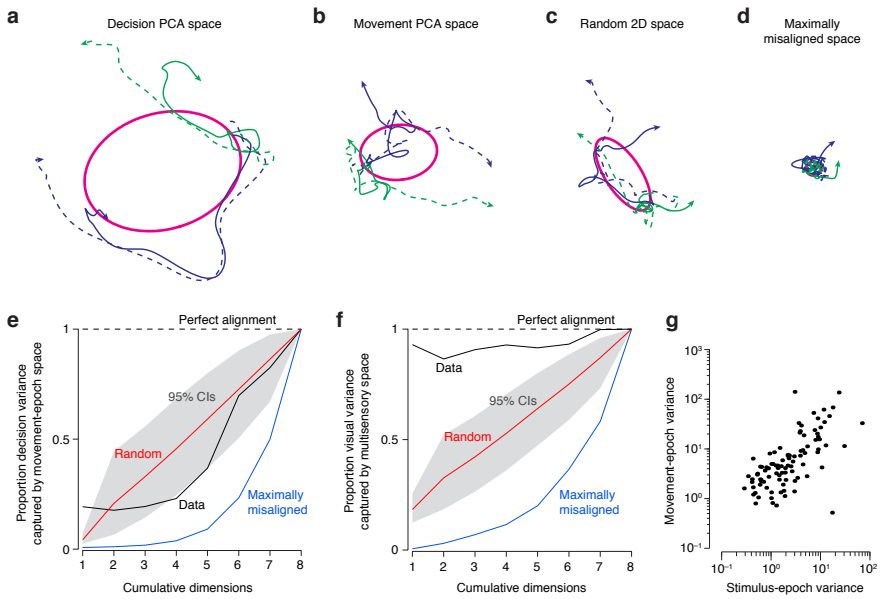

Figure 3.13: **PPC neurons exhibit different covariance patterns during decision formation and movement. a–d,** Two-dimensional projections of decision-epoch data (same data for all panels). Magenta ellipses indicate 1 s.d. of the data projected into the space specified by the panel's title. Color and line style same as in Figure 3.5. **a,** Space chosen as first two principal components (PCs) of decision-epoch data. **b,** Space chosen as first two PCs of movement-epoch data. **c,** Space chosen randomly from top 8 PCs. **d,** Space chosen as PCs 7 and 8 of decision-epoch data. **e,** Variance alignment analysis indicates that activity patterns across neurons differ substantially (and are not just, for example, scaled) for decision formation versus movement. Ordinate, decision variance captured in the dimensions used during movement, normalized by how much could maximally be captured in the same number of dimensions; abscissa, cumulative dimensions included. Black trace, data; other traces, alignment values expected under several scenarios for comparison (see labels). CI, confidence interval for the chance distribution. **f,** Same as h except that ordinate shows amount of decision variance for visual trials captured in the dimensions used on multisensory trials, normalized by how much could maximally be captured in the same number of dimensions. Note that, unlike in e, the black 'data' trace is close to 1, as expected. **g,** Strength of stimulus modulation for each neuron correlates with strength of movement modulation. Data from rat 4.

cases). This strong alignment indicates that the inherent noisiness of neural responses does not cause neural states to falsely appear misaligned and therefore provides reassurance that the misalignment of states during decision and movement indicates

a real difference in neural covariance. Thus, PPC employs highly similar patterns of population activity during visual and multisensory stimuli, but it explores quite different patterns of population activity during stimulus than during movement.

Finally, we asked whether the misalignment of stimulus and movement activity might be due to simply having different neurons active during these two epochs. This hypothesis predicts that neurons that are strongly modulated during the stimulus should be less modulated during movement, and vice versa. This was not the case: instead, we observed a strong correlation between modulation during stimulus and modulation during movement (Figure 3.13g; correlations of log(stimulus) to log(movement) for rats 1–5 were $r = 0.709$, $r = 0.655$, $r = 0.577$, $r = 0.666$, $r = 0.763$; all $p < 10^{-4}$). This implies that the misalignment of stimulus and movement activity is a population- level phenomenon, not due to having separate groups of neurons.

3.6 Discussion

We used a multisensory decision task to understand the organization and dynamics of PPC, an area that we demonstrate to be causal for visual decisions. We found that PPC neurons have mixed selectivity for two task parameters: the animal's developing choice and the modality of the stimulus. We used a new test, PAIRS, to demonstrate that task parameters and time-varying response features are distributed randomly across neurons. This configuration does not pose a problem for decoding: a linear SVM could accurately estimate the modality of the stimulus and the rat's choice on the basis of single-trial responses. A final analysis further demonstrated the flexibility of the population: our variance alignment test revealed that the network explores different dimensions during decision and movement. This may allow PPC to translate the decision about rate into an abstractly related action. Taken together, these results point to PPC neurons as a category-free population that is combined dynamically as the behavioral demands of a complex decision evolve.

Theoretical motivations for functionally specialized neurons, and their existence in early visual areas (Barlow, 1953), has driven a widespread assumption of cate-

gories that has influenced both experimental design (Roitman and Shadlen, 2002; Balan et al., 2008; Georgopoulos et al., 1982; Churchland et al., 2008) and analysis (Arimura et al., 2013; Viswanathan and Nieder, 2013; Roth et al., 2012; Russo et al., 2002). Our finding of a category-free neural population challenges these assumptions about the organization of cortical structures. As a caveat, we note that neural categories defined by other properties, such as cell type or connectivity, might reveal specialization. Indeed, a few studies have found projection-based categories that are functionally specific (Segraves, 1992; Movshon and Newsome, 1996; Chen et al., 2013), although many other studies report that connectivity-defined categories are functionally diverse (Churchland and Lisberger, 2005; El-Shamayleh et al., 2013; Paré and Wurtz, 2001). By demonstrating here that cortical areas can lack categories defined by selectivity to task parameters (Figure 3.8a–c) or by time-dependent response features (Figure 3.8d,e), our findings invite a new approach to interpreting population data. Specifically, future studies can test directly for the existence of categories and design appropriate analyses if neurons are shown to reflect random combinations of task parameters, as they are here.

Although individual neurons reflected random combinations of task components (as predicted by theory Salinas, 2004; Pouget and Sejnowski, 1997; Sussillo and Abbott, 2009), the observed responses were nonetheless structured. Specifically, we observed that most neurons that were driven by choice had 'tolerance' for modality: they retained their choice preference whether the stimulus was auditory, visual or multisensory (Figure 3.7a,b). Neurons in monkey inferotemporal cortex are likewise tolerant: many neurons have a preferred stimulus identity that is stable, though modulated, across many retinal positions (Rust and Dicarlo, 2010). Indeed, our task configuration is reminiscent of that used to study object recognition: just as a given object can be viewed from two different angles, a 'low rate' decision here can be informed by two different modalities. In inferotemporal cortex, the possibility of using the same linear decoder under many conditions, indicating tolerance, is taken as evidence that the neural data has been reformatted from an original, 'tangled' representation in earlier sensory areas (Cortes and Vapnik, 1995). In PPC, analo-

gously, a linear decoder was capable of reading out the animal's choice independent of modality. Combined with evidence that PPC responses are nearly linear functions of choice and modality, this suggests that PPC may likewise be at an advanced stage of processing where representations have been untangled to guide decisions. To obtain such a representation, multiple stages of reformatting may be required (Pagan et al., 2013); this may explain the surprising prevalence of multisensory neurons in early sensory areas (Ghazanfar et al., 2005).

In our study, as in primate work, neural responses in PPC seem likely to reflect a process of transforming ambiguous sensory information into action. As in primate vision studies (Roitman and Shadlen, 2002; Churchland et al., 2008), responses gradually diverged according to the eventual decision outcome (Figure 3.5a–e); the response divergence had a long latency, but was evident many hundreds of milliseconds before the animal reported the choice. This was true for both auditory and visual decisions. Primate PPC neurons are active in advance of movements driven by auditory stimuli as well (Linden et al., 1999; Mullette-Gillman et al., 2005). However, it was not known whether PPC neurons were causally involved. Our inactivation results were surprising in that auditory decisions were spared despite a clear signature of the developing choice in PPC neurons. Auditory responses in PPC, though apparently not necessary for this task, may be invoked by other decision tasks, such as those that require the animal to decide when to stop accumulating evidence (Churchland et al., 2008), those that require a report of confidence (Kiani and Shadlen, 2009) or those that require temporally precise multisensory information (Shams et al., 2002).

Two methodological differences between our study and primate decision-making studies are notable. First, our stimuli were full-field rather than spatially restricted, and were related abstractly to their required movement (for example, low rate, move left). These features may explain why we found no bias for contralateral movements (Figure 3.5f,g). Second, we recorded from all encountered neurons and used identical stimuli for each. The more traditional approach of using neuron selection criteria and customized stimuli is successful in identifying neurons with strong choice signals, but may leave unexamined neurons with subtler choice signals that nonetheless shape

the evolving decision. This point is underscored by our observation that most of our neurons contributed to the choice and modality decoding, including neurons that were modulated only weakly by those parameters (Figure 3.10d,h).

PPC thus represents multiple behaviorally relevant variables in the same population of neurons, with these representations structured in a way that could allow easy decoding by subsequent cortical areas — perhaps especially those that inform movements. These patterns of activity are dynamic and task dependent, and are determined by more than connectivity alone. This use of different patterns of activity could confer flexibility on PPC in converting stimuli into action, and it highlights the importance of understanding the population activity over the course of decision formation.

4

Optogenetic disruption of PPC

In the previous chapter we hypothesized that PPC is required for accurate visual decision-making by converting incoming visual signals into evidence for a decision. Our pharmacological and chemogenetic inactivation experiments (see Section 3.1; Raposo et al., 2014) indeed point to a causal role of this area in visual decision-making. However, the slow timescale and large spatial extent of the inactivations prevent us from establishing PPC as critical for visual decisions that require evidence integration.

In the following set of experiments we aimed to determine the role of PPC in the integration of evidence for visual decison-making, by disrupting the normal activity of the area on a fast timescale, using optogenetics.

Expressing the transmembrane ion channel channelrhodopsin-2 (ChR2) in neurons makes them permeable to cations when exposed to blue light. This allows a fast and robust cellular depolarization, inducing action potentials in response to brief flashes of blue light with millisecond precision (Boyden et al., 2005). We used this technique to disrupt the activity of PPC neurons of rats trained, as in previous experiments, to integrate evidence about the rate of visual events presented over 1000 ms (see Section 2.1). Rats were injected to express ChR2 pan-neuronally in PPC and were implanted with fibers to allow optical stimulation.

As reported in Section 3.2, electrophysiological recordings in PPC show that individual neurons in this area can either be suppressed or elevated during decision

formation. We have also shown that decision variables like choice and modality may be encoded at the population level, with many hundreds of neurons participating in that coding scheme (see Section 3.3; Raposo et al., 2014). This evidence suggested to us that pan-neuronal stimulation of PPC neurons could cause a disruption in the rats' decision-making by disrupting a dynamic population code. Indeed, optical stimulation presented throughout the decision period reliably reduced accuracy of rats' decisions on visual trials. This suggests that disruption of PPC impairs visual decision-making, even when disruption is rare and spatially restricted.

Stimulation could reduce decision accuracy by weakening the influence of visual evidence on choice or by allowing irrelevant task features to more strongly influence choice. To determine if either of these possibilities was true we fit a logistic regression model to the behavioral data. This analysis revealed that sensitivity to visual evidence was significantly weaker on stimulation trials, while bias and trial history dependence were not consistently affected.

Finally, to define the temporal dynamics governing PPC's involvement in decisions that require evidence integration, we disrupted neural activity during restricted epochs of the decision. Surprisingly, when stimulation took place during the first 250 ms of the decision, accuracy was reduced to the same extent as observed during full 1000 ms stimulation. By contrast, accuracy was largely unaffected when stimulation took place during the last 250 ms of the decision. The effect on accuracy during the middle of the decision (250-500 ms; 500–750 ms) was intermediate.

Taken together, these results suggest that PPC activity is required for the integration of evidence in visual decisions, but that the integrated evidence is maintained elsewhere (outside PPC) throughout the trial duration. The long-lasting effect of brief stimulation early in the trial suggests that stimulation interrupted an ongoing process that could not recover within the timescale of the trial. This suggests that several hundred milliseconds may be required for the network to re-establish a state that is receptive to visual evidence for decisions.

4.1 Pan-neuronal ChR2 stimulation of PPC neurons

We expressed ChR2 in the PPC of rats using the adeno-associated virus (AAV, serotype 9) carrying the gene ChR2 fused with green fluorescent protein (GFP) under the control of the CAG promoter (AAV9-CAG-ChR2-GFP). This promoter allows the expression of ChR2 in all cell types. Unilateral injections of this construct were made in the left PPC of two rats (3-4 weeks old), in three separate penetrations along the medial-lateral axis with the goal of maximizing expression in PPC and minimizing the spread outside of this area (stereotactic coordinates: -3.8 mm AP, -2.2 / -3.2 / -4.2 mm ML, relative to Bregma). We restricted injection depth to 800 μm below the pia to avoid viral spread to subcortical structures.

After allowing 2–3 weeks of recovery from surgery the rats were trained in the rate discrimination task described in Section 2.1. Both rats became proficient in the task and were subsequently subject to another surgery, this time with the goal of implanting optical fibers in PPC, which now expressed ChR2. These optical fibers provide us with a way to deliver blue light to ChR2-expressing neurons in a small region of the brain. A microdrive array carrying 8 individually movable optical fibers, each of them attached to a tetrode, was implanted in the center of the injected area. Fibers were sharpened using a diamond wheel to improve tissue penetration, maximize the angle of the light exit cone and increase light transmission. The spatial extent of the optical stimulation is dependent on the spread of the light in the brain, which drops off approximately with square of the distance (Aravanis et al., 2007), and the ChR2 expression levels, which may vary from neuron to neuron.

On a subset of randomly selected trials ("stimulation trials", 15–25%) we delivered blue light to activate ChR2-expressing neurons in PPC, using a 473 nm diode-pumped solid-state (DPSS) laser. On these trials the laser was triggered at the beginning of the stimulus (visual or auditory) presentation and was kept on throughout the entire decision formation period (1000 ms), delivering light pulses at a rate of 40 Hz (Figure 4.1a). On the remaining trials ("control trials", 75–85%) optical stimulation did not

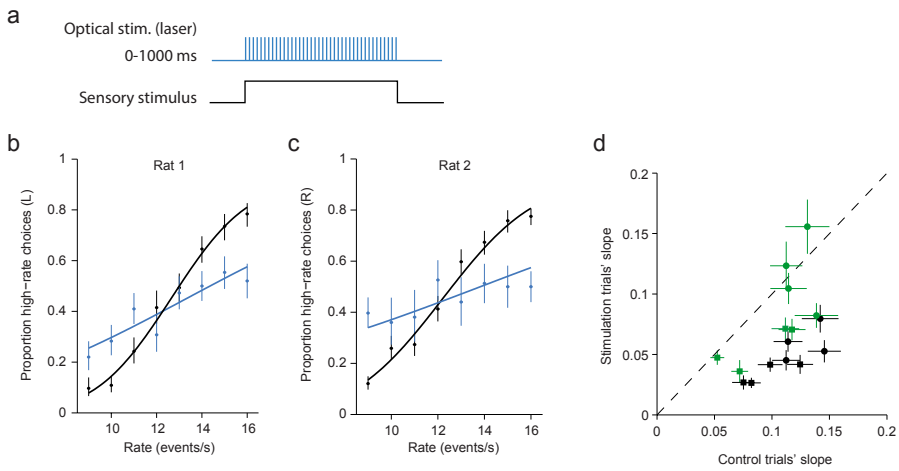

Figure 4.1: **Optical stimulation of PPC neurons disrupts visual decision-making. a,** Schematic of optical stimulation time course (blue) in a trial relative to onset and offset of sensory stimulus (black). **b,** Psychometric curves for one example rat (rat 1) and one example optical fiber site, on visual control trials (black) and visual trials with optical stimulation (blue). **c,** Same as in b but for a different rat (rat 2). **d,** Comparison between the slope ($\propto 1/\sigma$) of psychometric curves for stimulation (y axis) and control trials (x axis). Circles, different optical fiber sites for rat 1; squares, different optical fiber sites for rat 2. Black, visual trials; green, auditory trials. Dashed line, $x = y$. Points below the dashed line represent performance impairment.

occur. We covered the rats' implants with back insulating tape in the beginning of every session. This proved to be a good way to prevent the rats' behavior from being altered by the presence of an additional light source – i.e., the stimulation light (Figure 4.2a).

In both rats, we saw a significant and consistent decrease in accuracy for stimulation versus control trials in which decisions were based on visual stimuli (Figure 4.1b,c and Figure 4.1d, black symbols). Performance change was significant in 4 out of 4 fiber sites for rat 1 and in 4 out of 4 for rat 2, reinforcing the observations we previously made using pharmacological and chemogenetic manipulations (see Section 3.1). During decisions based on auditory stimuli the impairment was not systematic across fiber sites (Figure 4.1d, green symbols). Performance impairment was significant in 1 out of 4 fiber sites for rat 1 and in 3 out of 4 for rat 2.

We repeated these experiments on a third rat which was not injected and, as

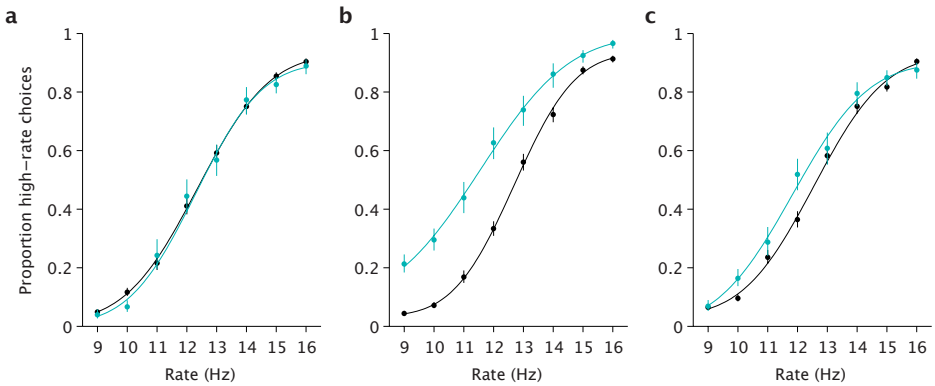

Figure 4.2: **Performance is unchanged during optical stimulation if PPC neurons do not express ChR2. a-c,** Psychometric curves for one uninjected rat (rat 3) and one optical fiber site, in control trials (black) and stimulation trials (cyan). Each plot shows data pooled across seven consecutive sessions. **a,** Condition 1: implant was covered with black tape to prevent light to be seen by the rat. **b,** Condition 2: implant was not covered and, as such, light from optical fiber was visible to the rat. **c,** Condition 3: implant was not covered and second optical fiber was used to mask light from stimulation fiber.

such, did not express ChR2 in PPC neurons. As we did in the previous optogenetic experiments, the rat's implant was covered with black tape to avoid that any light coming from the optical fiber could be seen by the rat. Under these conditions, optical stimulation showed no effect on this control rat (Figure 4.2a). We repeated this control experiment under two different conditions: one where we did not cover the implant with black tape and, therefore, the light coming from the optical fiber was visible to the rat during stimulation trials; another one where we did not cover the implant with black tape and used a second optical fiber – connected to a second laser source – which was attached to the implant near the stimulation fiber. The light coming from this second fiber was blocked from going into the rat's brain and was on on every trial (control trials and stimulation trials), serving as a mask to the actual stimulation light. Results from these two additional control experiments showed that the rat's behavior was influenced by the presence of a visible light coming from the optical fibers (Figure 4.2b,c). In particular, we observed a high-rate bias on conditions where the stimulation light was visible.

The observation that optical stimulation reduces decision accuracy could either be the result of weakening the influence of visual evidence on the choice or of allowing irrelevant task features to more strongly influence choice. To distinguish these two alternatives we used a probabilistic model in which the observer makes a decision based upon a weighted sum of a sensory term, two strategy terms and an overall bias (this model is identical to the one described in Busse et al., 2011). In this model the sensory term is a measure of the stimulus rate on each trial. More precisely, it measures the difference between the stimulus rate and the category boundary, ranging from -3.5 to 3.5 (events/s). The two strategy terms express the outcome of each trial's preceding trial. The first one reflects if the preceding trial was not correct (0), a correct trial where the subject chose high-rate (1) or a correct trial where the subject chose low-rate (-1). We call this term "success history". The second strategy term reflects if the preceding trial was not incorrect (0), incorrect where the subject chose high-rate (1) or incorrect where the subject chose low-rate (-1). We call this term "failure history". We fitted the four parameters in this model using logistic regression.

The model can be formalized by the following expression:

$$\ln(\frac{p}{1-p}) = \beta_0 + \beta_1\, r + \beta_2\, h_{succ} + \beta_3\, h_{fail} \tag{4.1}$$

where p is the probability of a high-rate choice, r is the sensory term, h_{suss} and h_{fail} are the success and failure history terms.

We were able to fit the rats' behavior well using this model both on control trials, where the performance was unaffected (Figure 4.3a) and on stimulation trials, where the performance was impaired (Figure 4.3b).

The coefficients fitted by the model (β_{0-3}) provide insight into how much each parameter of the model influences the choice on any given trial — stimulation or control. For both rats, on control trials, stimulus rate and success history had coefficients significantly different than zero while failure history did not (Figure 4.4a,b, left). This tells us two things: (1) as expected, the rats used the evidence provided

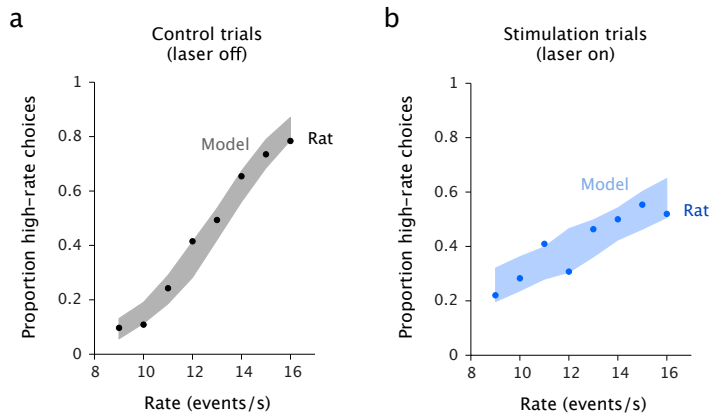

Figure 4.3: **Probabilistic model fits rats' behavioral data well. a,** Comparison between model performance and subject's behavior on control trials. Shaded area, model's performance (95% confidence intervals); circles, rat's behavior. **b,** Same as in b but for optical stimulation trials.

by the stimulus to make their decisions; (2) on each particular trial the rats' choice was affected by the choice they made on the preceding trial, but only if that trial was rewarded. In fact, because the success history coefficient was positive, we can say that, after a reward, rats had the tendency to repeat the choice they had just made. Even though the failure history coefficients did not significantly differ from zero, a propensity for taking negative values is noticeable. This means that after an incorrect trial (unrewarded and followed by a short time out) the rats had a slight preference to make the opposite choice. The bias coefficient fluctuated from session to session, but we did not observe a consistent bias across animals or sessions (Figure 4.4c, left). These observations were likewise true for auditory control trials (Figure 4.4d–f, left).

Comparing the coefficients obtained on control trials versus stimulation trials revealed that visual evidence had consistently lower weights on stimulation trials (lower coefficient for the sensory term, Figure 4.4a, right). This means that visual evidence had a lower weight on the rats' choices when optical stimulation occurred. This was not systematically observed on auditory trials (Figure 4.4d, right). Additionally, the influence of the preceding choice as well as the overall bias were not affected by the

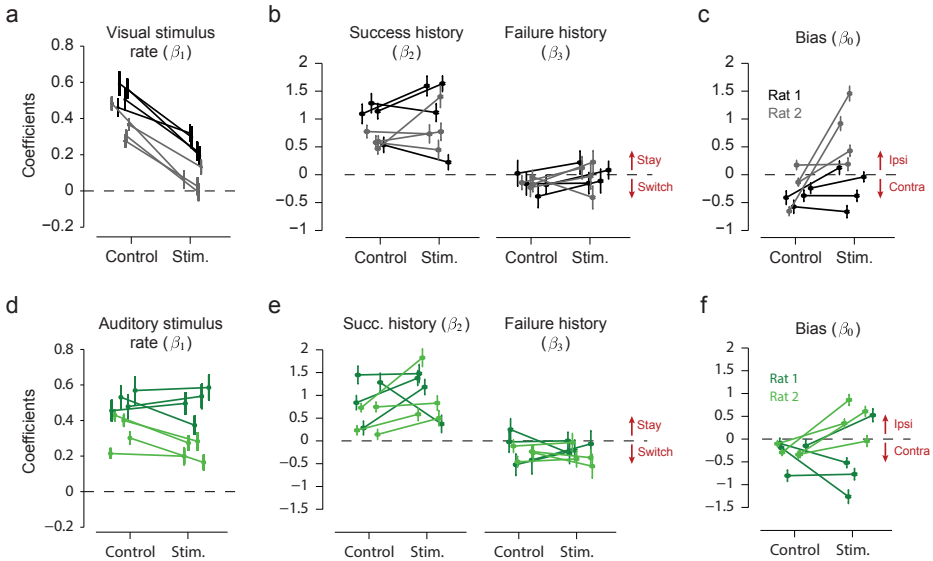

Figure 4.4: **Optical stimulation in PPC reduces influence of sensory evidence in visual decisions. a,** Coefficients fitted by the model for the sensory term, on visual control trials (left) and visual stimulation trials (right). Lines connect points corresponding to the same fiber site. Black, rat 1; Gray, rat 2. **b,** Same as in a but for two strategy terms: success history and failure history. **c,** Same as a and b but for the overall bias term. **d,e,f,** Same as in a,b,c, but for auditory trials. Dark green, rat 1; Light green, rat 2.

stimulation. This was true on both visual (Figure 4.4b,c, right) and auditory trials (Figure 4.4e,f, right). Together, these suggest that optical stimulation caused an impairment in the ability to use visual evidence to guide decisions but did not have an impact on the strategy used by the rats in the task.

4.2 Behavior disruption and recovery dynamics

Next, we aimed to understand the temporal dynamics guiding PPC's involvement in the integration of visual evidence for decision-making. To do that we repeated the experiments described in Section 4.1 but this time we disrupted neural activity in PPC during restricted epochs within the decision formation period. The optical stimulation was now limited to 250 ms and, on each particular stimulation trial (25%

of all trials), it could have one of four different start times: 0, 250, 500 or 750 ms relative to sensory stimulus onset (Figure 4.5a).

These experiments led once again to the observation that optical stimulation of PPC neurons disrupts rats' decision accuracy on visual trials. Remarkably, this disruption was strongest when stimulation took place during the first 250 ms of the decision formation period and this impairment was as effective as the one observed during full 1000 ms stimulation (Figure 4.5b,c, leftmost point and blue shaded area). By contrast, the ability to make visual decisions was largely spared when stimulation took place during the last 250 ms of the decision (Figure 4.5b,c, rightmost point and shaded gray area). The decline in accuracy was smaller but nevertheless significant when stimulation took place during the middle of the decision (Figure 4.5b,c, two middle points).

One possible explanation for the strong deficit observed in the rats' decision accuracy when stimulation occurred in the first 250 ms is that rats were only using visual evidence that was presented early in the trial to make their choices. This is unlikely to have happened because we know from previous experiments that rats tend to use most of the evidence throughout the trial in our task (see Section 2.4). An alternative hypothesis is that optical stimulation causes a disruption in the normal activity of the neurons from which it takes a long time (in the order of seconds or at least hundreds of milliseconds) to recover.

To investigate this question we computed psychophysical kernels to measure how rats weigh each moment of the evidence in their decisions. We employed a similar technique to the one described in Section 2.4, but this time directly modeling the subjects' choices by assigning weights to small portions of the stimulus. This analysis allowed us to have greater statistical power, given the larger number of conditions in these experiments, because it does not require discarding any trials.

This model used logistic regression to fit the behavioral data and it can be for-

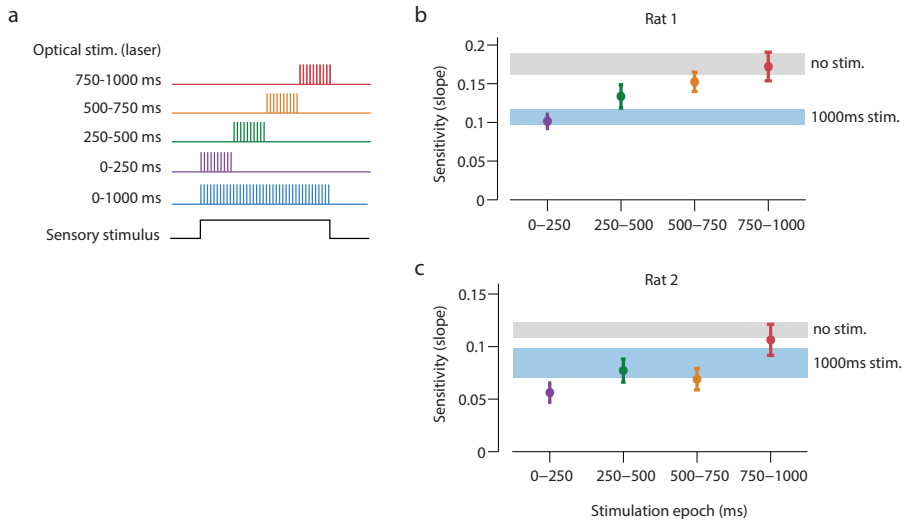

Figure 4.5: **Stimulation has a greater impact on decisions when it occurs early in decision formation. a,** Schematic of optical stimulation time course for different stimulation trials relative to onset and offset of sensory stimulus (black). Purple, green, yellow, red, represent short stimulation epochs during decision formation. Blue represents full 1000 ms stimulation. **b,** Ability of one example rat (rat 1) to make accurate decisions as measured by the slope of psychometric curves for different stimulation epochs. Lower values indicate greater impairment. Purple, green, yellow and red points show decision accuracy during short stimulation epochs. Color convention is the same as in a. Error bars represent SE. Thick blue line represents mean decision accuracy ± SE during full 1000 ms stimulation. Thick gray line represent mean decision accuracy ± SE during control trials. **c,** Same as in b but for a second rat (rat 2).

malized by the following expression:

$$\ln(\frac{p}{1-p}) = \beta_0 + \sum_{i=1}^{N} \beta_i C_i \tag{4.2}$$

where p is the probability of a high-rate choice, N is the total number of stimulus portions and C_i is the number of stimulus events that occur in the portion i of the stimulus. The coefficients of the model, β_i, reflect how much each portion of the stimulus is weighted in the rats' choices.

This analysis revealed two things. First, that rats do not weigh early evidence

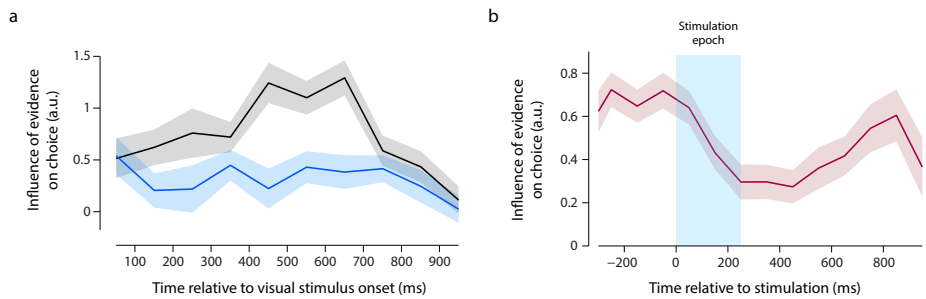

Figure 4.6: **Optical stimulation reduces influence of visual evidence in choices during and after stimulation epoch. a,** Influence of visual evidence on choices as measured by the coefficients fitted by the model for different time points during decision formation. Black, control trials; blue, full stimulation trials (0–1000 ms). **b,** Same as in a but for short stimulation epochs and aligned with the onset of optical stimulation.

more than they weigh evidence in the middle or the end of the decision formation period (Figure 4.6a, black line). The coefficients are elevated above zero throughout most of the trial. Second, that rats are not only unable to use the evidence provided by the visual stimulus during optical stimulation, but they are also unable to use that visual evidence for a long time after the stimulation ended (Figure 4.6b). If it were the case that optical stimulation had a short transient effect, we would expect to see the coefficients increase soon after the end of the stimulation epoch. But, as evident in Figure 4.6b, that increase does not occur, for at least another 300 ms. This explains the observations that optical stimulation has the strongest effect on decision accuracy early in decision formation (see Section 4.1). Moreover, it suggest that the disruption caused by optical stimulation of PPC is long lasting, requiring hundreds of milliseconds to fully recover.

4.3 Discussion

Previous pharmacological and chemogenetic experiments have implicated PPC in visual decision-making. However these manipulations did not establish for which aspect of the task PPC is required. It is plausible that PPC is required for visual evidence

integration but it is also possible that it is required to translate the integrated visual evidence into a motor command (e.g. action selection or movement preparation). By disrupting the activity of these neurons in a temporally precise manner we can get insights into the dynamics of PPC's involvement in the task and rule out hypotheses.

Our results using optogenetics to disrupt neural activity reinforce the idea that PPC is required for visual decisions in a task where subjects need to integrate evidence over time. We observed that PPC is mostly required early in decision formation rather than late. This suggests that PPC is not involved in the process of converting the accumulated evidence for or against a particular choice (e.g. evidence supporting a high-rate choice) into an action (e.g. moving body to the reward port on the right). If that were the case we would expect the impairment to be strong towards the end of the decision formation period, when the animals need to start planning a motor response.

The substantial impairment observed when we stimulated PPC early in the trial raises two possibilities: (1) there is a critical event in the decision process that is temporally restricted and happens early in decision formation; (2) optical stimulation of PPC neurons has a long lasting effect, in the order of hundreds of millisecond, that extends beyond the stimulation epoch. It is important to note that these two possibilities are not mutually exclusive. Our psychophysical kernel analysis provides evidence in support of the latter, but is insufficient to rule out the former. However, the fact that the impairment is still present when stimulation occurs in the middle of decision formation indicates that the first possibility may not be true. Yet, further experiments, with shorter stimulation epochs for example, need to be done to confirm this interpretation.

5

Materials and methods

5.1 Behavioral task and subjects' training

We examined the choice behavior of rodents and humans on a rate discrimination task described in Section 2.1. Stimuli consisted of 1-s streams of auditory and/or visual events separated by random sequences of short and long interevent intervals of fixed duration. The ratio of short to long intervals over the course of the whole trial determined the average event rate of each trial. Trials consisting solely of long intervals produced the lowest possible event rates; trials consisting of only short intervals produced the highest rates. Subjects made two-alternative low- / high-rate judgments by comparing the average rate of each trial to an enforced category boundary. Stimuli with more equal proportions of short and long intervals produced intermediate event rates difficult to classify as low or high.

5.1.1 Human subjects

We report data from 10 human volunteers (5 male, 5 female, age 22–60 years) with normal or corrected-to-normal vision and normal hearing. Two subjects were researchers connected to this study; the remaining eight subjects were naive about the experiment. Volunteers were recruited through fliers posted at Cold Spring Harbor Laboratory. Experiments were conducted in a large sound-isolating booth (Industrial Acoustics).

Visual stimuli were displayed on a CRT monitor (Dell M991) using a refresh rate of 100 Hz. Subjects were seated comfortably in front of the monitor; the distance from their eyes to the screen was ~ 51 cm. Stimulus presentation and data acquisition were controlled by the Psychophysics Toolbox (Pelli, 1997) running on MATLAB (Mathworks) on a Quad Core Macintosh computer (Apple). Subjects were instructed to fixate a central black spot ($0.22 \times 0.24^\circ$ of visual angle); eye position was not monitored because small deviations in eye position are unlikely to impact rate judgments about a large flashing stimulus. After a delay (500 ms), the stimulus presentation began.

Auditory events were pure tones (220 Hz) that were played from a single speaker attached to the left side of the monitor. Speakers were generic mini-USB speakers (4.8×7.2 cm; Hewlett Packard; azimuth $= 22.6^\circ$) that produced $78\,\mathrm{dB} - \mathrm{SPL}$ in the range of 200–240 Hz at the position of the subject (tested using a pressure-field microphone, Brüel & Kjær). Waveforms were created in software at a sampling rate of 44 kHz and delivered to speakers through a digital (TOSlink optical) audio output using the PsychPortAudio function in the Psychophysics Toolbox. The visual stimulus, a flashing square that subtended $10 \times 10^\circ$ of visual angle (azimuth $= 17.16^\circ$), was positioned eccentrically so that its leftmost edge touched the left side of the screen. This configuration meant that auditory and visual stimuli were separated by only 3.5 cm (the width of the plastic frame of the CRT). The top of the speaker was collinear with the top of the flashing visual square. We positioned the stimuli close together because spatial proximity has been previously shown to encourage multisensory binding (Slutsky and Recanzone, 2001; Körding et al., 2007). The timing of auditory and visual events was checked regularly by using a photodiode and a microphone connected to an oscilloscope. Both auditory and visual events were played amid background white noise. For the visual stimulus, the white noise was restricted to the region of the screen where the stimulus was displayed.

Subjects reported their decisions by pressing one of two keys on a standard keyboard. They received auditory feedback about their choices: correct choices resulted in a high tone (6400 Hz) and incorrect choices resulted in a low tone (200 Hz). We

provided feedback to the human subjects so that their experience with the task would be as similar as possible to the rats. Feedback for the rats was essential because the liquid rewards the rats received motivated them to do the task (see below). The two intervals used to generate the stimuli were 60 and 120 ms. Individual events were 10 ms. The resulting trials had fluctuating rates whose averages ranged from 7 to 15 Hz.

We trained subjects for 4–6 days so that they could learn the association between stimulus rate and the correct choice. We began by presenting very salient unimodal stimuli, both visual and auditory; initially, the rates used were uniformly low or uniformly high. Over the course of several days, we used a staircase procedure to gradually make the task more difficult by lowering the amplitude (contrast or volume) of the stimuli. We also began to include trials with mixtures of long and short interevent intervals so that the overall rate was harder to judge, as well as multisensory trials. Subjects typically achieved a high performance level on both unisensory and multisensory trials within 3 days. We typically used an additional 2-3 days for training during which we made slight adjustments to the auditory and visual background noise so that the two modalities were equally reliable (as measured by the subjects' thresholds on single modality trials). After this additional training, subjects' performance was typically well matched for the two modalities and also very stable from session to session. Once trained, subjects began each additional day with a 100 trial warm-up session. They then completed approximately five blocks of 160 trials on a given day.

5.1.2 Animal subjects

We collected data from adult male LongEvans rats (250–350 g; Taconic Farms) that were trained to do freely moving two-alternative forced-choice behavior in a sound isolating booth (Industrial Acoustics). Trials were initiated when the rats poked their snouts into a centrally positioned port. Placing their snouts in this port broke an infrared beam; this event triggered onset of the visual or auditory stimulus.

Auditory events were played from a single, centrally positioned speaker and con-

sisted of pure tones (15 kHz) or bursts of white noise with sinusoidal amplitude modulation. Speakers were generic electromagnetic dynamic speakers (Harman Kardon) calibrated by using a pressure-field microphone (Brüel & Kjær) to produce 75 dB − SPL in the range of 5–40 kHz at the position of the subject. Waveforms were created in software at a sampling rate of 200 kHz and delivered to speakers through a Lynx L22 sound card (Lynx Studio Technology).

Visual stimuli were presented on a centrally positioned panel of 96 LEDs that spanned 6 cm high × 7 cm wide (118° horizontal angle × 67° vertical angle). The bottom edge of the panel was ∼ 4 cm above the animals' eyes. Note that because the interior of the acoustic box was dark, it was not necessary for the rats to look directly at the LED panel to see the stimulus events. The use of a large, stationary visual stimulus ensured that small head or eye movements during the stimulus presentation period did not grossly distort the incoming visual information. The LEDs were driven by output from the same sound card that we used for auditory stimuli; the sound card has two channels (typically used for a left and right speaker), which can be controlled independently. Auditory and visual stimuli were sent to different channels on the sound card so that we could use different auditory/visual stimuli for the independent condition. The timing of auditory and visual events was checked regularly by using a photodiode and a microphone connected to an oscilloscope.

Animals were required to stay in the port for 1000 ms. Mean wait times were very close to 1000 ms for all three animals. Withdrawal from the center port before the end of the stimulus presentation resulted in a 2000–3000 ms "timeout" during which a new trial could not be initiated. These trials were excluded from further analysis. Animals typically displayed equal numbers of early withdrawal trials for auditory, visual, and multisensory stimuli. When animals successfully waited for the entire duration, they then had up to 2000 ms to report their decision by going to one of two eccentrically positioned reward ports, each of which was arbitrarily associated with either a high rate or a low rate. The time delay between leaving the center port and arriving at the reward port varied across animals. When the rats correctly went to the port corresponding to the presented rate, they received a drop of water (15-20 μl)

delivered directly into the port through tubing connected to a solenoid. Open times of the solenoid were regularly calibrated to ensure that equal amounts of water were delivered to each side.

In the experiments reported in Chapter 2, the two intervals used to generate the stimuli were slightly different for the three rats. For rat 1, intervals had durations of 30 and 70 ms. The resulting trials had fluctuating rates whose averages ranged from 12 to 22 Hz. For rat 2, intervals had durations of 17 and 67 ms. The resulting trials had fluctuating rates whose averages ranged from 12 to 32 Hz. Shorter intervals (and therefore higher rates) were used with the first two animals because we had originally feared that the lower rates used on the human task would be difficult for the rats to learn (lower rates require longer integration times because the information arrives more slowly). However, this proved to be incorrect: for rat 3, the intervals were very similar to those used in humans: intervals were 50 and 100 ms; the resulting trials had fluctuating rates whose averages ranged from 9 to 15 Hz. No major differences in multisensory enhancement were observed in the three animals. The main consequence of using different rates for each animal is that it prevented us from pooling data across animals for certain analyses. For these analyses, we report results from each animal individually. In the experiments reported in Chapters 3 and 4, the intervals used were the same for all rats: 50 and 100 ms.

Animals were first trained by using auditory stimuli alone. Once they had achieved proficiency with the task, we introduced a small proportion of multisensory trials where the auditory and visual events were played synchronously. Shortly thereafter, we introduced some trials that contained only the visual stimulus. Performance on these trials was typically near chance for the first few days and improved rapidly thereafter. Once proficiency was achieved on the visual task, animals were presented with equal numbers of auditory, visual, and multisensory trials interleaved in a single block.

All experimental procedures were in accordance with the National Institutes of Health's Guide for the Care and Use of Laboratory Animals and approved by the Cold Spring Harbor Animal Care and Use Committee.

5.1.3 Stimulus reliability

To manipulate sensory reliability, we adjusted the signal-to-noise ratios (SNRs) of the auditory and visual stimuli. The SNR of either modality could be independently manipulated since auditory and visual stimuli were presented amidst background noise. To gauge how strongly subjects weighted evidence from one sensory modality relative to the other for each pairing of sensory reliabilities, we presented multisensory trials in which the auditory and visual rates conflicted. To generate a multisensory trial, we first randomly selected a conflict level (for example, 2 events/s). Next, we randomly selected a pair of rates with the specified conflict (for example, 9 and 11 events/s). Between the two event rates chosen, the lower and higher rates were randomly assigned to the visual and auditory stimuli, respectively, leading to "positive" or "negative" cue conflicts in equal proportions. When the randomly selected conflict level was 0, the same rate was assigned to both modalities. Mixtures of long and short interevent intervals were then sampled randomly to generate independent auditory and visual event streams with the desired trial-averaged event rates.

Note that because event rates fluctuated in time due to the random sequences of short and long intervals in a trial, auditory and visual stimuli arrived at different moments and had different instantaneous rates on multisensory trials even when the trial-averaged event rates were equal. At the lowest and highest event rates (when all intervals were either short or long), auditory and visual stimuli still arrived at different times since a brief offset (humans: 20 ms; rats: 0-50 ms randomly selected for each trial) was imposed between the two event streams. Previous work indicates that this configuration leads to multisensory improvements in performance comparable to that observed when auditory and visual events are presented simultaneously. This is likely because the window of auditory-visual integration can be very flexible, depending on the task (Powers et al., 2009; Serwe et al., 2011).

5.2 Analysis of behavioral data

5.2.1 Psychometric curves

The performance of a subject on a perceptual task can be assessed by the subject's 'psychometric curve', which models their choices on the task as a function of the strength (or intensity) of the physical stimulus – e.g. the relation between the contrast of a visual stimulus and the observer's ability to detect it. A steeper psychometric curve corresponds to a greater ability of the subject to discriminate stimuli of different strengths.

In this work, four-parameter psychometric functions were fit to the subjects' choice data using the Psignifit version 3 toolbox for MATLAB (http://psignifit.sourceforge.net), following the maximum likelihood methods described by Wichmann and Hill (Wichmann and Hill, 2001a,b). Psychometric functions were parameterized as

$$f(r, \mu, \sigma, \gamma, \lambda) = \gamma + (1 - \gamma - \lambda)\,(1 + erf(\frac{r - \mu}{\sigma\sqrt{2}})) \tag{5.1}$$

where r is the trial event rate, μ and σ are the first and second moments of a cumulative Gaussian function, γ and λ are the guessing and lapse rates (constrained so that $0 \leq \gamma \leq 0.1$, $0 \leq \lambda \leq 0.1$), and erf is the error function. σ is referred to as the psychophysical threshold; smaller σ results in a steeper psychometric function. Standard errors for σ were computed via bootstrap analysis of the choice data (2000 resamples).

5.2.2 Optimal cue weighting

For a multisensory trial with auditory and visual event rate estimates $\hat{r}_A$ and $\hat{r}_V$, we model the subject's final rate estimate $\hat{r}$ on a multisensory trial as

$$\hat{r} = \hat{r}_A\, w_A + \hat{r}_V\, w_V \tag{5.2}$$

where w_A and w_V are linear weights such that $w_A + w_V = 1$ (Ernst and Banks, 2002; Young et al., 1993). Assuming $\hat{r}_A$ and $\hat{r}_V$ are unbiased, minimum variance in $\hat{r}$ is achieved by assigning sensory weights proportional to the relative reliabilities (i.e., reciprocal variances) of the estimates obtained from the two modalities (Landy and Kojima, 2001; Young et al., 1993). As in previous work, we estimated the single-sensory reliabilities (R) as the squared reciprocal of subjects' psychophysical thresholds obtained from their single sensory psychometric data: $R = 1/\sigma^2$ (Ernst and Banks, 2002; Young et al., 1993). Given only the single sensory thresholds σ_A and σ_V, an optimal maximum likelihood estimator assigns sensory weights

$$w_A = \frac{\sigma_V^2}{\sigma_A^2 + \sigma_V^2} \quad \text{and} \quad w_V = \frac{\sigma_A^2}{\sigma_A^2 + \sigma_V^2} \tag{5.3}$$

It follows that more reliable cues have a greater weighting in the bimodal (multisensory) estimate, and its variance is predicted to be lower than that of the unimodal estimates, according to

$$\sigma_{Bimodal}^2 = \frac{\sigma_A^2 \, \sigma_V^2}{\sigma_A^2 + \sigma_V^2} \tag{5.4}$$

Predicted weights can be compared to estimates of the subjects' actual sensory weights obtained from multisensory stimuli in which the conflict between auditory and visual event rates is systematically varied. In this conflict analysis, we assess each subject's point of subjective equality (PSE; the average event rate for which the subject is equally likely to make low- and high-rate decisions, estimated from the psychometric function) as a function of the sensory conflict Δ:

$$\Delta = r_V - r_A \tag{5.5}$$

where r_V and r_A are the presented visual and auditory rates. Rearranging Equation 5.2, we obtain

$$w_V = \frac{\hat{r} - r_A}{\Delta} \tag{5.6}$$

Neglecting choice biases, $\hat{r}$ will equal the category boundary rate (r_{CB}) when the average event rate, r_{mean}, is equal to PSE_{AV} (where $r_{mean} = r_A + \Delta/2$ and PSE_{AV}

is the PSE for the given multisensory trial type; see Fetsch et al., 2012; Young et al., 1993). Substituting these terms into Equation 5.6 and solving for PSE_{AV} yields

$$PSE_{AV} = \Delta\,(\frac{1}{2} - w_V) + r_{CB} \tag{5.7}$$

One can thus estimate the perceptual weights by measuring subjects' PSEs for multisensory trials presented across a range of conflict levels (Young et al., 1993), since the slope obtained from simple linear regression of PSE_{AV} against Δ provides an empirical estimate of w_V:

$$\hat{w}_V = \frac{1}{2} - slope \tag{5.8}$$

We used this approach to compare the empirically estimated weights to the weights predicted from subjects' single sensory thresholds (henceforth, observed and predicted weights). Standard errors for the predicted and observed weights were estimated by propagating the uncertainty associated with σ_A, σ_V, and PSE_{AV}. Statistical comparisons of observed and predicted weights in individual subjects were performed using Z-tests.

5.2.3 Excess Rate

The Excess Rate analysis, described in Section 2.4, complements the psychometric function as a means of quantifying the animal's decision-making behavior. The idea is to relate momentary fluctuations in the instantaneous rate with the animal's choice by computing a quantity termed "Excess Rate" in sliding 200 ms windows in the trial. Consider an example window from 0–200 ms after stimulus onset. Three steps are required. First, we select all trials in which the rate outside the window (e.g., 200–1000 ms) is neutral. The resulting group of trials differ only in the stimulus rate presented from 0–200 ms. Next, we separate trials into groups where the rat made a left vs. right choice. Finally, we average the rate for each group and take the difference in rate between trials preceding right vs. left choices. If the difference is zero, this indicates that trials preceding left and right choices were identical and that the time window under study did not influence the choice. Stimulus rates in excess

of zero indicate that the window under study did influence the choice. This process is repeated for sliding 200 ms windows, generating Excess Rates for every moment in time. Excess rate for data is compared to a shuffle in which trials are randomly assigned to a "left" and "right" pool.

5.3 Electrophysiology

Custom tetrode implants were prepared in-house following previously published methods (Znamenskiy and Zador, 2013). Briefly, each assembly contained up to 8 tetrodes. Tetrodes were connected to an EIB-36 narrow connector board (Neuralynx, Bozeman, MT) mounted on the assembly. The assembly was secured within a plastic enclosure prior to implanting. Tetrodes were gold-plated to 300–700 kΩ at 1 kHz; one additional tetrode was used as an internal reference for electrophysiological recordings and plated to $\sim 100\,\text{k}\Omega$.

Spike-triggered waveforms were recorded from each tetrode using Digital Lynx SX hardware and Cheetah data acquisition software (Neuralynx, Bozeman, MT). Data were acquired with a sampling rate of 32 kHz, and spike waveforms were bandpass filtered at frequency ranges of 600–6000 Hz. Tetrodes were moved 40–80 μm after each recording session to ensure that independent populations of neurons were sampled across sessions.

5.3.1 Monitoring of head/body orientation during recordings

We used two methods to monitor the animal's orientation during electrophysiology sessions. First, we connected red and green LEDs to the animal's implant and tracked head orientation throughout the behavioral session using Cheetah data acquisition software (Neuralynx, Bozeman, MT). LED positions were sampled at 30 Hz. Head angles were computed at each sample time and then smoothed with a Gaussian. For the second method, we used an open-source software package (Bonsai – https://bitbucket.org/horizongir/bonsai; Lopes et al., 2015) to track the animal's

whole body orientation. Body angle was sampled at 100 Hz. The estimates produced using the implant LEDs and body tracking were generally in good agreement, although there tended to be more variability in body angle than head angle (e.g., the rat's head could remain stationary in the central port despite small body movements).

5.3.2 Analysis of electrophysiological data

Raw spike-triggered waveforms were manually clustered using MClust software (A.D. Redish) for MATLAB (Mathworks). Only isolated clusters corresponding to single neurons were included for analysis. Neural recordings were also trimmed or excluded if a portion of the recording had a strongly non-stationary mean firing rate over time, based on automated criteria. In addition, neurons had to satisfy a signal-to-noise criterion. Specifically, the firing-rate range (over conditions and times) divided by the maximal s.e.m. (for all conditions and times) had to be greater than 3.3.

Peri-stimulus time histograms (PSTHs) were computed for two epochs in the trial: a "decision formation epoch" (the time during stimulus presentation and enforced central fixation) and a "movement epoch", for which the spike trains were aligned to the stimulus onset or to the movement onset, respectively. Firing rates were averaged across like trials and smoothed over time with a Gaussian kernel ($sd = 50$ ms).

Chapter 3 reports electrophysiological data from 5 rats. One animal in the cohort had stimulating fibers implanted alongside tetrodes. This animal was used as a control for a separate optogenetic study. For 9 of 18 electrophysiology sessions in this animal, laser stimulation (473 nm) was introduced through the fibers on 50% of trials. The animal expressed no light-activated ion channels in its brain, however, and laser stimulation had no effect on neural activity or behavior.

5.4 Choice selectivity and modality selectivity

PSTHs were constructed from spike trains by averaging firing rates within 10-ms bins and smoothing with a Gaussian kernel ($sd = 50$ ms). Correct trials were grouped according to two different aspects of the trials. The first way was based on the

animal's response: trials ending in a contralateral choice versus trials ending in an ipsilateral choice. The second way was based on the stimulus modality: visual trials versus auditory trials. We used ROC analysis (Green and Swets, 1966) to calculate the ability of an ideal observer to correctly classify the animal's choice or the stimulus modality. This was done on each trial from the smoothed spike trains, at intervals throughout the trial. Choice and modality preference were derived from the area under the ROC curve (AUC) and defined for each time point as $2\,(AUC - 0.5)$; this value ranged from -1 to 1 (Feierstein et al., 2006). A choice preference of -1 indicates that a cell always fired more during trials ending in an ipsilateral choice; a value of 1 means that the cell always fired more during trials ending in a contralateral choice. Modality preference was computed separately for rightward and leftward trials and averaged. A modality preference of -1 indicates that a cell always fired more during auditory trials; a modality preference of 1 means that the cell always fired more during visual trials.

Choice divergence was computed the same way as choice preference except that each neuron was assigned a "preferred" choice or modality based on its responses at the end of the trial (100–200 ms before movement onset). Choice divergence at other time points was computed based on this preference. This is a closely related measure to the absolute value of choice preference, but this way of computing the index has the advantage that it prevents small fluctuations in selectivity due to noise (either positive or negative) at the beginning of the trial from giving the incorrect impression that the neuron is selective before stimulus onset (Erlich et al., 2011). For choice and modality preference, significance ($p < 0.01$, one-sided) was assessed via bootstrapping (1000 iterations). A neuron was considered to have significant modality preference if this value was significant for either rightward or leftward trials.

5.5 Analysis of response clustering

To test for the presence of neural clusters, we developed a novel analysis, PAIRS: Projection Angle Index of Response Similarity. To calculate the statistic, we first

built a matrix of the trial-averaged neural data (the "A" matrix). This matrix had n rows by ct columns, where n is the number of neurons, c is the number of conditions (6 conditions: 2 choices $\times$ 3 sensory modality conditions), and t is the number of time points in the decision epoch (including 300 ms before stimulus onset). We then reduced the dimensionality of this matrix using one of two methods. One method was to perform principal component analysis (PCA) on the A matrix, reducing the dimensionality (number of rows) to 8. This dimensionality was estimated from the data, and the results were not sensitive to the exact dimensionality used. For the alternative "feature based" method, we used the two dimensions specified by our choice decoder and our modality decoder. In this case, the two dimensions were orthogonalized using the Gram-Schmidt algorithm (since they were nearly orthogonal but not perfectly so) to ensure that they captured independent variance. The PCA method is assumed for further description below.

The coefficients matrix resulting from PCA is of size 8 by n; that is, each neuron received a single 8-element vector representing its response profile across conditions and over time. If a pair of neurons had similar response profiles, they would receive similar vectors (i.e., the vectors would form a small angle). For each neuron, we found the angle it made with each of its k most similar partners (e.g., $k = 3$ partners). For each neuron, these k values were then averaged. This produced a distribution of near-neighbor angles, θ_{data}, with one angle per neuron. We took the median of this distribution, denoted $\tilde{\theta}_{data}$, which will be small for data with strong clustering of neural responses or larger if there is little or no clustering.

For comparison, we generated 10,000 simulated datasets composed of n random vectors from a 2- or 8-dimensional Gaussian distribution, as appropriate. For each simulated dataset, we then computed the distribution of angles θ_{random} using exactly the same method of k nearest neighbors. Note that the distribution for each simulated dataset depends on the number of neurons in the original dataset (n), the dimensionality (here 2 or 8), and k, and that each of the 10,000 datasets was independent from the others. We collected the resulting n $\times$ 10,000 angles, then computed the median near-neighbor angle $\tilde{\theta}_{random}$ from this grand distribution. For each rat, we

then computed the PAIRS statistic:

$$PAIRS = \frac{\tilde{\theta}_{random} - \tilde{\theta}_{data}}{\tilde{\theta}_{random}} \tag{5.9}$$

This statistic is 1 if all neurons have at least k identical partners, and 0 if clustering is only as strong as expected by chance. Since we could compute $\tilde{\theta}_{random}$ for each of the 10,000 simulated datasets separately, we used these values to find the distribution of the PAIRS statistic expected by chance. A two-sided p-value was then computed by comparing this distribution to the PAIRS statistic obtained from the neural data.

The value k was selected automatically. To do so, we found the smallest value of k for which $\tilde{\theta}_{random}$ exceeded a target value. When using the PCA method, this value was $\pi/4$ (halfway between 0 and orthogonal, $\pi/2$). For our data, this produced values of k from 2 to 4. When using the feature based method, the space was only two dimensional and therefore the feature vectors were packed more tightly. To avoid having overly large values of k (which would limit us to finding only large clusters), we chose a smaller value for the target angle: $\pi/8$. This produced values of k from 9 to 24.

We also compared the neural data with synthetic data that had artificial clusters introduced. To do so, we first selected one fifth of our neurons at random. For each neuron selected, we generated a quintet of "partner" neurons related to the original. These partners were produced by resampling trials with replacement, then producing PSTHs as in the real data. In the resulting synthetic data, there were as many faux neurons as in the original data, but each faux neuron was related to four others. These faux neurons had exactly the same amount of noise as their originating neurons. This process was repeated 1,000 times. The distribution of the resulting $\theta_{clustered}$ values is plotted as the dashed line in Figure 3.8e.

Finally, we note that PAIRS is not only a test for clustering, but also more generally for non-uniformity of the distribution of tuning across neurons. For example, if a strong majority of neurons "preferred" the high-rate stimulus, then the neurons' coefficient vectors would be mostly packed into half the space. The near-neighbor

angles would therefore be reduced relative to fully random, and PAIRS would detect "clustering" (properly, non-uniformity). While it is probably not possible to detect all conceivable ways in which the data might cluster, this method is a reasonably general test.

5.6 Decoding neural responses

The goal of the decoding analysis was to train a trial-by-trial classifier that could identify left versus right choices but was tolerant of modality, or separated auditory from visual trials but was tolerant of choice. That is, we looked for a weighted sum of neurons such that the result was high for one choice and low for the other regardless of modality, and a second weighted sum of neurons that was high for one modality and low for the other regardless of choice.

For a neuron to be included in this analysis, we required at least 20 successful trials each for all four choice/modality pairs (only visual and auditory modalities were used). Most of our neurons were not recorded simultaneously; we therefore constructed "pseudo-trials" by choosing random trials of the desired condition (defined by choice and stimulus modality) for each neuron. The epoch from 500 to 700 ms after stimulus onset was used for training the classifier. We assembled as many pseudo-trials as possible by randomly sampling trials from each neuron without replacement; because the number of trials from each neuron was balanced across conditions when training the classifiers, the process was limited by the neuron with the fewest trials in any one condition (21–32). We then used a standard machine learning technique, the linear Support Vector Machine (SVM), to train one classifier for choice and a second for modality. Training was repeated 1,000 times with different random samples of pseudo-trials, resulting in 1,000 trained classifiers each for choice and stimulus modality. These were combined using a standard technique called bootstrap aggregation ("bagging"; see Breiman, 1996), described below.

Each of these classifiers is a vector consisting of a set of linear weights, with one weight per neuron. We averaged the 1,000 trained classifier vectors to obtain a

final classifier orientation for choice and a final classifier orientation for modality. In addition, the classifiers required a threshold. To obtain the thresholds, we randomly sampled additional balanced sets of pseudo-trials, projected them onto our classifier vector, and found the optimal threshold based on Gaussian fits to the two classes (high vs. low rate or visual vs. auditory). Classifier thresholds were averaged across 25 iterations of this process.

To test the performance of the classifier, we randomly sampled additional sets of pseudo-trials. Spike trains were filtered with a 100 ms boxcar, then each time point was classified. This was repeated 1,000 times and performance was averaged. To assess statistical significance, we assessed generalization performance on the epoch from 700 to 800 ms after stimulus onset. Performance of the classifier on 1,000 pseudo-trials was compared with the performance of 10,000 random classifiers on the same number of pseudo-trials. To generate the random classifiers, we first chose a random vector with n elements (n the number of neurons). Since different neurons have unequal variances and high-variance neurons will tend to be used more heavily by a trained classifier, we multiplied each element of the random vector by the standard deviation of the corresponding neuron. P-values are two-sided.

To interpret the weights chosen by the classifier, we examined whether only a subset of neurons might be used heavily, or whether all the neurons were used. To do so, we compared the distribution of weights from the classifier found using the real data with the distribution of weights from the random classifiers described above (shown as purple lines in Figure 3.10d,h). To evaluate whether the real classifier was significantly different from the random ones, we determined the kurtosis of the distribution of weights from the data, and the kurtosis for each random classifier. To obtain a p-value, we could then compare the kurtosis for the real classifier's weights to the distribution of kurtosis expected by chance. If the real classifiers weight kurtosis differed from chance, this would indicate either that fewer neurons were strongly involved in the classifier compared to a random classifier, or that neurons contributed more uniformly to the classifier than expected by chance. Neither of these was observed (all $p > 0.1$, two-sided).

5.7 Variance Alignment analysis

We initially reduced the dimensionality of the data as above to k dimensions (chosen as 8) using PCA. This step de-noised the data. For this analysis, the A matrix on which we performed PCA contained data from both the decision and movement epochs together; this ensured that the resulting space captured the structure of both epochs. We then determined the shape of the variance ellipsoid for the movement epoch alone (-200 to 800 ms from movement onset). That is, we rotated the data in the k-dimensional space so that the first dimension captured as much movement-epoch variance as possible, the second the next most, etc. This was accomplished using PCA on the (k-dimensional) movement-epoch data alone, retaining all components. The decision data was then rotated into this movement-determined orientation. For each dimension d (1 to k, horizontal axis in Fig. 3.13e), we could then determine how much variance was present in the decision data. These values were normalized by the maximum possible variance that could be captured in the same number of dimensions: if the rotation were found using PCA on the decision-epoch data itself. Perfect alignment would produce a unity Variance Alignment value, while maximal misalignment defines the lower bound (i.e., if the highest-variance dimension during the movement epoch were the lowest-variance dimension during the decision epoch). To determine the chance Variance Alignment, 10,000 randomly oriented orthogonal bases for the k-space were chosen. The confidence intervals shown in Figure 3.13e,f were derived from these random bases (not corrected for multiple comparisons).

To obtain a summary "Variance Alignment index", we computed the area between the data curve and the chance curve. If the data curve was above the chance curve, the index was taken as positive and was normalized by the area between the perfect alignment curve and the chance curve. If the data curve was below the chance curve, the index was taken as negative and was normalized by the area between the chance curve and the maximally misaligned curve. The index thus ranges from -1 (maximally misaligned) to 1 (perfectly aligned). This index was also computed for each of the 10,000 random orientations. The resulting chance distribution was used

to calculate a p-value (two-sided).

For a control comparison, we repeated this analysis on two different modality conditions (visual and multisensory) during the decision epoch. This is a useful comparison because if activity patterns during the visual condition and multisensory condition are aligned, it demonstrates that the finding of chance-level alignment during decision formation and movement truly results from misaligned states and not noise. For this analysis, we determined the ordering of dimensions using data from multisensory trials. Then, data from visual trials was rotated into the multisensory-determined orientation. This analysis was performed on rats 1–4; Rat 5 was excluded because this animal had some neurons for which multisensory trials were not collected.

To better interpret the result, we asked whether neurons that had strong stimulus-epoch modulation tended to have strong or weak movement-epoch modulation. To measure the depth of modulation for each neuron, we first created a vector containing the trial-averaged firing rate at each time point for each condition. For each neuron, there was one vector for the stimulus epoch (starting 300 ms before stimulus onset) and one vector for the movement epoch (-200 to 800 ms from movement onset). The variance of each vector was then taken. Since the resulting distributions were approximately log-normal, we took the log of these values before correlating them.

5.8 Testing for linear and nonlinear components of neurons' responses

We wished to test how much of neurons' tuning was a linear function of choice or stimulus modality, and how much was a function of nonlinear interaction between choice and stimulus modality. To determine this, we considered one neuron at a time, and analyzed only successful visual and auditory trials (multisensory trials and failures were excluded). We first reduced the neurons response on each trial to a single number: the spike count in a 200 ms window of time (600 to 800 ms after stimulus onset). This produced a spike count vector y with as many elements as included

trials. Our model of the neuron's response was:

$$y = X\,\beta + \eta \tag{5.10}$$

where X is a design matrix (see below), β is a vector of regression coefficients, and η is a noise term. The design matrix X was of size r by 4, with r the number of trials. Each row summarized the conditions for the corresponding trial. For each row, the first element was always one, to capture the mean across trials. The second element captured choice preference, set to $+1$ for rightward trials and -1 for leftward trials. The third element captured modality preference, set to $+1$ for visual trials and -1 for auditory trials. The last element captured the interaction, set to $+1$ for visual rightward trials and auditory leftward trials, and -1 otherwise.

To find β, we performed a Generalized Linear Model regression (GLM regression; see Nelder and Wedderburn, 1972) with a Poisson noise distribution (since single-trial spike counts are typically assumed to have Poisson noise). In order to have orthogonal columns of X, it was necessary to have equal numbers of trials for each combination of left and right and visual and auditory. We therefore randomly downsampled trials to make these groups equal size before performing the regression. This was done 100 times for each neuron, and the resulting β's were averaged. For analysis, we examined the two linear terms of β and compared them with the final, interaction term of β.

5.9 Surgical procedures

All rats subject to surgery were anesthetized with isoflurane and administered 5 mg/kg ketoprofen before surgery for analgesia. Isoflurane anesthesia was maintained by monitoring respiration and foot pinch responses throughout the surgical procedure. Ophthalmic ointment was applied to keep the eyes moistened throughout surgery. Lidocaine solution (~ 0.1 mL) was injected below the scalp to provide local analgesia prior to performing scalp incisions. 0.05 mg/kg buprenorphine was administered daily for post-surgery analgesia (usually 2–3 days). All surgical procedures conformed to the guidelines established by the National Institutes of Health and were approved by

the Institutional Animal Care and Use Committee of Cold Spring Harbor Laboratory.

5.9.1 Injections

Two rats, 3–5 weeks of age, were anesthetized and placed in a stereotaxic apparatus (Kopf Instruments). Small craniotomies were made over PPC (3.8 mm posterior to Bregma; 2.2, 3.2, and 4.2 mm left/right of midline). One of the rats was subject to unilateral injections (left hemisphere), and the second rat was subject to bilateral injections. Small durotomies were performed at each craniotomy and virus was pressure injected at depths of 400, 600, and 800 μm below the pia (140 nL/depth) using calibrated pipettes and a syringe (rate of $\sim$ 1 nL/second). 2–3 minutes were allowed following injection at each depth to allow for diffusion of virus. Adeno-associated virus expressing muscarinic receptor hM4D-mCitrine under an hSyn promoter (AAV5-hSyn-HA-hM4D-IRES-mCitrine; construct provided by Bryan Roth, UNC; virus produced by UNC Gene Therapy Center) was used.

5.9.2 Cannulae implant

Rats were anesthetized and placed in the stereotax. Two craniotomies were made on each side of the brain; these were positioned to cover medial and lateral PPC on each side (4.0 mm posterior to Bregma and extending from 2.0 to 3.6 mm left/right of midline). Durotomies were performed and a double guide cannula (PlasticsOne, C235G-1.2) was placed in the brain 100–200 μm below the pia at each craniotomy. The exposed brain was covered with 2% agarose solution and both cannulae were anchored to the skull with dental acrylic (Lang Dental).

5.9.3 Tetrode array implant

After scalp shaving and incision, the skull was cleaned, and anchoring screws were drilled into 6 locations on the skull. Dental cement (Parkell, Inc.) was applied to the skull surface and a craniotomy was made above left PPC (4 mm posterior to Bregma; 2.5 mm left of midline; $\sim$ 2.4 mm anteroposterior $\times$ $\sim$ 3.4 mm mediolateral

in size). A durotomy was performed and the implant assembly was lowered until the tetrodes just penetrated the pial surface. 2% agarose solution was applied to cover the tetrodes and craniotomy, and dental acrylic (Lang Dental) was applied to secure the implant to the skull. The incision was closed around the base of the implant using Vetbond (3M). Following surgery, tetrodes were advanced in increments of 40–80 μm until action potentials were encountered.

5.10 Inactivations

5.10.1 Muscimol inactivation sessions

Muscimol was infused into PPC with a concentration of 0.5–1.0 mg/mL and a volume of 0.3 μL per site. A double-internal cannula (PlasticsOne, C235I/SP), connected to 2 microliter syringes (Hamilton microliter syringe, 7000 series), was inserted into each previously implanted guide cannula. Internal cannulae extended 0.5 mm below the guide (estimated 600–700 μm below the pia). Muscimol was delivered using an infusion pump (Harvard PHD 22/2000) at a rate of 0.1 μL/min. Internal cannulae were kept in the brain for 3–5 additional minutes to allow for diffusion of muscimol. Rats were removed from anesthesia and returned to cages for 30 minutes before beginning behavioral sessions. The same procedure was used in control sessions, where muscimol was replaced with sterile saline.

5.10.2 DREADD inactivation sessions

Prior to DREADD inactivation and control sessions, clozapine N-oxide (CNO, 1 mg/kg) or sterile saline was injected intraperitoneally into rats expressing the muscarinic receptor hM4D. Animals were returned to their cages for 30 minutes post-injection before beginning behavioral sessions.

5.11 Histology

At the conclusion of physiological experiments, animals were deeply anesthetized with ketamine and medetomidine. To indicate the final positions of electrodes, electrolytic lesions were made at the tetrode tips by passing 30 μA current through each electrode for $\sim$ 10–15 seconds. After lesioning, animals were perfused transcardially with 4% paraformaldehyde. Brains were extracted and post-fixed in 4% paraformaldehyde for 24–48 hours. After post-fixing, 100 μm coronal sections were cut from one of the brains on a vibratome (Leica).

At the conclusion of inactivation experiments, both animals that had been injected with DREADD were perfused transcardially with 4% paraformaldehye. One of the brains was extracted, post-fixed and sectioned following the protocol described above. The second brain was post-fixed, then kept in 30% sucrose solution for 48 hours, then frozen at -80° C. 20 μm coronal sections were cut from this brain using a cryostat (Leica CM1850). In both cases, brain sections were mounted on slides with Vectashield mounting medium.

5.11.1 Quantification of DREADD expression

Brain sections were imaged using an epifluorescence microscope. The resulting images were analyzed with MATLAB software. A region of interest (ROI) was manually defined for each brain section that was analyzed. The ROI extended from $\sim$ 1.5 to 5.0 mm lateral to the midline and $\sim$ 0.2 to 1 mm below the pia. A second, smaller ROI was defined near the first one, in a region that was not infected by the virus (which thus should have had no expression). This region was used as a measure for baseline pixel intensity. Average pixel intensity across columns of pixels was calculated inside the first ROI, then normalized by the average pixel intensity inside the second ROI (baseline). To quantify expression levels on a particular brain section, we calculated the area below the average pixel intensity curve for that section and above baseline (a flat line at unity). We used this measurement to compare the expression levels in two places: at the border between PPC and secondary visual cortex, and near the

injection site in PPC.

6

Final remarks

We developed a novel behavioral paradigm particularly useful for the study of multisensory decision-making in rodents. This paradigm allowed us to show that improvement in decision accuracy due to multisensory integration is not restricted to humans and non-human primates. We found that rats are, as primates, able to use visual and auditory information to make decisions, as it arrives over time, and they weigh that information in an optimal way, so as to minimize the variance of their perceptual judgments. Our results using this task open possibilities to further understand the computations that allow the brain to combine information across time and sensory modalities. It also opens doors for the rodent model to be more widely used both in multisensory and decision-making studies. The genetic and optogenetic techniques available nowadays for this animal model will be, in our view, critical to uncover the circuits and computations used by the brain during perceptual decisions.

The inactivation experiments presented here suggest that the posterior parietal cortex is required for accurate decisions informed by the visual system. This is, to our knowledge, the first study to reveal the impact of temporarily shutting down this area during perceptual judgments. Our results also suggest that, even though PPC receives inputs from primary auditory cortex as well as visual cortex, the area is not required for auditory decisions or multisensory integration. This argues in favor of a more sensory related, visual role for PPC, as it is defined today. Recent work have shown that PPC in rats exhibits significant differences along the medial-lateral

axis, defining subregions that may have distinct functions (Wilber et al., 2014). An important line of work would be to explore the role of these different subregions within PPC.

One of the main results of this work came from electrophysiological recordings that we have done in the PPC of rats performing our task. We have shown that the different responses of PPC neurons cannot be grouped into categories. In other words, neurons' response features are randomly distributed across the population. This configuration provides a flexible way for one single brain area to encode multiple variables which can be easily (linearly) decoded by single downstream neurons. An open question is then what variables, encoded in PPC, are being passed on and read out by downstream areas. One possibility is that PPC is providing information to premotor areas about abstract features of a visual stimulus, so that different categorical choices can be effectuated in different situations. It is conceivable that one of those features transmitted by PPC is the accumulated visual evidence in favor or against a particular choice, as suggested by the primate decision-making literature. Further experiments, in which the activity of PPC and one of its downstream areas is monitored simultaneously, would perhaps bring us closer to answering this question.

The optogenetic experiments developed in this work reveal, for the first time, the consequences of spatial and temporally precise disruption of PPC during a decision-making task. Our results point to a causal role of this area in visual decisions and suggest a slow recovery of the network to its normal state after a short disruption. Future experiments must take place to explain the nature of this causal role. It would be important to distinguish if the the optogenetic disruption causes an attentional deficit or, instead, an inability to integrate visual evidence, for example. An approach similar to the one we used in these experiments can be used to disrupt specific inputs to PPC. Stimulation of only the axonal terminals of neurons that project from visual cortex to PPC may provide insights into the computations implemented by PPC and, more generally, the nature of its role in visual decisions.

References

Alais, D. and Burr, D. The ventriloquist effect results from near-optimal bimodal integration. *Current Biology*, 14(3):257–262, February 2004.

Alais, D., Newell, F. N., and Mamassian, P. Multisensory processing in review: from physiology to behaviour. *Seeing and perceiving*, 23(1):3–38, 2010.

Albright, T. D., Desimone, R., and Gross, C. G. Columnar organization of directionally selective cells in visual area MT of the macaque. *Journal of neurophysiology*, 51(1):16–31, January 1984.

Andersen, R. A., Asanuma, C., Essick, G., and Siegel, R. M. Corticocortical connections of anatomically and physiologically defined subdivisions within the inferior parietal lobule. *The Journal of comparative neurology*, 296(1):65–113, June 1990.

Angelaki, D. E., Gu, Y., and DeAngelis, G. C. Multisensory integration: psychophysics, neurophysiology, and computation. *Current opinion in neurobiology*, 19(4):452–458, August 2009.

Aravanis, A. M., Wang, L.-P., Zhang, F., Meltzer, L. A., Mogri, M. Z., Schneider, M. B., and Deisseroth, K. An optical neural interface: in vivo control of rodent motor cortex with integrated fiberoptic and optogenetic technology. *Journal of neural engineering*, 4(3):S143–56, September 2007.

Arimura, N., Nakayama, Y., Yamagata, T., Tanji, J., and Hoshi, E. Involvement of the globus pallidus in behavioral goal determination and action specification. *The Journal of neuroscience*, 33(34):13639–13653, August 2013.

Avillac, M., Denève, S., Olivier, E., Pouget, A., and Duhamel, J.-R. Reference frames for representing visual and tactile locations in parietal cortex. *Nature neuroscience*, 8(7):941–949, July 2005.

Avillac, M., Ben Hamed, S., and Duhamel, J.-R. Multisensory integration in the ventral intraparietal area of the macaque monkey. *The Journal of neuroscience*, 27 (8):1922–1932, February 2007.

Balan, P. F. and Gottlieb, J. Functional significance of nonspatial information in monkey lateral intraparietal area. *The Journal of neuroscience*, 29(25):8166–8176, June 2009.

Balan, P. F., Oristaglio, J., Schneider, D. M., and Gottlieb, J. Neuronal correlates of the set-size effect in monkey lateral intraparietal area. *PLoS biology*, 6(7):e158, July 2008.

Barlow, H. B. Summation and inhibition in the frog's retina. *The Journal of physiology*, 119(1):69–88, January 1953.

Battaglia, P. W., Jacobs, R. A., and Aslin, R. N. Bayesian integration of visual and auditory signals for spatial localization. *Journal of the Optical Society of America. A, Optics, image science, and vision*, 20(7):1391–1397, July 2003.

Beck, J. M., Ma, W. J., Kiani, R., Hanks, T., Churchland, A. K., Roitman, J., Shadlen, M. N., Latham, P. E., and Pouget, A. Probabilistic population codes for Bayesian decision making. *Neuron*, 60(6):1142–1152, December 2008.

Benjamini, Y. and Hochberg, Y. Controlling the false discovery rate: A practical and powerful approach to multiple testing. *Journal of the Royal Statistical Society Series B (Methodological)*, 57(1):289–300, 1995.

Boyden, E. S., Zhang, F., Bamberg, E., Nagel, G., and Deisseroth, K. Millisecond-timescale, genetically targeted optical control of neural activity. *Nature neuroscience*, 8(9):1263–1268, September 2005.

Breiman, L. Bagging predictors. *Machine learning*, 24(2):123–140, 1996.

Britten, K. H., Shadlen, M. N., Newsome, W. T., and Movshon, J. A. The analysis of visual motion: a comparison of neuronal and psychophysical performance. *The Journal of neuroscience*, 12(12):4745–4765, December 1992.

Britten, K. H., Newsome, W. T., Shadlen, M. N., Celebrini, S., and Movshon, J. A. A relationship between behavioral choice and the visual responses of neurons in macaque MT. *Visual neuroscience*, 13(1):87–100, January 1996.

Brunton, B. W., Botvinick, M. M., and Brody, C. D. Rats and humans can optimally accumulate evidence for decision-making. *Science (New York, N.Y.)*, 340(6128): 95–98, April 2013.

Burr, D., Silva, O., Cicchini, G. M., Banks, M. S., and Morrone, M. C. Temporal mechanisms of multimodal binding. *Proceedings. Biological sciences / The Royal Society*, 276(1663):1761–1769, May 2009.

Busse, L., Ayaz, A., Dhruv, N. T., Katzner, S., Saleem, A. B., Schölvinck, M. L., Zaharia, A. D., and Carandini, M. The detection of visual contrast in the behaving mouse. *The Journal of neuroscience*, 31(31):11351–11361, August 2011.

Carandini, M., Heeger, D. J., and Movshon, J. A. Linearity and normalization in simple cells of the macaque primary visual cortex. *The Journal of neuroscience*, 17 (21):8621–8644, November 1997.

Chandler, H. C., King, V., Corwin, J. V., and Reep, R. L. Thalamocortical connections of rat posterior parietal cortex. *Neuroscience letters*, 143(1-2):237–242, August 1992.

Chen, J. L., Carta, S., Soldado-Magraner, J., Schneider, B. L., and Helmchen, F. Behaviour-dependent recruitment of long-range projection neurons in somatosensory cortex. *Nature*, 499(7458):336–340, July 2013.

Churchland, A. K. and Lisberger, S. G. Discharge properties of MST neurons that project to the frontal pursuit area in macaque monkeys. *Journal of neurophysiology*, 94(2):1084–1090, August 2005.

Churchland, A. K., Kiani, R., and Shadlen, M. N. Decision-making with multiple alternatives. *Nature neuroscience*, 11(6):693–702, June 2008.

Clark, J. and Yuille, A. Shape from shading via the fusion of specular and lambertian image components. 1:88–92, 1990.

Cordes, S., Gallistel, C. R., Gelman, R., and Latham, P. Nonverbal arithmetic in humans: light from noise. *Perception & psychophysics*, 69(7):1185–1203, October 2007.

Cortes, C. and Vapnik, V. Support-vector networks. *Machine Learning*, 20:273–297, 1995.

Corwin, J. V., Fussinger, M., Meyer, R. C., King, V. R., and Reep, R. L. Bilateral destruction of the ventrolateral orbital cortex produces allocentric but not egocentric spatial deficits in rats. *Behavioural brain research*, 61(1):79–86, March 1994.

Deneve, S., Latham, P. E., and Pouget, A. Efficient computation and cue integration with noisy population codes. *Nature neuroscience*, 4(8):826–831, August 2001.

Duffy, C. J. MST neurons respond to optic flow and translational movement. *Journal of neurophysiology*, 80(4):1816–1827, October 1998.

El-Shamayleh, Y., Kumbhani, R. D., Dhruv, N. T., and Movshon, J. A. Visual response properties of V1 neurons projecting to V2 in macaque. *The Journal of neuroscience*, 33(42):16594–16605, October 2013.

Erlich, J. C., Bialek, M., and Brody, C. D. A cortical substrate for memory-guided orienting in the rat. *Neuron*, 72(2):330–343, October 2011.

Ernst, M. O., Banks, M. S., and Bülthoff, H. H. Touch can change visual slant perception. *Nature neuroscience*, 3(1):69–73, January 2000.

Ernst, M. O. and Banks, M. S. Humans integrate visual and haptic information in a statistically optimal fashion. *Nature*, 415(6870):429–433, January 2002.

Ernst, M. O. and Bülthoff, H. H. Merging the senses into a robust percept. *Trends in cognitive sciences*, 8(4):162–169, April 2004.

Feierstein, C. E., Quirk, M. C., Uchida, N., Sosulski, D. L., and Mainen, Z. F. Representation of spatial goals in rat orbitofrontal cortex. *Neuron*, 51(4):495–507, August 2006.

Felleman, D. J. and Van Essen, D. C. Distributed hierarchical processing in the primate cerebral cortex. *Cerebral cortex (New York, N.Y.: 1991)*, 1(1):1–47, January 1991.

Fetsch, C. R., Turner, A. H., DeAngelis, G. C., and Angelaki, D. E. Dynamic reweighting of visual and vestibular cues during self-motion perception. *The Journal of neuroscience*, 29(49):15601–15612, December 2009.

Fetsch, C. R., Pouget, A., DeAngelis, G. C., and Angelaki, D. E. Neural correlates of reliability-based cue weighting during multisensory integration. *Nature neuroscience*, 15(1):146–154, January 2012.

Fine, I. and Jacobs, R. A. Modeling the combination of motion, stereo, and vergence angle cues to visual depth. *Neural computation*, 11(6):1297–1330, August 1999.

Freedman, D. J. and Assad, J. A. Experience-dependent representation of visual categories in parietal cortex. *Nature*, 443(7107):85–88, September 2006.

Freedman, D. J. and Assad, J. A. Distinct encoding of spatial and nonspatial visual information in parietal cortex. *The Journal of neuroscience*, 29(17):5671–5680, April 2009.

Fujisaki, W. and Nishida, S. Temporal frequency characteristics of synchrony-asynchrony discrimination of audio-visual signals. *Experimental brain research*, 166(3-4):455–464, October 2005.

Ganguli, S. and Sompolinsky, H. Compressed sensing, sparsity, and dimensionality in neuronal information processing and data analysis. *Annual review of neuroscience*, 35(1):485–508, 2012.

Georgopoulos, A. P., Kalaska, J. F., Caminiti, R., and Massey, J. T. On the relations between the direction of two-dimensional arm movements and cell discharge in primate motor cortex. *The Journal of neuroscience*, 2(11):1527–1537, November 1982.

Ghahramani, Z. and Wolpert, D. M. Modular decomposition in visuomotor learning. *Nature*, 386(6623):392–395, March 1997.

Ghazanfar, A. A., Maier, J. X., Hoffman, K. L., and Logothetis, N. K. Multisensory integration of dynamic faces and voices in rhesus monkey auditory cortex. *The Journal of neuroscience*, 25(20):5004–5012, May 2005.

Glickfeld, L. L., Histed, M. H., and Maunsell, J. H. R. Mouse primary visual cortex is used to detect both orientation and contrast changes. *The Journal of neuroscience*, 33(50):19416–19422, December 2013.

Gnadt, J. W. and Andersen, R. A. Memory related motor planning activity in posterior parietal cortex of macaque. *Experimental brain research*, 70(1):216–220, 1988.

Gold, J. I. and Shadlen, M. N. The neural basis of decision making. *Annual review of neuroscience*, 30(1):535–574, 2007.

Graham, N. V. S. *Visual pattern analysers*. Oxford University Press, Oxford, 1989.

Green, D. M. and Swets, J. A. Signal detection theory and psychophysics. 1966.

Gu, Y., Angelaki, D. E., and DeAngelis, G. C. Neural correlates of multisensory cue integration in macaque MSTd. *Nature neuroscience*, 11(10):1201–1210, October 2008.

Hanks, T. D., Ditterich, J., and Shadlen, M. N. Microstimulation of macaque area LIP affects decision-making in a motion discrimination task. *Nature neuroscience*, 9(5):682–689, May 2006.

Hardy, S. G. and Lynch, J. C. The spatial distribution of pulvinar neurons that project to two subregions of the inferior parietal lobule in the macaque. *Cerebral cortex*, 2(3):217–230, May 1992.

Harvey, C. D., Coen, P., and Tank, D. W. Choice-specific sequences in parietal cortex during a virtual-navigation decision task. *Nature*, 484(7392):62–68, April 2012.

Heeger, D. J. Normalization of cell responses in cat striate cortex. *Visual neuroscience*, 9(2):181–197, August 1992.

Heeger, D. J. Modeling simple-cell direction selectivity with normalized, half-squared, linear operators. *Journal of neurophysiology*, 70(5):1885–1898, November 1993.

Hillis, J. M., Watt, S. J., Landy, M. S., and Banks, M. S. Slant from texture and disparity cues: optimal cue combination. *Journal of vision*, 4(12):967–992, December 2004.

Hirokawa, J., Bosch, M., Sakata, S., Sakurai, Y., and Yamamori, T. Functional role of the secondary visual cortex in multisensory facilitation in rats. *Neuroscience*, 153(4):1402–1417, June 2008.

Hirokawa, J., Sadakane, O., Sakata, S., Bosch, M., Sakurai, Y., and Yamamori, T. Multisensory information facilitates reaction speed by enlarging activity difference between superior colliculus hemispheres in rats. *PloS one*, 6(9):e25283, 2011.

Huk, A. C. and Meister, M. L. R. Neural correlates and neural computations in posterior parietal cortex during perceptual decision-making. *Frontiers in integrative neuroscience*, 6:86, 2012.

Indyk, P. and Motwani, R. Approximate nearest neighbors: towards removing the curse of dimensionality. *Proc. Annu. ACM Symp. Theory Comput., 30th*, pages 604–613, 1998.

Jacobs, R. A. Optimal integration of texture and motion cues to depth. *Vision Research*, 39(21):3621–3629, 1999.

Jiang, W., Wallace, M. T., Jiang, H., Vaughan, J. W., and Stein, B. E. Two cortical areas mediate multisensory integration in superior colliculus neurons. *Journal of neurophysiology*, 85(2):506–522, February 2001.

Kaufman, M. T., Churchland, M. M., Ryu, S. I., and Shenoy, K. V. Cortical activity in the null space: permitting preparation without movement. *Nature neuroscience*, 17(3):440–448, March 2014.

Kiani, R. and Shadlen, M. N. Representation of confidence associated with a decision by neurons in the parietal cortex. *Science (New York, N.Y.)*, 324(5928):759–764, May 2009.

Kiani, R., Hanks, T. D., and Shadlen, M. N. Bounded integration in parietal cortex underlies decisions even when viewing duration is dictated by the environment. *The Journal of neuroscience*, 28(12):3017–3029, March 2008.

King, V. R. and Corwin, J. V. Comparisons of hemi-inattention produced by unilateral lesions of the posterior parietal cortex or medial agranular prefrontal cortex in rats: neglect, extinction, and the role of stimulus distance. *Behavioural brain research*, 54(2):117–131, April 1993.

Knill, D. C. and Pouget, A. The Bayesian brain: the role of uncertainty in neural coding and computation. *Trends in neurosciences*, 27(12):712–719, December 2004.

Knill, D. C. and Saunders, J. A. Do humans optimally integrate stereo and texture information for judgments of surface slant? *Vision research*, 43(24):2539–2558, November 2003.

Kolb, B. E. and Tees, R. C. *The cerebral cortex of the rat.* The MIT Press, 1990.

Körding, K. P., Beierholm, U., Ma, W. J., Quartz, S., Tenenbaum, J. B., and Shams, L. Causal inference in multisensory perception. *PloS one*, 2(9):e943, 2007.

Kuffler, S. W. Discharge patterns and functional organization of mammalian retina. *Journal of neurophysiology*, 16(1):37–68, January 1953.

Landy, M. S. and Kojima, H. Ideal cue combination for localizing texture-defined edges. *Journal of the Optical Society of America. A, Optics, image science, and vision*, 18(9):2307–2320, September 2001.

Li, C. S., Mazzoni, P., and Andersen, R. A. Effect of reversible inactivation of macaque lateral intraparietal area on visual and memory saccades. *Journal of neurophysiology*, 81(4):1827–1838, April 1999.

Linden, J. F., Grunewald, A., and Andersen, R. A. Responses to auditory stimuli in macaque lateral intraparietal area. II. Behavioral modulation. *Journal of neurophysiology*, 82(1):343–358, July 1999.

Link, S. W. and Heath, R. A. A sequential theory of psychological discrimination. *Psychometrika*, 40:77–105, 1975.

Lopes, G., Bonacchi, N., Frazão, J., Neto, J. P., Atallah, B. V., Soares, S., Moreira, L., Matias, S., Itskov, P. M., Correia, P. A., Medina, R. E., Calcaterra, L., Dreosti, E., Paton, J. J., and Kampff, A. R. Bonsai: an event-based framework for processing and controlling data streams. *Frontiers in neuroinformatics*, 9:7, 2015.

Lovelace, C. T., Stein, B. E., and Wallace, M. T. An irrelevant light enhances auditory detection in humans: a psychophysical analysis of multisensory integration in stimulus detection. *Brain research. Cognitive brain research*, 17(2):447–453, July 2003.

Ma, W. J., Beck, J. M., Latham, P. E., and Pouget, A. Bayesian inference with probabilistic population codes. *Nature neuroscience*, 9(11):1432–1438, November 2006.

Mante, V., Sussillo, D., Shenoy, K. V., and Newsome, W. T. Context-dependent computation by recurrent dynamics in prefrontal cortex. *Nature*, 503(7474):78–84, November 2013.

Maunsell, J. H. and Gibson, J. R. Visual response latencies in striate cortex of the macaque monkey. *Journal of neurophysiology*, 68(4):1332–1344, October 1992.

Mazurek, M. E., Roitman, J. D., Ditterich, J., and Shadlen, M. N. A role for neural integrators in perceptual decision making. *Cerebral cortex (New York, N.Y.: 1991)*, 13(11):1257–1269, November 2003.

Mazzoni, P., Bracewell, R. M., Barash, S., and Andersen, R. A. Motor intention activity in the macaque's lateral intraparietal area. I. Dissociation of motor plan from sensory memory. *Journal of neurophysiology*, 76(3):1439–1456, September 1996.

Meister, M. L. R., Hennig, J. A., and Huk, A. C. Signal multiplexing and single-neuron computations in lateral intraparietal area during decision-making. *The Journal of neuroscience*, 33(6):2254–2267, February 2013.

Meredith, M. A., Nemitz, J. W., and Stein, B. E. Determinants of multisensory integration in superior colliculus neurons. I. Temporal factors. *The Journal of neuroscience*, 7(10):3215–3229, October 1987.

Miller, E. K. and Cohen, J. D. An integrative theory of prefrontal cortex function. *Annual review of neuroscience*, 24(1):167–202, 2001.

Miller, L. M. and D'Esposito, M. Perceptual fusion and stimulus coincidence in the cross-modal integration of speech. *The Journal of neuroscience*, 25(25):5884–5893, June 2005.

Morgan, M. L., DeAngelis, G. C., and Angelaki, D. E. Multisensory integration in macaque visual cortex depends on cue reliability. *Neuron*, 59(4):662–673, August 2008.

Movshon, J. A. and Newsome, W. T. Visual response properties of striate cortical neurons projecting to area MT in macaque monkeys. *The Journal of neuroscience*, 16(23):7733–7741, December 1996.

Mullette-Gillman, O. A., Cohen, Y. E., and Groh, J. M. Eye-centered, head-centered, and complex coding of visual and auditory targets in the intraparietal sulcus. *Journal of neurophysiology*, 94(4):2331–2352, October 2005.

Myskiw, J. C. and Izquierdo, I. Posterior parietal cortex and long-term memory: some data from laboratory animals. *Frontiers in integrative neuroscience*, 6:8, 2012.

Nelder, J. A. and Wedderburn, R. W. M. Generalized linear models. *Journal of the Royal Statistical Society. Series A (General)*, 135(3):370–384, 1972.

Newsome, W. T. and Paré, E. B. A selective impairment of motion perception following lesions of the middle temporal visual area (MT). *The Journal of neuroscience*, 8(6):2201–2211, June 1988.

Newsome, W. T., Britten, K. H., and Movshon, J. A. Neuronal correlates of a perceptual decision. *Nature*, 341(6237):52–54, September 1989.

Nieder, A. and Miller, E. K. A parieto-frontal network for visual numerical information in the monkey. *Proceedings of the National Academy of Sciences of the United States of America*, 101(19):7457–7462, May 2004.

Nienborg, H. and Cumming, B. G. Macaque V2 neurons, but not V1 neurons, show choice-related activity. *The Journal of neuroscience*, 26(37):9567–9578, September 2006.

Ohshiro, T., Angelaki, D. E., and DeAngelis, G. C. A normalization model of multisensory integration. *Nature neuroscience*, 14(6):775–782, June 2011.

Pagan, M., Urban, L. S., Wohl, M. P., and Rust, N. C. Signals in inferotemporal and perirhinal cortex suggest an untangling of visual target information. *Nature neuroscience*, 16(8):1132–1139, August 2013.

Palmer, J., Huk, A. C., and Shadlen, M. N. The effect of stimulus strength on the speed and accuracy of a perceptual decision. *Journal of vision*, 5(5):376–404, 2005.

Paré, M. and Wurtz, R. H. Progression in neuronal processing for saccadic eye movements from parietal cortex area lip to superior colliculus. *Journal of neurophysiology*, 85(6):2545–2562, June 2001.

Park, I. M., Meister, M. L. R., Huk, A. C., and Pillow, J. W. Encoding and decoding in parietal cortex during sensorimotor decision-making. *Nature neuroscience*, 17 (10):1395–1403, October 2014.

Pelli, D. G. The videotoolbox software for visual psychophysics: Transforming numbers into movies. *Spatial vision*, 10(4):437–442, 1997.

Pfingst, B. E. and O'Connor, T. A. Characteristics of neurons in auditory cortex of monkeys performing a simple auditory task. *Journal of neurophysiology*, 45(1): 16–34, January 1981.

Platt, M. L. and Glimcher, P. W. Neural correlates of decision variables in parietal cortex. *Nature*, 400(6741):233–238, July 1999.

Pouget, A. and Sejnowski, T. J. Spatial transformations in the parietal cortex using basis functions. *Journal of cognitive neuroscience*, 9(2):222–237, March 1997.

Pouget, A., Dayan, P., and Zemel, R. Information processing with population codes. *Nature reviews. Neuroscience*, 1(2):125–132, November 2000.

Powers, A. R., Hillock, A. R., and Wallace, M. T. Perceptual training narrows the temporal window of multisensory binding. *The Journal of neuroscience*, 29(39): 12265–12274, September 2009.

Raposo, D., Sheppard, J. P., Schrater, P. R., and Churchland, A. K. Multisensory decision-making in rats and humans. *The Journal of neuroscience*, 32(11):3726–3735, March 2012.

Raposo, D., Kaufman, M. T., and Churchland, A. K. A category-free neural population supports evolving demands during decision-making. *Nature neuroscience*, 17 (12):1784–1792, December 2014.

Ratcliff, R. A theory of memory retrieval. *Psychological Review*, 85(2):59–108, March 1978.

Recanzone, G. H., Guard, D. C., and Phan, M. L. Frequency and intensity response properties of single neurons in the auditory cortex of the behaving macaque monkey. *Journal of neurophysiology*, 83(4):2315–2331, April 2000.

Recanzone, G. H. Auditory influences on visual temporal rate perception. *Journal of neurophysiology*, 89(2):1078–1093, February 2003.

Reep, R. L., Chandler, H. C., King, V., and Corwin, J. V. Rat posterior parietal cortex: topography of corticocortical and thalamic connections. *Experimental brain research*, 100(1):67–84, 1994.

Reep, R. L. and Corwin, J. V. Posterior parietal cortex as part of a neural network for directed attention in rats. *Neurobiology of learning and memory*, 91(2):104–113, February 2009.

Reynolds, J. H. and Heeger, D. J. The normalization model of attention. *Neuron*, 61 (2):168–185, January 2009.

Rigotti, M., Barak, O., Warden, M. R., Wang, X.-J., Daw, N. D., Miller, E. K., and Fusi, S. The importance of mixed selectivity in complex cognitive tasks. *Nature*, 497(7451):585–590, May 2013.

Rishel, C. A., Huang, G., and Freedman, D. J. Independent category and spatial encoding in parietal cortex. *Neuron*, 77(5):969–979, March 2013.

Robinson, S. and Bucci, D. J. Damage to posterior parietal cortex impairs two forms of relational learning. *Frontiers in integrative neuroscience*, 6:45, 2012.

Rogan, S. C. and Roth, B. L. Remote control of neuronal signaling. *Pharmacological reviews*, 63(2):291–315, June 2011.

Roitman, J. D. and Shadlen, M. N. Response of neurons in the lateral intraparietal area during a combined visual discrimination reaction time task. *The Journal of neuroscience*, 22(21):9475–9489, November 2002.

Roth, E. D., Yu, X., Rao, G., and Knierim, J. J. Functional differences in the backward shifts of CA1 and CA3 place fields in novel and familiar environments. *PloS one*, 7(4):e36035, 2012.

Russo, G. S., Backus, D. A., Ye, S., and Crutcher, M. D. Neural activity in monkey dorsal and ventral cingulate motor areas: comparison with the supplementary motor area. *Journal of neurophysiology*, 88(5):2612–2629, November 2002.

Rust, N. C. and Dicarlo, J. J. Selectivity and tolerance ("invariance") both increase as visual information propagates from cortical area V4 to IT. *The Journal of neuroscience*, 30(39):12978–12995, September 2010.

Sakata, S., Yamamori, T., and Sakurai, Y. Behavioral studies of auditory-visual spatial recognition and integration in rats. *Experimental brain research*, 159(4): 409–417, December 2004.

Saleem, A. B., Ayaz, A., Jeffery, K. J., Harris, K. D., and Carandini, M. Integration of visual motion and locomotion in mouse visual cortex. *Nature neuroscience*, 16 (12):1864–1869, 2013.

Salinas, E. and Abbott, L. F. Vector reconstruction from firing rates. *Journal of computational neuroscience*, 1(1-2):89–107, June 1994.

Salinas, E. Context-dependent selection of visuomotor maps. *BMC neuroscience*, 5 (1):47, 2004.

Salzman, C. D., Britten, K. H., and Newsome, W. T. Cortical microstimulation influences perceptual judgements of motion direction. *Nature*, 346(6280):174–177, July 1990.

Sanger, T. D. Probability density estimation for the interpretation of neural population codes. *Journal of neurophysiology*, 76(4):2790–2793, October 1996.

Sclar, G. and Freeman, R. D. Orientation selectivity in the cat's striate cortex is invariant with stimulus contrast. *Experimental brain research*, 46(3):457–461, 1982.

Segraves, M. A. Activity of monkey frontal eye field neurons projecting to oculomotor regions of the pons. *Journal of neurophysiology*, 68(6):1967–1985, December 1992.

Senkowski, D., Schneider, T. R., Foxe, J. J., and Engel, A. K. Crossmodal binding through neural coherence: implications for multisensory processing. *Trends in neurosciences*, 31(8):401–409, August 2008.

Serwe, S., Körding, K. P., and Trommershäuser, J. Visual-haptic cue integration with spatial and temporal disparity during pointing movements. *Experimental brain research*, 210(1):67–80, April 2011.

Shadlen, M. N. and Newsome, W. T. Motion perception: seeing and deciding. *Proceedings of the National Academy of Sciences of the United States of America*, 93 (2):628–633, January 1996.

Shadlen, M. N., Britten, K. H., Newsome, W. T., and Movshon, J. A. A computational analysis of the relationship between neuronal and behavioral responses to visual motion. *The Journal of neuroscience*, 16(4):1486–1510, February 1996.

Shadlen, M. N. and Kiani, R. Decision making as a window on cognition. *Neuron*, 80(3):791–806, October 2013.

Shams, L., Kamitani, Y., and Shimojo, S. Visual illusion induced by sound. *Brain research. Cognitive brain research*, 14(1):147–152, June 2002.

Sheppard, J. P., Raposo, D., and Churchland, A. K. Dynamic weighting of multisensory stimuli shapes decision-making in rats and humans. *Journal of vision*, 13(6): 4–4, 2013.

Slutsky, D. A. and Recanzone, G. H. Temporal and spatial dependency of the ventriloquism effect. *Neuroreport*, 12(1):7–10, January 2001.

Stanford, T. R., Quessy, S., and Stein, B. E. Evaluating the operations underlying multisensory integration in the cat superior colliculus. *The Journal of neuroscience*, 25(28):6499–6508, July 2005.

Sugrue, L. P., Corrado, G. S., and Newsome, W. T. Matching behavior and the representation of value in the parietal cortex. *Science (New York, N.Y.)*, 304 (5678):1782–1787, June 2004.

Sugrue, L. P., Corrado, G. S., and Newsome, W. T. Choosing the greater of two goods: neural currencies for valuation and decision making. *Nature reviews. Neuroscience*, 6(5):363–375, May 2005.

Sussillo, D. and Abbott, L. F. Generating coherent patterns of activity from chaotic neural networks. *Neuron*, 63(4):544–557, August 2009.

Uchida, N., Kepecs, A., and Mainen, Z. F. Seeing at a glance, smelling in a whiff: rapid forms of perceptual decision making. *Nature reviews. Neuroscience*, 7(6): 485–491, June 2006.

Viswanathan, P. and Nieder, A. Neuronal correlates of a visual "sense of number" in primate parietal and prefrontal cortices. *Proceedings of the National Academy of Sciences of the United States of America*, 110(27):11187–11192, July 2013.

Wichmann, F. A. and Hill, N. J. The psychometric function: I. Fitting, sampling, and goodness of fit. *Perception & psychophysics*, 63(8):1293–1313, November 2001a.

Wichmann, F. A. and Hill, N. J. The psychometric function: II. Bootstrap-based confidence intervals and sampling. *Perception & psychophysics*, 63(8):1314–1329, November 2001b.

Wilber, A. A., Clark, B. J., Demecha, A. J., Mesina, L., Vos, J. M., and McNaughton, B. L. Cortical connectivity maps reveal anatomically distinct areas in the parietal cortex of the rat. *Frontiers in neural circuits*, 8, 2014.

Young, M. J., Landy, M. S., and Maloney, L. T. A perturbation analysis of depth perception from combinations of texture and motion cues. *Vision research*, 33(18): 2685–2696, December 1993.

Zemel, R. S. and Dayan, P. Combining probabilistic population codes. pages 1114–1119, 1997.

Znamenskiy, P. and Zador, A. M. Corticostriatal neurons in auditory cortex drive decisions during auditory discrimination. *Nature*, 497(7450):482–485, May 2013.

ITQB-UNL | Av. da República, 2780-157 Oeiras, Portugal
Tel (+351) 214 469 100 | Fax (+351) 214 411 277

www.itqb.unl.pt